BIO-INSPIRED FIRST-ROW TRANSITION METAL COMPLEXES FOR SMALL MOLECULE ACTIVATION

BY

YUN JI PARK

DISSERTATION

Submitted in partial fulfillment of the requirements
for the degree of Doctor of Philosophy in Chemistry
in the Graduate College of the
University of Illinois at Urbana-Champaign, 2016

Urbana, Illinois

Doctoral Committee:

Assistant Professor Alison R. Fout, Chair
Professor Gregory S. Girolami
Professor Yi Lu
Assistant Professor Damien Guironnet

Abstract

Secondary coordination spheres play many important roles in the activity and function of metalloenzymes: they can help stabilize reactive intermediates and shuttle protons or electrons over the course of enzymatic transformations. Accordingly, there have been numerous efforts to mimic these advantageous structural and functional features; indeed, secondary coordination spheres are now employed in a number of synthetic inorganic systems. Our lab has recently designed first-row transition metal complexes bearing secondary coordination spheres. Such complexes have been designed to: 1) be tautomerizable to traverse between hydrogen bond donating and accepting within the secondary coordination 2) facilitate activation of molecules such as O_2, NO_2^- and NO_3^- 3) catalytically reduce nitrogen-containing oxyanions. In the case of the latter, mechanistic studies have been performed to understand the role of the secondary coordination sphere, revealing its ability to stabilize intermediate as well as shuttle protons/electrons.

Early work focused on the synthesis of a tautomerizable ligand platform and its metalation with various first-row transition metal centers. This ligand platform can tautomerize from a pyrrole-2-imine to an azafulvene-amine form, resulting in either hydrogen bond acceptors or hydrogen bond donors in the secondary coordination sphere depending on the binding mode. The synthesis and characterization of a series of Mn(II) complexes with this platform have been described. Of especial importance, intramolecular hydrogen bond interactions between bound substrates and the secondary coordination sphere, as well as independent tautomerization of each arm of the ligand platform, have confirmed that our metal complexes are useful to mimic metalloenzyme.

Interested in probing the reactivity of these metal complexes towards biologically relevant molecules, O_2, NO_2^- and NO_3^- were reacted with metal derivatives of the ligand platform. Upon addition, high-valent Mn(III) and Fe(III) complexes were generated, with noticeable stabilization of the generated species by the secondary coordination sphere. Furthermore, in order to assess the possibility of rendering these reactions catalytic, reduction of the Fe(III) complexes back to the starting Fe(II) complexes was undertaken and accomplished. This result intrigued me and led me to study the catalytic reduction of the nitrogen-containing anions in

particular given their significant interest in biological and environmental studies. Mechanistic studies revealed the importance of the secondary coordination sphere in stabilizing intermediates, as well as shuttling protons and electrons throughout the catalytic reaction. Thus, this research demonstrates that metal complexes bearing flexible secondary coordination sphere can model functional and structural features of metalloenzymes, thereby providing important insights into the design of new catalysts to address unmet needs.

To My Family

Acknowledgements

I would first like to thank my parents and my sister. My parents have always been supportive throughout my life. They trusted me with every decision I have made, and supported me with everything they have. My sister Sojin has been a good friend even from Korea, and I would like to thank her for the entertaining phone conversations that made me laugh. Without my family, I could not have finished my PhD program.

I would like to thank my advisor, Professor Alison Fout. Since the first time we have met, she has always been supportive of me. Her knowledge of chemistry and her scientific intuition inspired me to become a better chemist. I truly appreciate her understanding, patience, and encouragements that she showed me for the last four years. She has been the best advisor to me. I would also like to thank my committee members, Professor Girolami, Professor Lu, and Professor Guironnet, for their support, providing me with great insights, and sharing their knowledge of chemistry during my graduate studies.

I would like to thank our previous post-doc, Professor Ellen Matson. She was an enormous help to me when I started as a graduate student, and I appreciate her caring which helped me become a better chemist. I would also like to thank my group members, Zack Gordon, Abdulrahman Ibrahim, Gabriel Espinosa Martinez, Courtney Ford, Bailey Jackson, Kenan Tokmic, Michael Drummond, Jack Killion, Tabitha Miller and Joe Nugent for their incredible support, thoughtful suggestions on my talk and papers, the interesting discussions about chemistry, and telling me funny stories all the time. I had a great time during my graduate school career thanks to my group members.

I would like to thank Connie Knight as well as all other secretaries in the IMP office, Beth Myler, Karen Neuman, Theresa Struss, and Stacy Dudzinski, for making everything run smoothly within the department. Also, I would like to thank Dr. Danielle Gray and Dr. Jeffery Bertke for teaching me X-ray crystallography; and Dr. Mark Nilges for helping me with EPR spectroscopy.

Lastly, I would like to thank my husband and best friend, John (Wookyung) Lee. His support has been incredible. Without him I would not have made it until today.

Table of Contents

Chapter 1

Secondary coordination spheres in metalloenzymes and their applications in synthetic inorganic systems

1.1 The roles of the secondary coordination sphere in metalloenzymes

Metalloenzymes are critical in biological systems where they play prominent roles in small molecule activation, signal transduction, as well as transport or storage processes.[1–4] In order to probe how metalloenzymes operate and interact with substrates, the active sites containing redox active metal centers have been extensively studied. The primary coordination sphere, which is directly bound to the metal center in metalloenzymes, is known to be a key contributor towards determining the electronic structure and Lewis acidity of the metal.[5] For example, the porphyrin platform present in metalloproteins such as hemoglobin, myoglobin or cytochrome P450 provides a ligand environment that facilitates redox events at the metal center.[6–8]

However, scientists have also found that hydrogen bonds within the secondary coordination sphere play an important role. Although hydrogen bond interactions are much weaker (ranging from 5 to 15 kcal/mol)[9] than formal bonds in the primary coordination sphere, such interactions in the protein scaffold can control substrate binding, stabilize intermediates, and tune redox activity over the course of enzymatic reactions.[5,10] For instance, in cytochrome P450, hydrogen bond interactions from Thr-252 and Asp-251 aid in activating dioxygen. It is proposed that these residues stabilize the iron-peroxo intermediate and protonate the terminal oxygen atom, resulting in the formation of an Fe^{III}–OOH species (Figure 1.1A).[11–13] In the case of the oxygen evolving complex (OEC), which is responsible for catalytic water oxidation in photosystem II, several amino acid residues in the secondary coordination sphere are utilized: Asp-61 can facilitate proton exit from the Mn_4CaO_5 cluster; His-337 can stabilize the cubane structure; and Tyr-161 is responsible for mediating electron transfer between the Mn_4CaO_5 cluster and the photosystem II reaction center (Figure 1.1B).[14–16] Mutation studies on these metalloenzymes have shown that changing the amino acid residues that are engaged in hydrogen bonding with the active site can result in the loss of enzymatic reactivity.

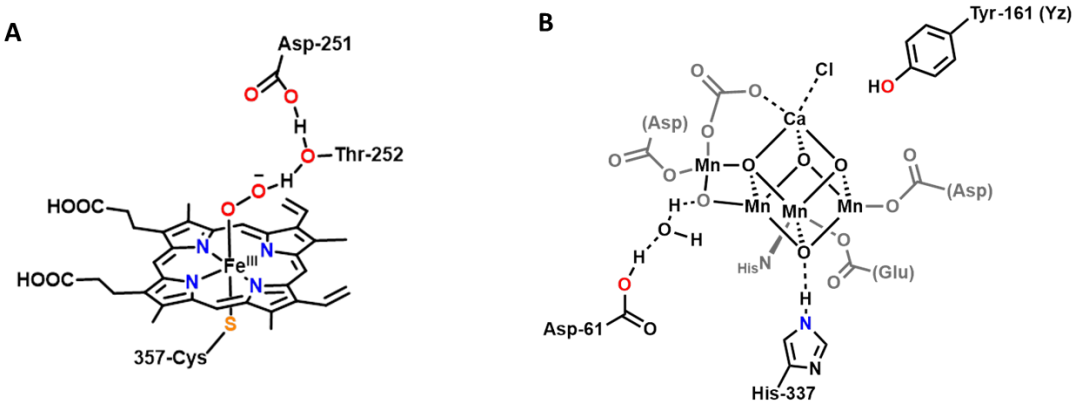

Figure 1.1 (A) The active site of cytochrome P450 featuring hydrogen bond interactions with Thr-252 and Asp-251.[13] (B) OEC with amino acid residues in the secondary coordination sphere.[14]

As shown above, both the primary and secondary coordination spheres are crucial to achieve ideal reactivity in metalloenzymes. Accordingly, understanding their roles should provide important insights that will inform the design of ligand platforms and synthetic inorganic systems capable of mimicking enzymatic structures and reactivities. Incorporation of secondary coordination spheres, in particular, would help overcome many of the current challenges that synthetic inorganic chemists face.

1.2 Synthetic inorganic systems utilizing secondary coordination spheres for small molecule activation

1.2.1 Synthetic heme complexes

Due to the advantage of the heme complexes capable of performing redox reactions readily, porphyrin platforms having a secondary coordination sphere were synthesized and studied. Introducing the secondary coordination sphere was expected to increase the substrate binding affinity to the metal center and stabilize their intermediates. Reed's urea/amide-appended porphyrins called "picket-fence porphyrins" revealed an enhanced affinity of O_2 to the iron center and better stabilization of the Fe-O_2 adduct, which was proposed as a key intermediate in cytochrome P450 (Figure 1.2A).[17] Another example by Nocera was a "hangman porphyrin" that uses xanthane units to position H-bond in the heme complexes.[18] In the crystal structure, they observed that a water molecule is hydrogen bonding to the hydroxyl ligand bound to the metal center and the carboxylic acid moiety of the secondary coordination sphere. They

suggested that this can be demonstrated as a model platform of the water channel in cytochrome P450 (Figure 1.2B).

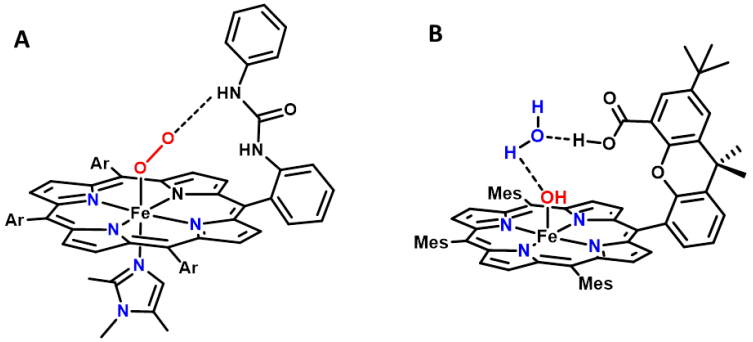

Figure 1.2 Hydrogen bonding stabilization in (A) Reed's urea-appended "picket-fence porphyrin"[17] and (B) Nocera's Fe^{III}-OH "hangman porphyrin" complex.[18]

1.2.2 Synthetic non-heme and other first-row transition metal complexes

Non-heme complexes bearing intramolecular hydrogen bonding frameworks have also been studied. Despite the usefulness of the porphyrin containing metal complexes, modifying porphyrins to introduce functional groups is synthetically challenging. Thus, development of non-heme complexes has the advantage of relatively facile installation of functional groups as well as having a variety of metal geometries compared to the porphyrin platforms. One of the earliest examples of such a non-heme system was reported by Kitajima, who synthesized a monomeric side-on Mn(III)-peroxo complex in a distorted trigonal bipyramidal geometry stabilized by an intramolecular hydrogen bond (Figure 1.3A).[19] Using polypyridine tripodal ligand frameworks, Masuda et al. were able to show the first example of a stable Cu^{II}-OOH complex, where two amines in the secondary coordination sphere are hydrogen bonding to the oxygen atoms of the hydroperoxide (Figure 1.3B).[20]

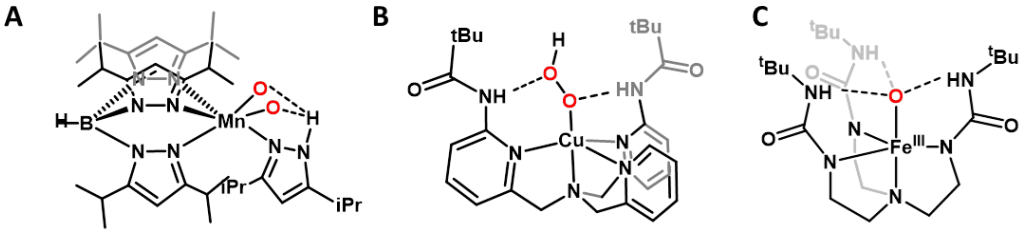

Figure 1.3 (A) A side-on Mn(III)-peroxo complex.[19] (B) Cu(II)-OOH complex.[20] (C) Fe(III)-oxo complex.[21]

More recently, Borovik has extensively worked on first-row transition metal complexes with tripodal ligands that possess urea moieties functioning as hydrogen bond donors in the secondary coordination sphere. Utilizing this platform they were able to activate O_2 or water, generating M(III)-oxo, M(III)-OH, and M(IV)-oxo molecules (M = Mn, Fe, and Co), which were stabilized by the hydrogen bonding interaction in the secondary coordination sphere (Figure 1.3C).[21–25] Interested in the stabilizing effect of the secondary coordination sphere, they modified the ligand platform with a different number of urea moieties in the ligand scaffold. In this study, the resulting Co(III)-OH complex with a smaller number of intramolecular hydrogen bond interactions was less stable, resulting in a shorter half life time (Figure 1.4).[26]

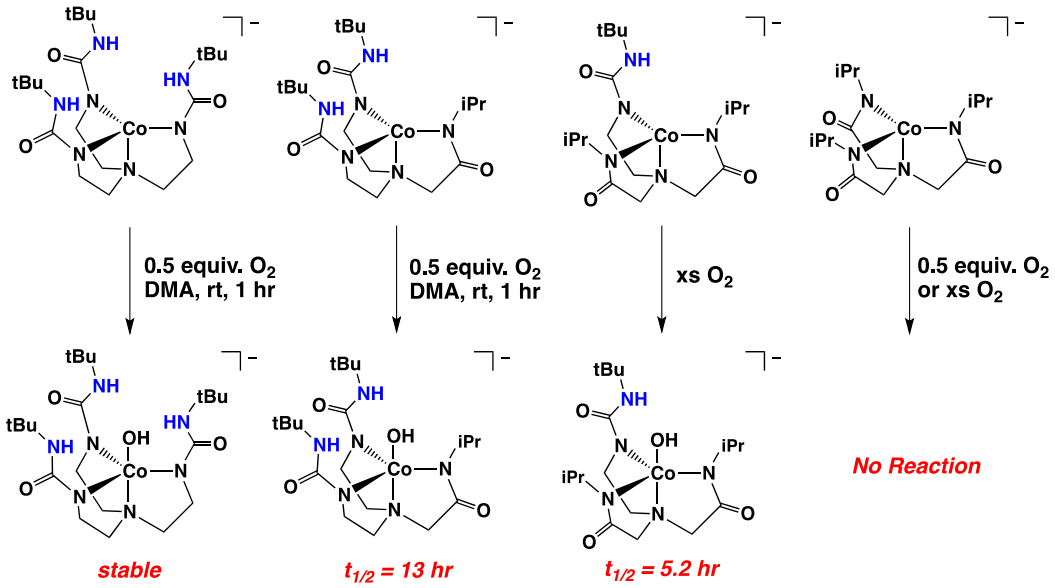

Figure 1.4 Dioxygen reactivity with a series of Co(II) complexes featuring a different number of hydrogen bond donors.[26]

While there are a number of reported metal complexes having hydrogen bond donors in the secondary coordination sphere, examples of metal complexes bearing hydrogen bond acceptors are very rare. For example, Borovik installed a sulfonamide group on the tripodal ligand to stabilize the Fe(III)-OH complex,[27] and Gilbertson and Pluth demonstrated that the pendant tertiary amine in the secondary coordination sphere can stabilize the Zn(II)-hydrosulfide complex.[28]

Thus, previous studies have shown that hydrogen bond interactions can aid in activating small molecules and stabilizing reactive intermediates including high-valent metal-oxo, metal-hydroxyl, and metal-peroxo species. However, there are a limited number of examples of metal complexes capable of traversing between hydrogen bond donating and accepting within the secondary coordination sphere as well as shuttling electrons and protons to/from the substrates, which are necessary roles to complete catalytic cycles in metalloenzymes. In our research group, we sought to expand the research of secondary coordination spheres to feature various roles demonstrated in the metalloenzymes by using tautomerizable ligand platforms, eventually aiming to perform catalytic small molecule activations.

1.3 A tripodal ligand platform capable of tautomerization

Our research group previously synthesized and reported a ligand capable of tautomerization between pyrrole-imine and azafulvene-amine, presenting a flexible secondary coordination sphere (Figure 1.5).[29] This ligand, tris(5-cyclohexyliminopyrrol-2-ylmethyl)amine ($H_3[N(pi^{Cy})_3]$), was designed to be a tetradentate tripodal ligand where the primary coordination sphere contains an apical nitrogen and three pyrroles. Depending on the tautomeric form, the secondary coordination can serve as either a hydrogen bond acceptor when in the pyrrole-imine form or a hydrogen bond donor in azafulvene-amine tautomer. This hydrogen bond interaction via tautomerization was expected to stabilize reactive intermediates as well as be able to transfer protons or electrons between substrates and the metal complexes. This is reminiscent of certain amino acids such as aspartic acid, histidine, and tyrosine, in the secondary coordination sphere of the oxygen evolving complex described above.[14]

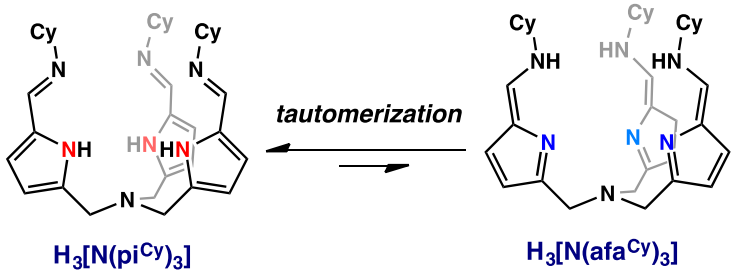

Figure 1.5 Tautomerization of the ligand platform ($H_3[N(pi^{Cy})_3]$).[29]

Utilizing this ligand platform, our group reported the synthesis of a series of Fe(II) complexes featuring different tautomeric forms of the ligand platform depending on the reaction

conditions (Figure 1.6). The bound substrates such as H_2O or OH can have hydrogen bonding interaction to the secondary coordination sphere, suggesting that the secondary coordination sphere is within the appropriate hydrogen bonding range. Moreover, each arm of the ligand can tautomerize independently as demonstrated in the $[N(pi^{Cy})(afa^{Cy})_2]Fe(OH)$ complex. Early studies with $H_3[N(pi^{Cy})_3]$ showed that this ligand platform would be appropriate for modelling metalloenzymes; it demonstrated not only hydrogen bonding interactions to stabilize the bound substrates, but also flexible tautomerization within the ligand arm which enabled proton/electron transfers, a primary role of secondary coordination spheres in metalloenzymes.

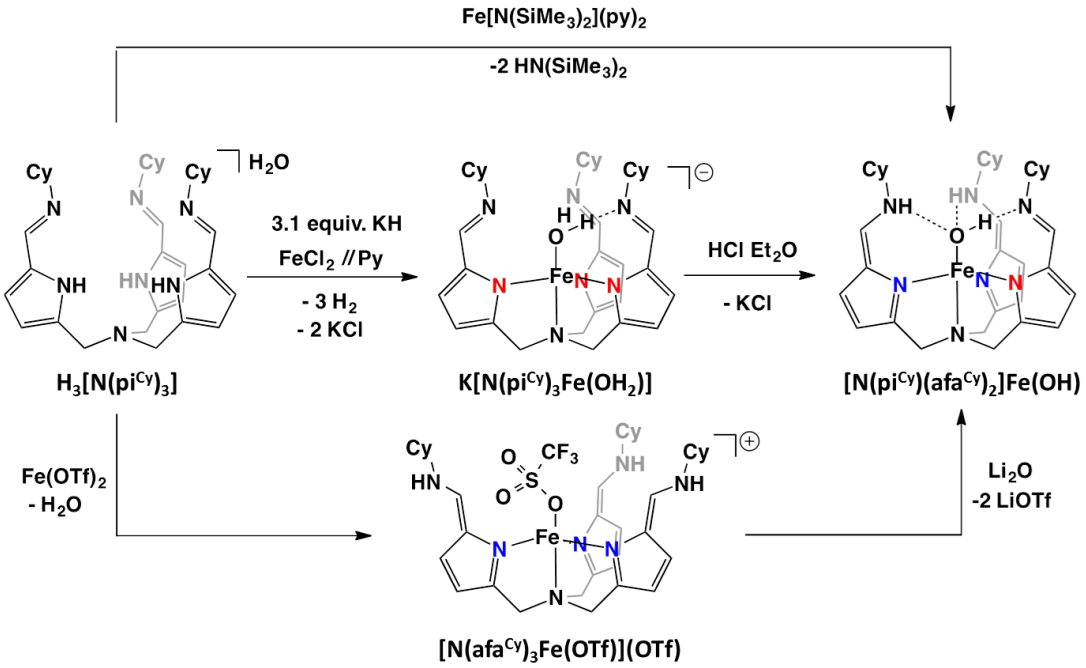

Figure 1.6 Synthesis of a series of Fe(II) complexes with $H_3[N(pi^{Cy})_3]$.[29]

1.4 References

(1) Thomson, A. J.; Gray, H. B. Bio-Inorganic Chemistry. *Curr. Opin. Chem. Biol.* **1998**, *2*, 155–158.

(2) Aisen, P.; Listowsky, I. Iron Transport and Storage Proteins. *Annu. Rev. Biochem.* **1980**, *49*, 357–393.

(3) Waldron, K. J.; Rutherford, J. C.; Ford, D.; Robinson, N. J. Metalloproteins and Metal Sensing. *Nature* **2009**, *460*, 823–830.

(4) Silaghi-Dumitrescu, R. Redox Activation of Small Molecules at Biological Metal Centers. In *Applications of Density Functional Theory to Biological and Bioinorganic Chemistry*; Putz, M. V.; Mingos, D. M. P., Eds.; Springer Berlin Heidelberg: Berlin, Heidelberg, 2013; Vol. 150, pp. 97–117.

(5) Shook, R. L.; Borovik, A. S. Role of the Secondary Coordination Sphere in Metal-Mediated Dioxygen Activation. *Inorg. Chem.* **2010**, *49*, 3646–3660.

(6) Fleischer, E. B. Structure of Porphyrins and Metalloporphyrins. *Acc. Chem. Res.* **1970**, *3*, 105–112.

(7) Suslick, K. S. *The Porphyrin Handbook*; Kadish, K. M.; Smith, K. M.; Guilard, R., Eds.; Academic Press: New York, 2000.

(8) Ivanov, A. S.; Boldyrev, A. I. Deciphering Aromaticity in Porphyrinoids via Adaptive Natural Density Partitioning. *Org. Biomol. Chem.* **2014**, *12*, 6145.

(9) Etter, M. C. Encoding and Decoding Hydrogen-Bond Patterns of Organic Compounds. *Acc. Chem. Res.* **1990**, *23*, 120–126.

(10) Colquhoun, H. M.; Stoddart, J. F.; Williams, D. J. Second-Sphere Coordination–a Novel R??le for Molecular Receptors. *Angew. Chem. Int. Ed. Engl.* **1986**, *25*, 487–507.

(11) Williams, P. A.; Cosme, J.; Ward, A.; Angove, H. C.; Matak Vinković, D.; Jhoti, H. Crystal Structure of Human Cytochrome P450 2C9 with Bound Warfarin. *Nature* **2003**, *424*, 464–468.

(12) Meunier, B.; de Visser, S. P.; Shaik, S. Mechanism of Oxidation Reactions Catalyzed by Cytochrome P450 Enzymes. *Chem. Rev.* **2004**, *104*, 3947–3980.

(13) Denisov, I. G.; Makris, T. M.; Sligar, S. G.; Schlichting, I. Structure and Chemistry of Cytochrome P450. *Chem. Rev.* **2005**, *105*, 2253–2278.

(14) Umena, Y.; Kawakami, K.; Shen, J.-R.; Kamiya, N. Crystal Structure of Oxygen-Evolving Photosystem II at a Resolution of 1.9 Å. *Nature* **2011**, *473*, 55–60.

(15) McEvoy, J. P.; Brudvig, G. W. Water-Splitting Chemistry of Photosystem II. *Chem. Rev.* **2006**, *106*, 4455–4483.

(16) McEvoy, J. P.; Gascon, J. A.; Batista, V. S.; Brudvig, G. W. The Mechanism of Photosynthetic Water Splitting. *Photochem. Photobiol. Sci.* **2005**, *4*, 940.

(17) Wuenschell, G. E.; Tetreau, C.; Lavalette, D.; Reed, C. A. Hydrogen-Bonded Oxyhemoglobin Models with Substituted Picket-Fence Porphyrins: The Model Compound Equivalent of Site-Directed Mutagenesis. *J. Am. Chem. Soc.* **1992**, *114*, 3346–3355.

(18) Yeh, C.-Y.; Chang, C. J.; Nocera, D. G. “Hangman” Porphyrins for the Assembly of a Model Heme Water Channel. *J. Am. Chem. Soc.* **2001**, *123*, 1513–1514.

(19) Kitajima, N.; Komatsuzaki, H.; Hikichi, S.; Osawa, M.; Moro-oka, Y. A Monomeric Side-On Peroxo Manganese(III) Complex: Mn(O2)(3,5-iPr2pzH)(HB(3,5-iPr2pz)3). *J. Am. Chem. Soc.* **1994**, *116*, 11596–11597.

(20) Wada, A.; Harata, M.; Hasegawa, K.; Jitsukawa, K.; Masuda, H.; Mukai, M.; Kitagawa, T.; Einaga, H. Structural and Spectroscopic Characterization of a Mononuclear Hydroperoxo-Copper(II) Complex with Tripodal Pyridylamine Ligands. *Angew. Chem. Int. Ed.* **1998**, *37*, 798–799.

(21) MacBeth, C. E. O2 Activation by Nonheme Iron Complexes: A Monomeric Fe(III)-Oxo Complex Derived From O2. *Science* **2000**, *289*, 938–941.

(22) Shirin, Z.; Hammes, B. S.; Young, V. G.; Borovik, A. S. Hydrogen Bonding in Metal Oxo Complexes: Synthesis and Structure of a Monomeric Manganese(III)−Oxo Complex and Its Hydroxo Analogue. *J. Am. Chem. Soc.* **2000**, *122*, 1836–1837.

(23) MacBeth, C. E.; Hammes, B. S.; Young, V. G.; Borovik, A. S. Hydrogen-Bonding Cavities about Metal Ions: Synthesis, Structure, and Physical Properties for a Series of Monomeric M−OH Complexes Derived from Water. *Inorg. Chem.* **2001**, *40*, 4733–4741.

(24) Gupta, R.; MacBeth, C. E.; Young, V. G.; Borovik, A. S. Isolation of Monomeric $Mn^{III/II}$−OH and Mn^{III} −O Complexes from Water: Evaluation of O−H Bond Dissociation Energies. *J. Am. Chem. Soc.* **2002**, *124*, 1136–1137.

(25) Borovik, A. S. Bioinspired Hydrogen Bond Motifs in Ligand Design: The Role of Noncovalent Interactions in Metal Ion Mediated Activation of Dioxygen. *Acc. Chem. Res.* **2005**, *38*, 54–61.

(26) A Modular Approach toward Regulating the Secondary Coordination Sphere of Metal Ions: Differential Dioxygen Activation Assisted by Intramolecular Hydrogen Bonds [*J. Am. Chem. Soc.* **2006** , *128* , 15476−15489]. *J. Am. Chem. Soc.* **2007**, *129*, 723–723.

(27) Cook, S. A.; Ziller, J. W.; Borovik, A. S. Iron(II) Complexes Supported by Sulfonamido Tripodal Ligands: Endogenous versus Exogenous Substrate Oxidation. *Inorg. Chem.* **2014**, *53*, 11029–11035.

(28) Hartle, M. D.; Delgado, M.; Gilbertson, J. D.; Pluth, M. D. Stabilization of a Zn(II) Hydrosulfido Complex Utilizing a Hydrogen-Bond Accepting Ligand. *Chem Commun* **2016**, *52*, 7680–7682.

(29) Matson, E. M.; Bertke, J. A.; Fout, A. R. Isolation of Iron(II) Aqua and Hydroxyl Complexes Featuring a Tripodal H-Bond Donor and Acceptor Ligand. *Inorg. Chem.* **2014**, *53*, 4450–4458.

Chapter 2

Exploration of Mn complexes containing Mn–O bonds stabilized by secondary coordination sphere: synthesis of Mn^{III}–O by small molecule activation†

2.1 Introduction

Manganese is considered one of the most important first-row transition metals capable of performing various catalytic reactions in biological systems, including the oxygen evolving complex (OEC) of photosystem II,[1,2] peroxidases,[3] catalases[4,5] and manganese oxidizing bacteria.[6] In all examples, high-valent Mn-oxo complexes are proposed as key intermediates over the course of the enzymatic reactions. The OEC, comprised of a Mn_4CaO_5 cluster, is supported by both bridging hydroxo or oxo ligands, and aspartic acid and histidine side chains from the protein, with the manganese metal centers ranging in oxidation state from three to five.[1,7–10] Key intermediates in the water oxidation reaction include manganese aqua, hydroxyl and oxo species. As discussed in the previous chapter, hydrogen bonding also plays a significant role in this enzymatic reaction by influencing the structure-function relationship of metalloenzymes. Several amino acids (tyrosine, histidine, tryptophan and cysteine) have been shown to mediate proton transfer, stabilize the cubane structure, and facilitate electron transfer, alleviating the electronic burden often placed on the metal center.[1]

Complexes featuring Mn–O bonds have played an important role in chemical catalysis.[11–16] Several reports have illustrated the generation of Mn–O bonds from a variety of substrates. However, prior to the work by Borovik,[17–19] reports of Mn–oxo complexes were limited to peroxo or bridging oxo moieties.[4,20,21] Stabilization of the terminal Mn^{III}–oxo was realized in 2000, when a ligand architecture that featured a hydrogen-bonding cavity was used.[17] This remains the only example of a terminal Mn^{III}–oxo complex. Isolation of Mn^{III}–oxo complexes is critical in both inorganic chemistry and biochemistry to study reactive high-valent Mn-oxo species to gain insights into biological systems.

† Portions of this chapter are reproduced from the following publication with permission from the authors. Park, Y.J.*; Matson, E. M.*; Nilges, M. J.; Fout, A.R. *Chem Commun* **2015**, *51*, 5310-5313.

Given our group's previous work on the tautomerizable ligand platform and Fe(II) complexes,[22] we were interested in examining the relationship between the tautomeric states accessible for the ligand platform and their role in the stabilization of Mn-O bonds. Herein we describe the facile generation of key intermediates found in water oxidation including a Mn^{II}–OH, Mn^{II}–OH_2, and Mn^{III}–O stabilized by either hydrogen-bond donating (afa^{Cy}) or accepting (pi^{Cy}) groups. The facile generation of a Mn(III)-oxo from a variety of reagents, including O-atoms transfer reagents, O_2, and NO_2^-, is described, whereby the latter reaction represents the first example of facile nitrite reduction to afford a Mn(III)-oxo complex.

2.2 Results and discussion

2.2.1 Synthesis of a series of Mn(II) complexes

Synthesis of the desired manganese complexes, K[N(pi^{Cy})$_3$Mn(OH_2)] (**Mn^{II}-OH_2**), [N(afa^{Cy})$_3$Mn(OTf)](OTf) (**Mn^{II}-OTf**) and N(pi^{Cy})(afa^{Cy})$_2$Mn(OH) (**Mn^{II}-OH**) was accomplished following the previously reported synthetic procedures for the iron derivatives in comparable yields (Scheme 2.1).[22] As complexes are ^{1}H NMR silent, characterization of these species was performed by X-ray crystallography, IR spectroscopy and magnetism by Evans' method (Figure 2.1, Table 2.1).

Addition of 3.1 eq. of KH to the ligand followed by $MnCl_2$ resulted in the formation of **Mn^{II}-OH_2**, where the ligand is anionically coordinated to the manganese center. As expected, the X-ray crystal structure showed that the Mn(II) species was in a distorted trigonal bipyramidal geometry with a water molecule bound to the metal center *trans* to the apical nitrogen, analogous to the reported K[N(pi^{Cy})$_3$Fe(OH_2)] complex (Figure 2.1). The Mn1—O1 distance of 2.096(2) Å compares favorably to that of five-coordinate Mn(II)-aqua complexes in the literature, ranging from 2.081 to 2.189 Å.[23–27] By locating hydrogens of the water molecule in the difference map, we were able to observe that the water molecule was engaged in hydrogen bonding with two of the pendant imine moieties in the secondary coordination sphere, supported by N···H bond distances of 1.88(2) and 1.85(4) Å within the range of donor-acceptor atoms participating in hydrogen bonding.[28] The solution magnetic moment of **Mn^{II}-OH_2** as determined by the Evans' method was 6.15(15) μ_B, consistent with the formation of high-spin Mn(II) complex (high-spin Mn(II) μ_{SO} = 5.92 μ_B)

Synthesis of **Mn^{II}-OTf** was accomplished by adding ligand, $H_3N(pi^{Cy})_3$, to the THF solution of $Mn(OTf)_2(MeCN)_2$ without base. In **Mn^{II}-OTf**, the ligand was tautomerized to the azafulvene-amine form which features dative coordination to the metal center. X-ray crystal structure determination of **Mn^{II}-OTf** revealed that the five-coordinate Mn(II) center was in a pseudo-trigonal bipyramidal geometry bound to the tripodal ligand platform (Figure 2.1). Even though the gross structures of the bound ligand in **Mn^{II}-OH_2** and **Mn^{II}-OTf** are similar, comparison of intraligand bond distances revealed that three arms were tautomerized to the azafulvene-amine moieties in **Mn^{II}-OTf** (Figure 2.2). Moreover, the protons from the pyrroles in the primary coordination sphere moved to the secondary coordination sphere, resulting in the formation of amine moieties which can be potential hydrogen bond donors to the bound substrate. However, due to the sterics of the bound triflate anion and the secondary coordination sphere, the arms were rotated outwards, having hydrogen bonding interaction to the outer sphere triflate anion. The effective magnetic moment of **Mn^{II}-OTf** by Evans' method was 5.88(7) μ_B, consistent with the formation of high-spin Mn(II) complex.

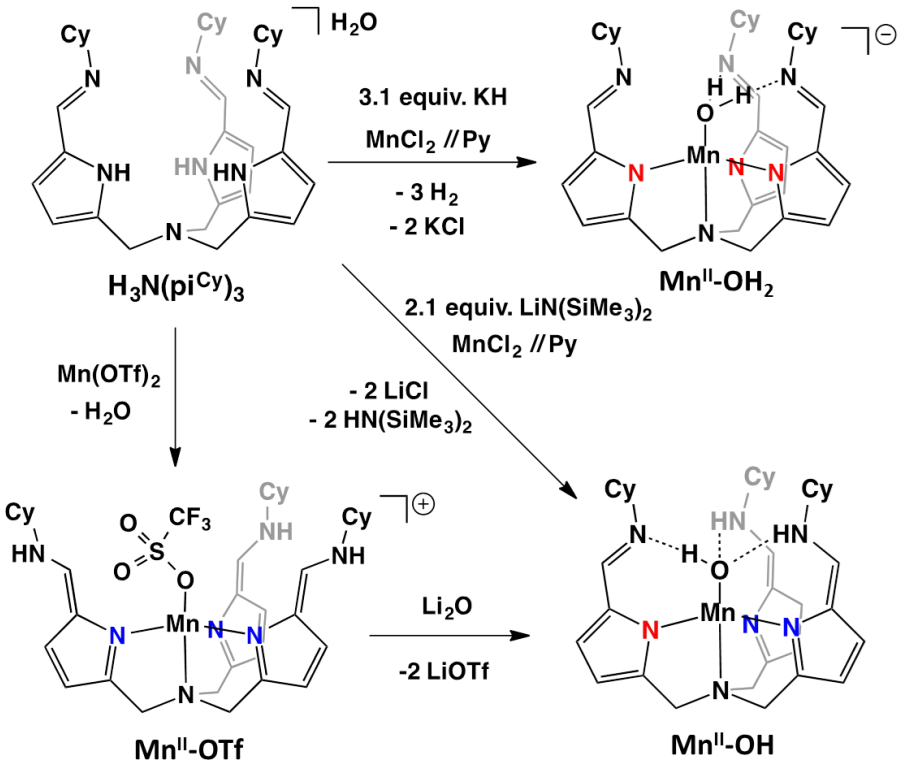

Scheme 2.1 Synthesis of **Mn^{II}-OH_2**, **Mn^{II}-OH**, and **Mn^{II}-OTf**.

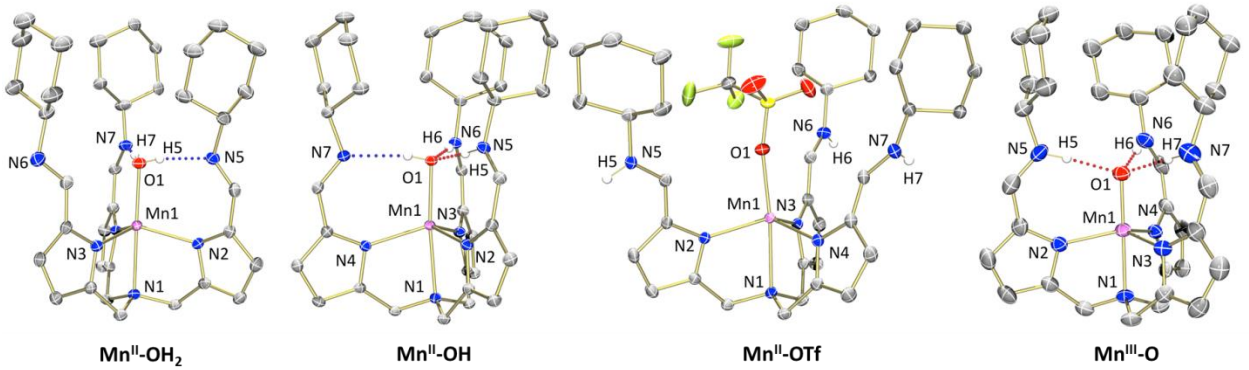

Figure 2.1 Molecular structures of **Mn^{II}-OH_2**, **Mn^{II}-OH**, **Mn^{II}-OTf** and **Mn^{III}-O** shown with 30% probability ellipsoids.

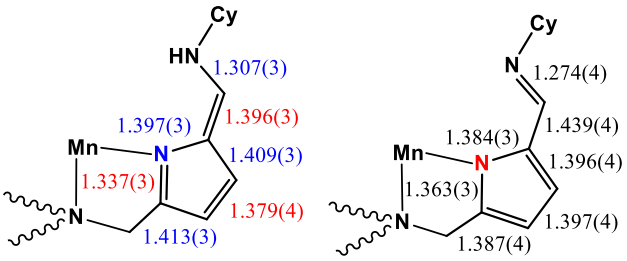

Figure 2.2 Bond length comparisons between **Mn^{II}-OTf** (left) and **Mn^{II}-OH_2** (right). Bond distances of the azafulvene substituent (**Mn^{II}-OTf**) listed in red denote contraction, while those in blue signify elongation from anionically coordinated pyrrole-imine (**Mn^{II}-OH_2**) arm.

The preparation of **Mn^{II}-OH** is also comparable to the previously reported [N(pi^{Cy})(afa^{Cy})$_2$]FeOH compound and was achieved by two different synthetic routes which are described in Scheme 2.1. H_3[N(pi^{Cy})$_3$] was deprotonated by the addition of 2.2 equivalents of LiN(SiMe$_3$)$_2$ and subsequent addition of the deprotonated ligand to an $MnCl_2$ in the presence of adventitious water resulted in the formation of **Mn^{II}-OH**. Alternatively, synthesis of **Mn^{II}-OH** was achieved by adding Li_2O to **Mn^{II}-OTf**.

Structural analysis of **Mn^{II}-OH** revealed that the manganese center was in a pseudo-trigonal bipyramidal geometry, consisting of the tripodal ligand and a hydroxyl ligand *trans* to the apical nitrogen (Figure 2.1). The Mn1—O1 distance of 2.0524(12) Å was shorter than that of complex **Mn^{II}-OH_2** and comparable to the Mn—O distance of Borovik's Mn(II)-OH complex (2.059(2)Å).[19] Interestingly, two different tautomeric forms were observed in the crystal

structure of **Mn^{II}-OH**. Two of the three arms were revealed as azafulvene-amine moieties presenting hydrogen bond donors in the secondary coordination sphere. Those two amines were hydrogen bonding to the oxygen of the hydroxyl ligand with O···H distance of 1.75(2) and 1.66(2) Å. The third arm, however, was determined to be the pyrrole-imine moiety, functioning as a hydrogen bond acceptor from the hydroxyl ligand with a N···H distance of 2.09(2) Å. The O···H and N···H distances are within the range of appropriate hydrogen bonding interaction. As previously reported with the Fe complex, this Mn complex demonstrated that each arm of this ligand is capable of independent tautomerization, resulting in two different tautomers in the same complex. Characterization of **Mn^{II}-OH** by Evans' method, however, was unsuccessful due to low solubility.

The solid-state infrared spectra (FTIR-ATR) of **Mn^{II}-OH_2, Mn^{II}-OTf,** and **Mn^{II}-OH** feature bands corresponding to the C=N stretches of the ligand platform (Table 2.1) similar to those reported for iron (**Fe^{II}-OH_2**: 1603 cm^{-1}; **Fe^{II}-OTf**: 1637 cm^{-1}; **Fe^{II}-OH**: 1624, 1655 cm^{-1})[22] and supported analogous coordination modes of the ligand between the different metal centers.

Table 2.1 Selected structural parameters of **Mn^{II}-OH_2**, **Mn^{II}-OH**, **Mn^{II}-OTf** and **Mn^{III}-O**.

Bond	**Mn^{II}-OH_2** (Å)	**Mn^{II}-OH** (Å)	**Mn^{II}-OTf** (Å)	**Mn^{III}-O** (Å)
Mn1-N1	2.347(2)	2.3295(15)	2.3398(17)	2.114(5)
Mn1-N(pyr)	2.126(2) – 2.165(2)	2.1427(15) – 2.1784(15)	2.1201(17) – 2.1480(18)	2.056(5) – 2.067(5)
Mn1-O1	2.096(2)	2.0524(12)	2.1450(16)	1.789(4)
O1-H5	0.74(4)	1.75(2)	--	--[b]
O1-H6	--	1.66(2)	--	--[b]
O1-H7	0.89(5)	0.78(2)	--	--[b]
C=N stretch	1617 cm^{-1}	1645 cm^{-1}	1641 cm^{-1}	1659 cm^{-1}
Magnetic Moment	6.15(15) μ_B	--[a]	5.88(7) μ_B	5.22(16) μ_B

[a]A reliable magnetic moment could not be obtained for complex **Mn^{II}-OH** due to its insolubility. [b]H atoms were calculated in this structure, therefore hydrogen-bonding distances are not pertinent. O1-NX (X =5, 6, 7) distances ranging from 2.673(7) – 2.747(16) Å support hydrogen-bonding interactions.

2.2.2 Reactivity of Mn^{II}-OTf towards small molecules: synthesis of Mn(III)-oxo complex

Following the synthesis of **Mn^{II}-OH_2**, **Mn^{II}-OH**, and **Mn^{II}-OTf**, oxidation experiments were explored to evaluate the propensity of these complexes to activate small molecules. Exposure of complex **Mn^{II}-OH_2** to an atmosphere of oxygen quickly afforded decomposition,

indicated by free ligand noted in the ^{1}H NMR spectrum. In contrast, complex **Mn^{II}-OH** was completely inert to oxygen. We propose this is a result of the hydrogen bonding observed in the structure of **Mn^{II}-OH**, protecting the metal center from external substrates. Furthermore, the presence of H-bonding likely disfavors ligand dissociation which is required for the reactivity of O_2 to occur.

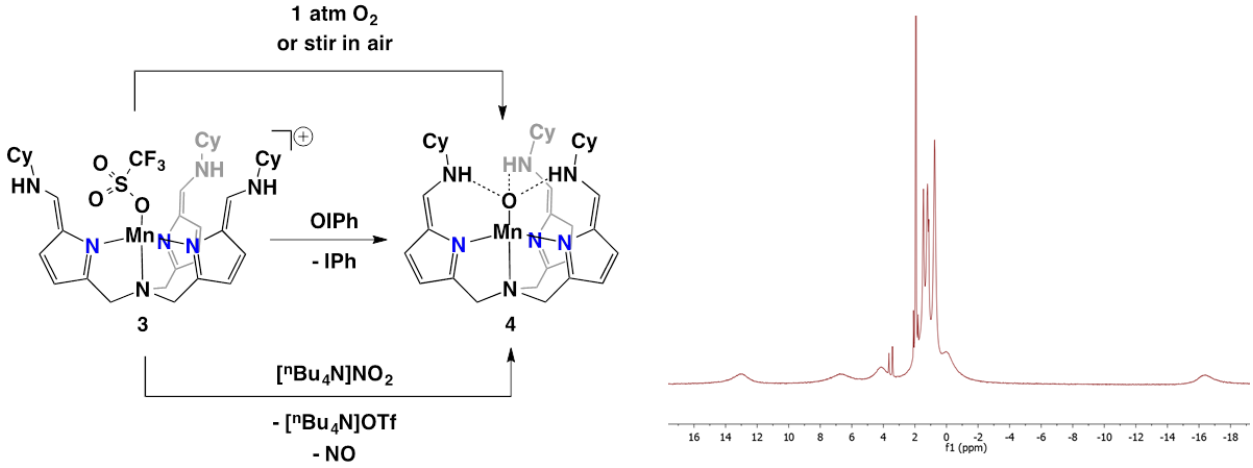

Figure 2.3 Synthesis of [N(afa^{Cy})$_3$MnO](OTf) (left). ^{1}H NMR Spectrum of [N(afa^{Cy})$_3$MnO](OTf) (right).

Oxidation of **Mn^{II}-OTf** was attempted via exposure to O_2, resulting in a gradual color change from yellow to green over the course of 24 hours (Figure 2.3, left). The green solid was obtained in 75% yield following workup. Characterization by ^{1}H NMR spectroscopy revealed 5 paramagnetically broadened and shifted features, ranging from -16.4 to 13.1 ppm (Figure 2.3, right). The solution magnetic moment of the product in dimethyformamide (μ_{eff} = 5.22(16) μ_B), as determined by the Evans' method, corresponds to high-spin Mn(III).

In order to confirm the formation of high-spin Mn(III) complex, the solution X-Band EPR spectrum of crystalline **Mn^{III}-O** in a 1:1 DCM/Toluene mixture (5 mM) was collected in perpendicular mode, displaying a weak and broad transition centered at g = 8 (Figure 2.4). In parallel mode, the spectrum displays a forbidden, ±2 transition with a six-line hyperfine splitting centered at g_{eff} = 7.9 and simulated with the following: g_z = 1.95; E/D = 0.09; A_z = 262 MH_z (Figure 2.4).

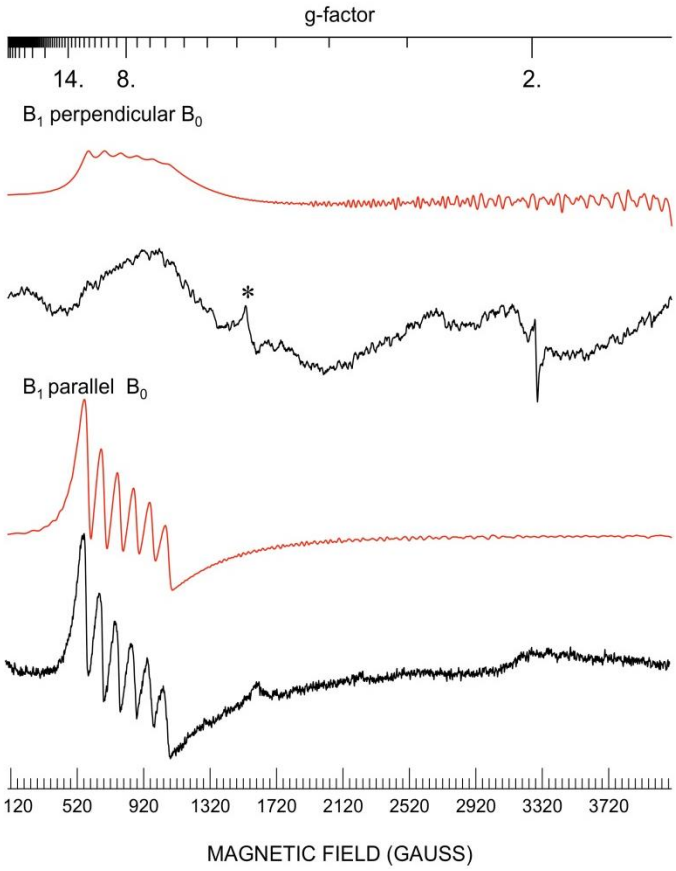

Figure 2.4 EPR Spectrum (X Band, Perpendicular Mode (top, simulation red, experimental black) Parallel Mode (bottom, simulation red, experimental black) of **Mn^{III}-O** (4K) (5 mM solution of **Mn^{III}-O** in a 1:1 dichloromethane/toluene mixture). The microwave frequency = 9.1008 GHz; receiver gain = 6.40E+3; modulation amplitude = 20.00G; Power = 10.00dB. The experimental data is shown in green and simulated spectrum in black g = 1.95 (E/D = .09). *denotes signal due to cavity background.

Independent synthesis of **Mn^{III}-O** was attempted via oxygen-atom transfer reagents. Exposure of **Mn^{II}-OTf** to an equivalent of pyridine-*N*-oxide resulted in recovery of starting materials despite prolonged reaction periods. Heating the mixture gave rise to decomposition of **Mn^{II}-OTf**, as identified by the presence of free ligand in the ^{1}H NMR spectrum. However, addition of an equivalent of iodosylbenzene (PhIO) to an acetonitrile solution of **Mn^{II}-OTf** resulted in a gradual color change from yellow to green-brown (Figure 2.3, left). Trituration with THF resulted in the isolation of a green solid, confirmed as **Mn^{III}-O** by ^{1}H NMR

spectroscopy and mass spectrometry, albeit in depreciated yields (41%). ESI-MS revealed the parent ion of **Mn^{III}-O** ($[N(afa^{Cy})_3Mn(O)]^+$, m/z = 652.35), which matches the predicted isotope pattern for the product and is consistent with the proposed molecular formula. Furthermore addition of 90% isotopically enriched $PhIO^{18}$ showed the parent ion for the O^{18} isotopologue of **Mn^{III}-O (**m/z = 654.35) with 60% incorporation of O^{18}. We believe the depreciation in O^{18} incorporation is due to rather fast exchange with water, which has previously been observed.[29] The infrared spectrum of **Mn^{III}-O** does not indicate any O-H or N-H stretches consistent with this fast water exchange.

Refinement of structural data obtained from green crystals of **Mn^{III}-O** revealed a pseudo trigonal bipyramidal manganese center with three datively coordinated azafulvene rings composing the equatorial plane, and a terminal oxygen bound *trans* to the apical nitrogen of the ligand platform (Figure 2.1, Table 2.1). As in the structure of the previously reported Fe(III)-oxo, $[N(afa^{Cy})_3Fe(O)]^+$,[30] all three arms of the ligand platform are rotated inwards, with the amino hydrogen atoms composing a secondary coordination sphere and engaging in hydrogen-bonding interactions with the oxygen atom [$O1^{\cdots}NX$ = 2.673(7) Å (X=5), 2.747(16) Å (X=6), 2.706(7) Å (X=7)] (Note: Due to the quality of the crystal structure, H-atoms could not be located in the difference map but calculated, thus evidence for hydrogen-bonding comes from the O–N distances consistent with that of $[N(afa^{Cy})Fe(O)]^+$). The Mn1–O1 distance of 1.789(4) Å is statistically identical to that of Borovik's Mn(III)-oxo (1.771(5) Å).[18] Furthermore, the Mn–O distance of **Mn^{III}-O** is significantly shorter than that of reported Mn(III)–OH bond distances which range from 1.806(13) – 1.8540(8) Å, consistent with our assignment of the product as the Mn(III) terminal-oxo species.[11,17,31]

To investigate the electronic changes upon oxidation of **Mn^{II}-OTf**, electronic absorption spectroscopy was employed (Figure 2.5). In the case of **Mn^{II}-OTf** a single band centered at 327 nm (ε = 84386 $M^{-1}cm^{-1}$), attributed to the $\pi \rightarrow \pi^*$ transition of the ligand platform, is detected in the UV region of the spectrum. Upon oxidation to **Mn^{III}-O**, this $\pi \rightarrow \pi^*$ transition is slightly red-shifted, as a result of the reduction of electron density at the metal centre [λ_{max} (ε_m) = 335 nm (33620 $M^{-1}cm^{-1}$)]. Additionally, the spectrum of **Mn^{III}-O** resembles that previously reported for $[Mn(III)H_3buea(O)]^{2-}$ [λ_{max} (ε_m) = 498 nm (490 M^{-1} cm^{-1}), 725 nm (240 $M^{-1}cm^{-1}$)], with notable bands blue-shifted, located at 458 nm (ε = 507 $M^{-1}cm^{-1}$) and 621 nm (ε = 477 $M^{-1}cm^{-1}$).[32] These

energy differences are proposed to arise from the dative versus anionic coordination, respectively, of the ligand platforms.

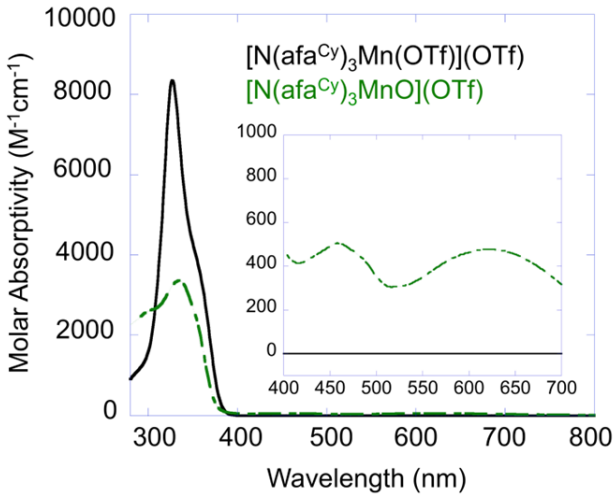

Figure 2.5 Electronic absorption spectrum of **Mn^{II}-OTf** and **Mn^{III}-O** in MeCN at ambient temperature.

In an effort to explore alternative synthetic routes to access **Mn^{III}-O**, the reactivity of the Mn(II) azafulvene complex (**Mn^{II}-OTf**) towards the reduction of nitrite was investigated (Figure 2.3). Previously, our research group has reported the facile reduction of NO_2^- by an iron(II) non-heme species, [N(afa^{Cy})$_3$Fe(OTf)](OTf), resulting in the isolation of a terminal Fe(III)oxo complex, [N(afa^{Cy})$_3$Fe(O)](OTf).[30] Due to the similarities in the structures of the iron and manganese starting materials, the ability of the manganese system to perform the analogous anion reduction was explored. Upon exposure of **Mn^{II}-OTf** to an equivalent of [NBu_4][NO_2], formation of **Mn^{III}-O** was noted over a period of 24 hours at elevated temperatures (61%). This extended reaction time is in contrast to the immediate reduction noted by iron. Reduction of nitrite by a manganese center is exceedingly rare, with the sole example reported for a Mn-porphyrin system induced by photolysis of the Mn-nitrito precursor.[7]

Structural characterization of Mn(III)-oxo complexes is exceedingly rare. To the best of our knowledge, the only synthesized complex preceding the example reported here is derived from the urea functionalized tris(2-aminoethyl)amine ligand platform studied by Borovik.[17] The ability to access the terminal metal oxo species is attributed to the presence of three amine

moieties composing a hydrogen-bonding secondary coordination sphere to stabilize the terminal oxo ligand. Additionally, structural parameters of the starting material depict three amine moieties pointing away from the pocket of the complex, engaging in hydrogen-bonding interactions with the outer sphere triflate anion. Simple rotation about the C=C bond of the azafulvene moiety is not possible without tautomerization, suggesting dissociation of the arm of the ligand prior to appropriate positioning of the secondary coordination sphere. The amino groups of the ligand platform reposition themselves for the stabilization of the Mn(III)-oxo species.

2.3 Conclusion

Our ligand scaffold ($H_3[N(pi^{Cy})_3]$) that is capable of each arm tautomerizing independently, as reflected in the intraligand bond lengths of complex **Mn^{II}-OH**, may adequately mimic the electronic nuances of the amino acids found within the protein superstructure of metalloenzymes. Capable of participating in bond cleavage events, dioxygen activation and subsequent formation of the Mn^{III}–O species may be assisted by the hydrogen-bonding network found in the secondary coordination sphere of our ligand. Furthermore, the various synthetic protocols established to access the Mn^{III}–O complex (summarized in Figure 2.3) illustrate the propensity of this system to cleave E–O multiple bonds (where E = N, O and I).

2.4 Experimental section

General Considerations. All manipulations were carried out in the absence of water and dioxygen using standard Schlenk techniques, or in an MBraun inert atmosphere drybox under a dinitrogen atmosphere except where specified otherwise. All glassware was oven dried for a minimum of 8 h and cooled in an evacuated antechamber prior to use in the drybox. Solvents were dried and deoxygenated on a Glass Contour System (SG Water USA, Nashua, NH) and stored over 4 Å molecular sieves purchased from Strem following literature procedure prior to use. Acetontrile-d_3 was purchased from Cambridge Isotope Labs and stored over 4 Å molecular sieves prior to use. Manganese(II) chloride was purchased from Strem and used as received. Manganese bis(trifluoromethanesulfonate) was prepared according to literature procedures.[33] $H_3[N(pi^{Cy})_3]$ was prepared according to literature procedures.[22] Lithium oxide was purchased from Sigma-Aldrich and used as received. Lithium hexamethyldisilazane was purchased from

Sigma-Aldrich and recrystallized from toluene under an inert atmosphere prior to use. Celite® 545 (J. T. Baker) was dried in a Schlenk flask for 24 h under dynamic vacuum while heating to at least 150℃ prior to use in a drybox. ^{1}H NMR spectra were recorded on a Varian spectrometer operating at 500 MHz (^{1}H NMR). All chemical shifts were reported relative to the peak of the residual solvent as a standard. Solid-state infrared spectra were recorded using a Perkin-Elmer Frontier FT-IR spectrophotometer equipped with a KRS5 Thallium Bromide/Iodide Universal Attenuated Total Reflectance accessory. ESI-MS data was collected on a Thermo Scientific LTQ Orbitrap. The data was collected using sonic spray ionization (SSI) with a solvent pumping rate of 6 microliters/min and a nitrogen pressure of 200 psi. Elemental analysis was performed the University of Illinois at Urbana-Champaign School of Chemical Sciences Microanalysis Laboratory in Urbana, IL. EPR samples were prepared in an MBraun glovebox. The sample concentration is approximately 5mM in dichloromethane/toluene (1:1) mixture. EPR spectra were recorded on a Varian E-line 12" Century series X-band CW spectrometer and the spectra were simulated using the program SIMPOW6.

Preparation of K[(N(pi^{Cy})$_3$Mn(OH$_2$)]. $H_3[N(pi^{Cy})_3]$ (0.060 g, 0.103 mmol) was deprotonated by addition of 3.1 equivalent of KH (0.013 g, 0.32 mmol) to an approximately 10 mL of tetrahydrofuran solution. After it was stirred for two hours at room temperature, the mixture was filtered through Celite to remove excess KH. Addition of deprotonated ligand to the $MnCl_2$ (0.013 g, 0.0103 mmol) slurry in tetrahydrofuran resulted in a color change from colorless to yellow. After stirring overnight and all $MnCl_2$ was consumed, the reaction mixture was filtered through Celite to remove KCl. Following removal of the volatiles, the yellow oil was washed with diethyl ether. The product was isolated as a yellow powder in quantitative yields (0.068 g, 0.097 mmol, 95 %). Crystals of $K[(N(pi^{Cy})_3Mn(OH_2)]$ suitable for X-ray analysis were grown at room temperature via slow diffusion of hexanes into a concentrated solution of tetrahydrofuran. Analysis for $KMnC_{36}H_{50}N_7O{\cdot}OC_4H_8$: Calcd. C, 62.97; H, 7.66; N, 12.85. Found C, 63.46; H, 7.60; N, 12.47. IR = 1617 cm^{-1} (C=N). μ_{eff} = 6.15(15) μ_B.

Preparation of [N(afa^{Cy})$_3$Mn(OTf)](OTf). A 20 mL scintillation vial was charged with $Mn(OTf)_2(MeCN)_2$ (0.043 g, 0.100 mmol) and approximately 10 mL of tetrahydrofuran. With vigorous stirring, $H_3[N(pi^{Cy})_3]$ (0.060 g, 0.103 mmol) was added and resulted in an instantaneous

color change from colorless to yellow. The mixture was stirred for one hour, after which time solvents were removed under reduced pressure. The yellow oil was washed with diethyl ether three times. The product, $[N(afa^{Cy})_3Mn(OTf)](OTf)$, was isolated as a yellow powder in quantitative yields (0.087 g, 0.094mmol, 94%). Crystals of $[N(afa^{Cy})_3Mn(OTf)](OTf)$ suitable for X-ray analysis were grown at room temperature from a concentrated solution of tetrahydrofuran layered with pentane. Analysis for $MnC_{38}H_{51}N_7S_2F_6O_6 \cdot OC_4H_8$: Calcd. C, 50.47; H, 5.87; N, 9.91. Found C, 50.31; H, 5.82; N, 9.81. IR = 1641 cm^{-1} (C=N), 3230, 3290 cm^{-1} (N-H). μ_{eff} = 5.89(7) μ_B.

Preparation of $N(pi^{Cy})(afaCy)_2Mn(OH)$. A 20 mL scintillation vial was charged with $Mn(OTf)_2(MeCN)_2$ (0.043 g, 0.100 mmol) and approximately 10 mL of tetrahydrofuran. With vigorous stirring, $H_3[N(pi^{Cy})_3]$ (0.060 g, 0.103 mmol) was added and resulted in an instantaneous color change from colorless to yellow. After stirring for one hour, lithium oxide (0.003 g, 0.100 mmol) was added as a solid. The mixture was stirred for three hours, giving rise to formation of yellow precipitates. The solvents were removed under reduced pressure and the resulting yellow residue was washed with diethyl ether/ tetrahydrofuran mixture to remove lithium triflate. The product, $N(pi^{Cy})(afaCy)_2Mn(OH)$, was isolated as a yellow powder in quantitative yields (0.075 g, 0.093 mmol, 93%). Crystals of $N(pi^{Cy})(afaCy)_2Mn(OH)$ suitable for X-ray analysis were grown at room temperature from a dilute solution of tetrahydrofuran. Analysis for $MnC_{36}H_{51}N_7O$: Calcd C, 66.24; H, 7.87; N, 15.02. Found C, 65.95; H, 7.51; N, 14.91. IR = 1645 cm^{-1} (C=N). 3226 cm^{-1} (NH). μ_{eff} = 5.87(28) μ_B.

Alternetive Synthesis of $N(pi^{Cy})(afaCy)_2Mn(OH)$. $H_3[N(pi^{Cy})_3]$ (0.060 g, 0.103 mmol) was deprotonated by addition of 2.1 equivalents of $LiN(SiMe_3)_2$ (0.036 g, 0.216 mmol) to an approximately 10 mL of tetrahydrofuran solution. After was stirring for one hour at room temperature, the deprotonated ligand was added dropwise to another 20 mL scintillation vial, charged with $MnCl_2$ (0.012 g, 0.100 mmol), 2 drops of pyridine (to aid in solubility), and approximately 2 mL of tetrahydrofuran with vigorous stirring. After this solution was stirred for 3 h at room temperature and the solvents were removed under reduced pressure. The product was isolated as yellow powder with LiCl as a contaminant.

Preparation of [N(afa^{Cy})$_3$MnO](OTf) from O_2. A 20 mL scintillation vial was charged with [N(afa^{Cy})$_3$Mn(OTf)](OTf) (0.100 g, 0.108 mmol) approximately 10 mL of acetonitrile. The vial was sealed with a 14/20 septum and tape and removed from the glovebox. A standard party balloon attached to a syringe was filled with O_2 and injected through the septum with a needle. The atmosphere was purged with O_2, resulting in an instantaneous color change to green. The mixture was stirred overnight to ensure completion. Volatiles were removed under reduced pressure and the product, [N(afa^{Cy})$_3$MnO](OTf) (0.065 g, 0.081 mmol, 75 %) was isolated via recrystallization in good yields via slow diffusion of diethyl ether through a concentrated acetonitrile solution at room temperature.

Independent Preparation of [N(afa^{Cy})$_3$MnO](OTf). A 20 mL scintillation vial was charged with [N(afa^{Cy})$_3$MnO](OTf) (0.050 g, 0.054 mmol) approximately in 10 mL of acetonitrile. The mixture was cooled to -35 °C. An equivalent of iodosylbenzene (0.012 g, 0.054 mmol) was weighed and added as a solid to the pale-yellow solution. A gradual color change to green was noted over the course of two hours. Volatiles were removed under reduced pressure, leaving a brown-green residue. The oil was washed with tetrahydrofuran and filtered over Celite until the filtrate ran clear. The product was subsequently washed through the frit with acetonitrile. After removing solvents *in vaccuo*, the product, [N(afa^{Cy})$_3$MnO](OTf), was isolated as a green, crystalline powder in modest yields (0.018 g, 0.022 mmol, 41 %). Crystals suitable for X-ray analysis were grown from the slow evaporation of a concentrated acetonitrile solution of [N(afa^{Cy})$_3$MnO](OTf) via slow diffusion of diethyl ether. Analysis for $C_{37}H_{51}N_7MnO_4F_3S$: Calcd. C, 55.42; H, 6.41; 12.23. Found C, 55.28; H, 6.37; N, 12.08. ^{1}H NMR (CD_3CN, 21 °C): δ = 13.06 (539, 3H, C*H*), 6.78 (447, 3H, C*H*), 4.17 (348, 3H, C*H*), 1.47 – 0.75 (33H, Cy-C*H*), 0.06 (274, 6H, C*H*), -16.39 (491, 3H, C*H*). IR = 1659 cm^{-1} (C=N). ESI-MS m/z = 652.3525 for [N(afa^{Cy})$_3$MnO](OTf). ESI-MS m/z = 654.3549 for [N(afa^{Cy})$_3$MnO^{18}](OTf).

Preparation of [N(afa^{Cy})$_3$MnO](OTf) via Reduction of Nitrite. A 20 mL scintillation vial was charged with [N(afa^{Cy})$_3$MnO](OTf) (0.050 g, 0.054 mmol) and approximately 5 mL of acetonitrile. An equivalent of [^{n}Bu$_4$N][NO_2] (0.016 g, 0.056 mmol) was weighed by difference and added as a solid to the pale-yellow solution. Over the course of 24 hours at 40 °C, a gradual color change to red was noted. Volatiles were removed under reduced pressure, leaving a green

solid. Following trituation with a diethylether and tetrahydrofuran mixture (1:1) to remove the byproduct, [^{n}Bu$_4$N][OTf], the product [N(afa^{Cy})$_3$MnO](OTf) was recrystallized from a concentrated acetonitrile solution via slow diffusion of diethyl ether. After removing residual solvents *in vaccuo*, the product, [N(afa^{Cy})$_3$MnO](OTf), was isolated as a green, crystalline powder in modest yields (0.027 g, 0.033 mmol, 61 %). Formation of the desired product was confirmed by ^{1}H NMR spectroscopy and X-ray diffraction.

2.5 References

(1) Umena, Y.; Kawakami, K.; Shen, J.-R.; Kamiya, N. Crystal Structure of Oxygen-Evolving Photosystem II at a Resolution of 1.9 Å. *Nature* **2011**, *473*, 55–60.

(2) Meyer, T. J.; Huynh, M. H. V.; Thorp, H. H. The Possible Role of Proton-Coupled Electron Transfer (PCET) in Water Oxidation by Photosystem II. *Angew. Chem. Int. Ed.* **2007**, *46*, 5284–5304.

(3) Nick, R. J.; Ray, G. B.; Fish, K. M.; Spiro, T. G.; Groves, J. T. Evidence for a Weak Mn:O Bond and a Non-Porphyrin Radical in Manganese-Substituted Horseradish Peroxidase Compound I. *J. Am. Chem. Soc.* **1991**, *113*, 1838–1840.

(4) Pecoraro, V. L.; Baldwin, M. J.; Gelasco, A. Interaction of Manganese with Dioxygen and Its Reduced Derivatives. *Chem. Rev.* **1994**, *94*, 807–826.

(5) Dismukes, G. C. Manganese Enzymes with Binuclear Active Sites. *Chem. Rev.* **1996**, *96*, 2909–2926.

(6) Nealson, K. H. The Manganese-Oxidizing Bacteria. In *The Prokaryotes*; Dworkin, M.; Falkow, S.; Rosenberg, E.; Schleifer, K.-H.; Stackebrandt, E., Eds.; Springer New York: New York, NY, 2006; pp. 222–231.

(7) Zouni, A.; Witt, H. T.; Kern, J.; Fromme, P.; Krauss, N.; Saenger, W.; Orth, P. Crystal Structure of Photosystem II from Synechococcus Elongatus at 3.8 A Resolution. *Nature* **2001**, *409*, 739–743.

(8) Yano, J.; Kern, J.; Sauer, K.; Latimer, M. J.; Pushkar, Y.; Biesiadka, J.; Loll, B.; Saenger, W.; Messinger, J.; Zouni, A.; *et al.* Where Water Is Oxidized to Dioxygen: Structure of the Photosynthetic Mn4Ca Cluster. *Science* **2006**, *314*, 821–825.

(9) Loll, B.; Kern, J.; Saenger, W.; Zouni, A.; Biesiadka, J. Towards Complete Cofactor Arrangement in the 3.0 Å Resolution Structure of Photosystem II. *Nature* **2005**, *438*, 1040–1044.

(10) McEvoy, J. P.; Brudvig, G. W. Water-Splitting Chemistry of Photosystem II. *Chem. Rev.* **2006**, *106*, 4455–4483.

(11) Shirin, Z.; S. Borovik, A.; G. Young Jr., V. Synthesis and Structure of a MnIII(OH) Complex Generated from Dioxygen. *Chem. Commun.* **1997**, 1967.

(12) Goldsmith, C. R.; Cole, A. P.; Stack, T. D. P. C−H Activation by a Mononuclear Manganese(III) Hydroxide Complex: Synthesis and Characterization of a Manganese-Lipoxygenase Mimic? *J. Am. Chem. Soc.* **2005**, *127*, 9904–9912.

(13) Parsell, T. H.; Yang, M.-Y.; Borovik, A. S. C−H Bond Cleavage with Reductants: Re-Investigating the Reactivity of Monomeric Mn $^{III/IV}$ −Oxo Complexes and the Role of Oxo Ligand Basicity. *J. Am. Chem. Soc.* **2009**, *131*, 2762–2763.

(14) Wijeratne, G. B.; Corzine, B.; Day, V. W.; Jackson, T. A. Saturation Kinetics in Phenolic O–H Bond Oxidation by a Mononuclear Mn(III)–OH Complex Derived from Dioxygen. *Inorg. Chem.* **2014**, *53*, 7622–7634.

(15) Hong, S.; Lee, Y.-M.; Sankaralingam, M.; Vardhaman, A. K.; Park, Y. J.; Cho, K.-B.; Ogura, T.; Sarangi, R.; Fukuzumi, S.; Nam, W. A Manganese(V)–Oxo Complex: Synthesis by Dioxygen Activation and Enhancement of Its Oxidizing Power by Binding Scandium Ion. *J. Am. Chem. Soc.* **2016**, *138*, 8523–8532.

(16) Borovik, A. S. Role of Metal–oxo Complexes in the Cleavage of C–H Bonds. *Chem. Soc. Rev.* **2011**, *40*, 1870.

(17) Shirin, Z.; Hammes, B. S.; Young, V. G.; Borovik, A. S. Hydrogen Bonding in Metal Oxo Complexes: Synthesis and Structure of a Monomeric Manganese(III)−Oxo Complex and Its Hydroxo Analogue. *J. Am. Chem. Soc.* **2000**, *122*, 1836–1837.

(18) MacBeth, C. E.; Gupta, R.; Mitchell-Koch, K. R.; Young, V. G.; Lushington, G. H.; Thompson, W. H.; Hendrich, M. P.; Borovik, A. S. Utilization of Hydrogen Bonds To Stabilize M−O(H) Units: Synthesis and Properties of Monomeric Iron and Manganese Complexes with Terminal Oxo and Hydroxo Ligands. *J. Am. Chem. Soc.* **2004**, *126*, 2556–2567.

(19) Gupta, R.; MacBeth, C. E.; Young, V. G.; Borovik, A. S. Isolation of Monomeric Mn $^{III/II}$ −OH and Mn ^{III} −O Complexes from Water: Evaluation of O−H Bond Dissociation Energies. *J. Am. Chem. Soc.* **2002**, *124*, 1136–1137.

(20) Wieghardt, K. The Active Sites in Manganese-Containing Metalloproteins and Inorganic Model Complexes. *Angew. Chem. Int. Ed. Engl.* **1989**, *28*, 1153–1172.

(21) Kitajima, N.; Singh, U. P.; Amagai, H.; Osawa, M.; Morooka, Y. Oxidative Conversion of a $Mn(\mu\text{-}OH)_2Mn$ to a $Mn(\mu\text{-}O)_2Mn$ Moiety. Synthesis and Molecular Structures of a (μ-Hydroxo)dimanganese (II,II) and (μ -oxo)dimanganese(III,III) Complex with a Hindered N3 Ligand. *J. Am. Chem. Soc.* **1991**, *113*, 7757–7758.

(22) Matson, E. M.; Bertke, J. A.; Fout, A. R. Isolation of Iron(II) Aqua and Hydroxyl Complexes Featuring a Tripodal H-Bond Donor and Acceptor Ligand. *Inorg. Chem.* **2014**, *53*, 4450–4458.

(23) Zhao, P.-Z.; Yan, F.-M.; Wang, J.-G. Aqua(2,9-Dimethyl-1,10-Phenanthroline-κ^2*N*, *N*′)bis(2-Hydroxybenzoato-κ*O*)-manganese(II)2,9-Dimethyl-1,10-Phenanthroline Hemisolvate. *Acta Crystallogr. Sect. E Struct. Rep. Online* **2009**, *65*, m194–m195.

(24) Williamson, M. M.; Hill, C. L. Isolation and Characterization of a Five-Coordinate manganese(III) Porphyrin Cation. Crystal and Molecular Structure of aquo(tetraphenylporphinato)manganese(III) Triflate. *Inorg. Chem.* **1986**, *25*, 4668–4671.

(25) Rich, J.; Rodríguez, M.; Romero, I.; Vaquer, L.; Sala, X.; Llobet, A.; Corbella, M.; Collomb, M.-N.; Fontrodona, X. Mn(ii) Complexes Containing the Polypyridylic Chiral Ligand (−)-pinene[5,6]bipyridine. Catalysts for Oxidation Reactions. *Dalton Trans.* **2009**, 8117.

(26) Ferrari, M. B.; Fava, G. G.; Pelizzi, C.; Tarasconi, P.; Tosi, G. Thiosemicarbazones as Co-Ordinating Agents. Part 2. Synthesis, Spectroscopic Characterization, and X-Ray Structure of Aquachloro(pyridoxal thiosemicarbazone)manganese(II) Chloride and Aqua(pyridoxal Thiosemicarbazonato)-copper(II) Chloride Monohydrate. *J. Chem. Soc. Dalton Trans.* **1987**, 227.

(27) Alexandru, M.-G.; Velickovic, T.; Jitaru, I.; Grguric-Sipka, S.; Draghici, C. Synthesis, Characterization and Antitumor Activity of Cu(II), Co(II), Zn(II) and Mn(II) Complex Compounds with Aminothiazole Acetate Derivative. *Open Chem.* **2010**, *8*, 649–645.

(28) Jeffrey, G. A. *An Introduction to Hydrogen Bonding*; Topics in physical chemistry; Oxford University Press: New York, 1997.

(29) Company, A.; Prat, I.; Frisch, J. R.; Mas-Ballesté, D. R.; Güell, M.; Juhász, G.; Ribas, X.; Münck, D. E.; Luis, J. M.; Que, L.; *et al.* Modeling the Cis-Oxo-Labile Binding Site Motif of Non-Heme Iron Oxygenases: Water Exchange and Oxidation Reactivity of a Non-Heme Iron(IV)-Oxo Compound Bearing a Tripodal Tetradentate Ligand. *Chem. - Eur. J.* **2011**, *17*, 1622–1634.

(30) Matson, E. M.; Park, Y. J.; Fout, A. R. Facile Nitrite Reduction in a Non-Heme Iron System: Formation of an Iron(III)-Oxo. *J. Am. Chem. Soc.* **2014**, *136*, 17398–17401.

(31) Coggins, M. K.; Brines, L. M.; Kovacs, J. A. Synthesis and Structural Characterization of a Series of Mn ^{III} OR Complexes, Including a Water-Soluble Mn ^{III} OH That Promotes Aerobic Hydrogen-Atom Transfer. *Inorg. Chem.* **2013**, *52*, 12383–12393.

(32) Parsell, T. H.; Behan, R. K.; Green, M. T.; Hendrich, M. P.; Borovik, A. S. Preparation and Properties of a Monomeric Mn ^{IV} −Oxo Complex. *J. Am. Chem. Soc.* **2006**, *128*, 8728–8729.

(33) Riedel, P. J.; Arulsamy, N.; Mehn, M. P. Facile Routes to manganese(II) Triflate Complexes. *Inorg. Chem. Commun.* **2011**, *14*, 734–737.

Chapter 3

Manganese complexes and their X_3^- derivatives interacting with secondary coordination sphere†

3.1 Introduction

One of the important small molecules in biology is O_2 which reacts with metalloenzymes to perform various catalytic reactions including water oxidation by the oxygen evolving complex (OEC),[1,2] oxygenase reactions by cytochrome P450,[3,4] oxygen reduction to water by cytochrome *c* oxidase,[5,6] etc. Exposure of these metalloenzymes to molecular oxygen results in the formation of reactive high-valent metal species such as metal-oxo, hydroxyl, superoxo or peroxo complexes, which can be stabilized by hydrogen bonding interactions from the secondary coordination sphere.[1-6] However, due to the rapid reactivity of oxygen with metalloenzymes, understanding mechanisms and identifying reaction intermediates are not straightforward. To gain insights into O_2 reactivity and its interaction with secondary coordination sphere, pseudohalide ligands such as azide (N_3^-), thiocyanate (NCS^-) or isocyanate (NCO^-) can be utilized as surrogates for molecular oxygen or superoxide (O_2^-). Azide can bind to the active site of the metalloenzymes similar to oxygen or superoxide, but subsequent reactivity is limited.[7–9] In cytochrome *c* oxidase, for example, it has been shown that the azide competitively binds to copper over oxygen, resulting in the chemical asphyxiation of cells.[10] Moreover, multiple hydrogen bonding sites of such ligands will allow for studying non-covalent interaction between bound substrates and the secondary coordination sphere, as shown in Brayer's work with myoglobin where histidine side chain can stabilize the azide bound to the iron center.[8]

As discussed in Chapter 2, a Mn(II) complex can react with O_2 and nitrite, resulting in the formation of a Mn(III)-oxo complex. Since it readily reacts with those small molecules, identifying reaction intermediates is challenging. In order to gain further insights into the hydrogen bonding ability of our metal complexes with such small molecules, we shifted our interest to expand the generation of pseudohalide derivatives of Mn complexes.

† Portions of this chapter are reproduced from the following publication with permission from the authors. Matson, E.M.; Park, Y.J.; Fout, A.R. *Dalton Trans.* ***2015****, 44, 10377-10384.*

Herein, the synthesis and characterization of a family of azafulvene Mn complexes with X_3^- ligands, [N(afa^{Cy})$_3$MnX](OTf) (X = N_3, OCN and SCN) will be explored to understand how the binding of anionic and axial substrates influence the coordination of the ligand and non-covalent interactions of the secondary coordination sphere. The surprising ability of the ligand to span multiple hydrogen bonding motifs presented herein demonstrates a novel, biomimetic scaffold capable of conformational changes to optimally stabilize M–X interactions.

3.2 Results and discussion

With the [N(afa^{Cy})$_3$Mn(OTf)](OTf) complex in hand, installation of a variety of anions possessing lone pairs of electrons capable of engaging in hydrogen bonding with the secondary coordination sphere was attempted. The purpose of the synthesis of these variants was to develop an increased understanding of the interaction of substrates with the secondary coordination sphere to elucidate how the substrate can influence the coordination mode of the ligand scaffold. The pseudohalides thiocyanate (NCS^-), isocyanate (NCO^-), and azide (N_3^-) were selected due to their commercial availability and propensity to serve as model substrates for biological intermediates. Binding of the linear functionality anionically to the metal center has been shown to serve as a mimic for hydroxyl, peroxide, or nitrite intermediates, with lone pairs of electrons available for hydrogen bonding with the amino moieties of the ligand. Furthermore, these anions possess characteristic infrared stretching frequencies that provide electronic information on the interaction between metal center and substrate.

In an effort to synthesize the desired [N(afa^{Cy})$_3$MnX]$^+$ species (X = NCS^-, NCO^-, N_3^-), salt metathesis with the corresponding [NBu_4]X salt was employed for functionalization of the complex [N(afa^{Cy})$_3$Mn(OTf)](OTf) (Scheme 3.1). Initial experiments focused on the synthesis and characterization of the thiocyanate derivative in order to understand the ligand's ability to hydrogen bond with an anionic substrate without the complexity of variable coordination modes due to the ambidentate nature of the anion. Addition of an equivalent of [NBu_4][NCS] to a THF slurry of the manganese azafulvene precursor resulted in yellow precipitate from the solution, suspended as a fine powder. Following work-up, the product, [N(afa^{Cy})$_3$Mn(NCS)](OTf) (**Mn-NCS**) was isolated as a powder in quantitative yield. For the isolation of analytically pure samples, recrystallization was accomplished by slow diffusion of diethyl ether into a concentrated solution of DMA and acetonitrile (1:10). The magnetic moment of **Mn-NCS** is

consistent with a high-spin Mn(II) complex (μ_{eff} = 5.96(12) μ_B). The complex was also characterized by infrared spectroscopy to confirm the installation of the new thiocyanate functional group. The shifted, asymmetric stretch of the NCS^- at 2016 cm^{-1} was noted by comparison to the values reported for the starting material [$^nBu_4N$][NCS] (2060 cm^{-1}) (Table 3.1).

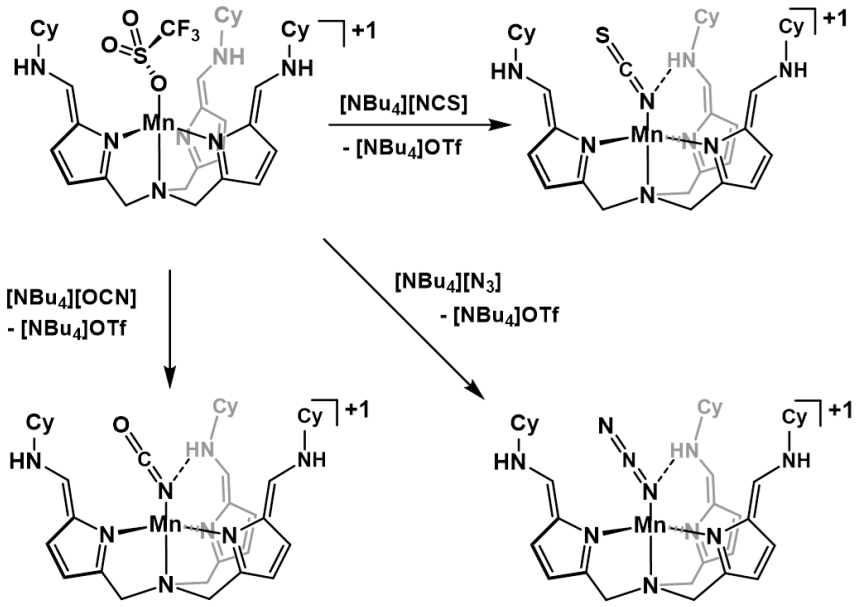

Scheme 3.1 Synthesis of $[N(afa^{Cy})_3MnX]^+$ complexes (X = NCS^-, NCO^-, N_3^-).

To gain insight into the structural parameters of the thiocycanate complexes, crystallographic characterization was performed (Figure 3.1, Table 3.1). Crystals suitable for X-ray analysis were grown from a concentrated solution of DMA and acetonitrile in a 1:10 ratio, layered with diethyl ether. Upon refinement of the data, a pseudo trigonal bipyramidal geometry was noted. Mn1-NX (X = 1-4) distances are consistent with that of $[N(afa^{Cy})_3Mn(OTf)](OTf)$ starting material presented in the previous chapter, indicating analogous primary coordination interactions of the ancillary ligand platform with manganese. Intraligand bond distances are of the appropriate values to confirm presence of the tautomeric azafulvene-amine form of the ligand backbone.

A new feature of the system was observed following installation of the thiocyanate anion, resulting from the rotation of a single arm of the ligand platform inward, giving rise to a hydrogen bonding interaction between an amino moiety of the secondary coordination sphere and the nitrogen atom of the pseudohalide. The position of the hydrogen atom engaging in

hydrogen bonding with the axial ligand could be reliably determined and independently refined in the electron density map. The N10-H5 distance of 2.12 Å and the N5–N10 distance of 2.992(3) Å are well within the range of distances established as hydrogen-bonding interactions.[11] Further support of the presence of a hydrogen bonding interaction is the nearly linear N5–H5–N10 bond angle of 168.8°.

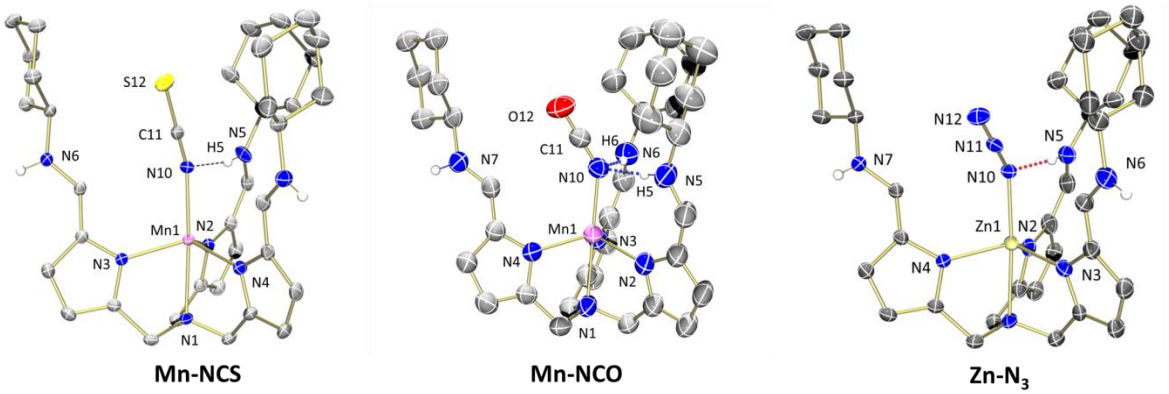

Figure 3.1 Crystal structures of **Mn-NCS**, **Mn-NCO** and **Zn-N_3** shown with 50% probability ellipsoids. Select hydrogen atoms, counter ions, and solvent molecules have been removed for clarity.

Table 3.1 Selected structural parameters of complexes, **Mn-NCS**, **Mn-NCO**, **Mn-N_3** and **Zn-N_3.**

Bond	Mn-NCS	Mn-NCO	Mn-N_3	Zn-N_3
M1-N1	2.3337(16)	2.3398(17)	—	2.267(2)
M1-N(pyr)	2.1427(18) – 2.1491(16)	2.1201(17) – 2.1480(18)	—	2.059(3) – 2.069(2)
M1-NX0	2.1322(17)	2.1450(16)	—	2.081(7)
N10-H5	2.126(2)	2.06[a]	—	2.16(4)
N10···N5	2.993(2)	2.93(2)	—	2.921(14)
N10-H5-N5	168(1)°	175.7[a]	—	174(4)
N-H stretch	3218, 3280 cm^{-1}	3202, 3288 cm^{-1}	3221cm^{-1}	3226, 3294 cm^{-1}
C=N stretch	1646 cm^{-1}	1640 cm^{-1}	1655 cm^{-1}	1651 cm^{-1}
IR stretch, X	2016 cm^{-1}	2178 cm^{-1}	2066 cm^{-1}	2067 cm^{-1}
μ_{eff}	5.96(12) μ_B	5.90(11) μ_B	5.88(4) μ_B	—

The observation of the formation of a new hydrogen bonding interaction between the amino moiety and the substrate supports the hypothesis of the flexible nature of the ligand

platform. The participation of the ligand framework in hydrogen bonding with the newly installed thiocyanate moiety is remarkable, as free rotation around the C=C bond of the azafulvene-amine tautomer is prohibited.

Interested in investigating the electronic and structural properties of isocyanate derivatives of the metal azafulvene complexes, synthesis was accomplished by addition of an equivalent of $[NBu_4][NCO]$ to $[N(afa^{Cy})_3Mn(OTf)](OTf)$. The primary motivation for the exploration of the oxygen-containing pseudohalide was to generate a complex resembling the structural properties of a peroxide moiety, with a M–O single bond stabilized through H-bonding interactions. Following salt metathesis, installation of the psuedohalide was confirmed by infrared spectroscopy; $[N(afa^{Cy})_3Mn(NCO)]^+$ (**Mn-NCO**) bears sharp bands assigned to a bound isocyanate moiety at 2178 cm^{-1}, shifted from that of the starting material, $[NBu_4][NCO]$ (2160 cm^{-1}).

Crystallographic characterization of **Mn-NCO** was possible by diffraction of single crystals grown from a concentrated solution of acetonitrile and DMA (10:1) layered with diethyl ether (Figure 3.1). A single component was identified in the asymmetric unit, consisting of two disordered species. In the minor component (25%), a single arm of the tripodal framework has been rotated inwards, engaging in hydrogen bonding with the nitrogen located closest to the metal center in the axial isocyanate substituent (Figure 3.1). However, compared to the **Mn-NCS** having only single arm hydrogen bonding to the substrate, the major component has two arms of the ligand platform engaging in hydrogen bonding with the substrate presumably due to the smaller size of the isocyanate.

Structural refinement of **Mn-NCO** revealed a distorted trigonal bipyramidal geometry about the metal center, similar to that of the thiocyanate complex. The isocyanate moiety has replaced the triflate as anticipated, driving N–H bonds to rotate inward and stabilizing the substrate via a new hydrogen bonding interaction. The disorder of one of ligand arms gives rise to a metal-isocyanate complex where two ligand arms are now participating in hydrogen bonding. To accommodate this increase in ligand-anion H-bonding, the isocyanate moiety is positioned at a slightly more acute angle (Mn1–N10–C11 = 142.5(16)°) in comparison to the minor component of the crystal structure (Mn1–N10B–C11B = 152(4)°). The ability of the ligand to participate in this remarkable structural transformation highlights the ability of this tripodal

platform to adequately mimic amino acid binding sites present in metalloenzymes by adjusting the number of hydrogen bonding interactions to best suit the stabilization needs of the complex.

Intrigued by the participation of the secondary coordination sphere in stabilization of the thiocyanate and isocyanate moieties, synthesis of the structurally analogous **Mn-N_3** complex was subsequently explored. An azide moiety has been shown to spectroscopically mimic metal peroxide species and have been utilized to investigate the electronic properties of proposed intermediates in enzymatic pathways. In recent EPR spectroscopic studies, Rivera and coworkers observed the presence of an iron(III)peroxo, while the electronically similar species were studied utilizing azide and cyanide ligands as models for the reactive peroxo substrate.[12–14] Additionally, metal azide complexes are well-established precursors for metal nitrides. As our research group is primarily interested in the utilization of secondary coordination spheres for the stabilization of intermediates along biologically relevant mechanistic pathways including water oxidation, oxygen reduction, nitrite or nitrogen reduction, the synthesis of a manganese azide complex was explored.

The synthesis and purification of the azide derivative, **Mn-N_3**, were accomplished in a similar fashion to that discussed for the synthesis of **Mn-NCS** and **Mn-NCO**. Following work-up, the product, $[N(afa^{Cy})_3Mn(N_3)](OTf)$, was isolated as a powder in a quantitative yield. Magnetic properties of the products revealed similar electronic states to that of the respective starting materials (μ_{eff} = 5.88(4) μ_B). The effective magnetic moment of the complex also resembles those obtained for the corresponding thiocyanate and isocyanate derivatives.

To confirm the installation of the azide moiety, infrared spectroscopy was employed to determine the stretching frequency of the coordinated [N_3^-]. A strong band was located at 2067 cm^{-1}, shifted from that of the azide starting material, $[NBu_4][N_3]$ (2022 cm^{-1}). The C=N stretches observed in the infrared spectra of **Mn-N_3** at 1640 cm^{-1} is similar to that of the tripodal starting material (1636 cm^{-1}), and is consistent with the dative azafulvene-amine binding mode of the tripodal ligand.

However, since crystallographic characterization of **Mn-N_3** was not performed due to its needle like shape, $[N(afa^{Cy})_3Zn(N_3)](OTf)$ (**Zn-N_3**) complex which is isomorphous to **Mn-N_3** was synthesized and characterized instead. Analysis of **Zn-N_3** by ^{1}H NMR spectroscopy revealed diamagnetic resonances which are in a similar range with the previously reported

[N(afa^{Cy})$_3$Zn(OTf)](OTf), but revealing an asymmetric distribution of resonances suggesting that arm rotations varied within the product (Figure 3.2).

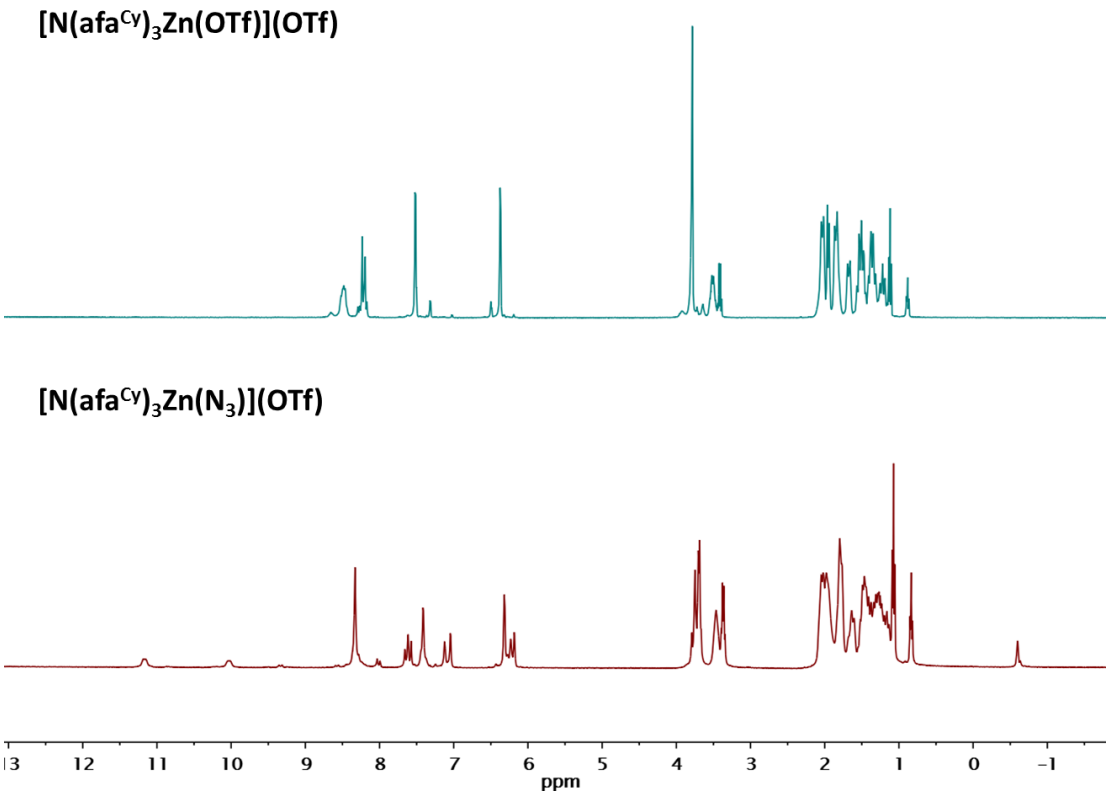

Figure 3.2 ^{1}H NMR spectrum of [N(afa^{Cy})$_3$Zn(OTf)](OTf) and [N(afa^{Cy})$_3$Zn(N$_3$)](OTf) (20°C, MeCN-d_3).

Crystallographic analysis of **Zn-N$_3$** revealed a similar molecular configuration as **Mn-NCS**, having a single arm hydrogen bonding to the bound azide (Figure 3.1). Again, the N10-H5 bond distance of 2.16(4) Å and the N5–N10 bond distance of 2.921(14) Å are well within the range of established hydrogen-bonding interactions.[11] Further supporting the presence of a hydrogen bonding interaction is the nearly linear N5–H5–N10 bond angle of 174(4)°.

The synthesis of metal azide complexes by salt metathesis is a common strategy to access precursors to metal nitride species. In recent work, Smith and coworkers have presented the synthesis and characterization of the terminal Fe(IV) nitride species, generated by photolysis of a Fe(II) azide complex, PhB(^{t}Bulm)$_3$FeN$_3$.[15,16] Likewise, Meyer and coworkers have recently reported a Co(II) azide complex that releases an equivalent of N_2 to form a transient Co(IV)

nitride upon exposure to UV light.[17] Despite extensive attempts to access the desired complexes "[N(afa^{Cy})$_3$MN]" via thermolysis, photolysis and chemical reduction, isolation of the terminal nitride remains elusive.

3.3 Conclusions

Our previous report in *Dalton Transactions* summarized the syntheses and characterizations of a series of late first-row transition metal complexes (Mn, Fe and Co) with pseudohalide ligands (N_3^-, NCO^-, and NCS^-).[18] In all cases, we were able to observe substrates binding over a triflate anion and various hydrogen bonding interactions within the secondary coordination sphere depending on the bound substrates. Compared to the starting compounds, [N(afa^{Cy})$_3$M(OTf)](OTf), having all arms rotated outwards, addition of hydrogen bonds to the substrates in [N(afa^{Cy})$_3$MX](OTf) is not simple, as free rotation around the C=C bond of the azafulvene-amine tautomer is prohibited. Tautomerization of the ligand scaffold allows for this fluxional behavior of the ligand platform, resulting in variable hydrogen bonding motifs.

3.4 Experimental section

General Considerations. All manipulations were carried out in the absence of water and dioxygen using standard Schlenk techniques, or in an MBraun inert atmosphere drybox under a dinitrogen atmosphere except where specified otherwise. All glassware was oven dried for a minimum of 8 h and cooled in an evacuated antechamber prior to use in the drybox. Solvents were dried and deoxygenated on a Glass Contour System (SG Water USA, Nashua, NH) and stored over 4 Å molecular sieves purchased from Strem following literature procedure prior to use. $H_3N(pi^{Cy})_3$,[19] [N(afa^{Cy})Mn(OTf)](OTf)[20] and [N(afa^{Cy})Zn(OTf)](OTf)[21] were prepared according to literature procedures. [^{n}Bu$_4$N][X] (X = NCS, NCO, N_3) were purchased from Sigma Aldrich and used as received.

Infrared spectra were recorded using a Perkin-Elmer Frontier FT-IR spectrophotometer equipped with a KRS5 Thallium Bromide/Iodide Universal Attenuated Total Reflectance accessory. Elemental analysis was performed by Complete Analysis Laboratories, Inc. in Parsippany, NJ and the University of Illinois at Urbana-Champaign School of Chemical Sciences Microanalysis Laboratory in Urbana, IL. All crystal structures were collected on a Bruker APEX II Duo three-circle goniometer equipped with an Oxford cryostream cooling device.

Procedure for synthesis of [N(afa^{Cy})$_3$M(NCS)](OTf). A 20 mL scintillation vial was charged with [N(afa^{Cy})$_3$Mn(OTf)](OTf) (0.093 g, 0.100 mmol) and approximately 10 mL of tetrahydrofuran. With vigorous stirring, [^{n}Bu$_4$N][NCS] (0.030 g, 0.102 mmol) was weighed and added as a white solid. The mixture was stirred for one hour, after which time solvents were removed under reduced pressure. The resulting yellow powder was washed three times with diethylether to remove the byproduct, tetrabutylammonium triflate. The product was isolated as a yellow powder in quantitative yields (0.079 g, 0.094 mmol, 94%). Yellow crystals suitable for X-ray analysis were grown from acetonitrile-DMA mixture(10:1) layered with diethyl ether. Analysis for $MnC_{37}H_{51}N_8O{\cdot}SO_3CF_3$: Calcd. C, 55.13; H, 6.21; N, 13.54. Analysis for $MnC_{37}H_{51}N_8S{\cdot}SO_3CF_3$: Calcd. C, 54.08; H, 6.09; N, 13.28. Found C, 53.75; H, 6.21; N, 12.80. μ_{eff} = 5.96(12) μ_B. IR: 1646 cm^{-1} (C=N), 2016 cm^{-1} (NCS), 3218, 3280 cm^{-1} (NH).

Procedure for the synthesis of [N(afa^{Cy})$_3$Mn(NCO)](OTf). A 20 mL scintillation vial was charged with [N(afa^{Cy})$_3$Mn(OTf)](OTf) (0.093g, 0.100mmol) and approximately 10 mL of tetrahydrofuran. With vigorous stirring, [^{n}Bu$_4$N][OCN] (0.029 g, 0.102 mmol) was weighed and added as a white solid. The mixture was stirred for one hour, after which time solvents were removed under reduced pressure. The resulting yellow powder was washed three times with diethylether to remove the byproduct, tetrabutylammonium triflate. The product, **7**, was isolated as a yellow powder in quantitative yields (0.079 g, 0.096 mmol, 96%). Yellow crystals suitable for X-ray analysis were grown from acetonitrile-DMA mixture (10:1) layered with diethyl ether. Analysis for $MnC_{37}H_{51}N_8O{\cdot}SO_3CF_3$: Calcd. C, 55.13; H, 6.21; N, 13.54. Found C, 55.37; H, 6.34; N, 13.05.. μ_{eff} = 5.90(11) μ_B. IR: 1640 cm^{-1} (C=N), 2178 cm^{-1} (NCO), 3202 cm^{-1} (NH).

Procedure for synthesis of [N(afa^{Cy})$_3$Mn(N$_3$)](OTf). A 20 mL scintillation vial was charged with [N(afa^{Cy})$_3$Mn(OTf)](OTf) (0.093g, 0.100 mmol) and approximately 10 mL of tetrahydrofuran. With vigorous stirring, [^{n}Bu$_4$N][N$_3$] (0.029 g, 0.102 mmol) was weighed by difference and added as a white solid. The mixture was stirred for one hour, after which time solvents were removed under reduced pressure. The resulting pale yellow powder was washed three times with a 1:1 diethylether and THF mixture to remove the byproduct, tetrabutylammonium triflate. The remaining powder was dried under reduced pressure to yield the product in high yields (0.077 g, 0.094 mmol, 94%). Analysis for [$MnC_{36}H_{51}N_{10}{\cdot}SO_3CF_3$]

·C_4H_8O: Calcd. C, 54.72; H, 6.61; N, 15.56. Found C, 54.40; H, 6.50; N, 15.59. μ_{eff} = 5.88(4) μ_B. IR: 1655 cm^{-1} (C=N), 2067 cm^{-1} (N_3), 3216 cm^{-1} (NH).

Procedure for synthesis of [N(afa^{Cy})$_3$Zn(N$_3$)](OTf). A 20 mL scintillation vial was charged with [(afa^{NCy})$_3$Zn(OTf)](OTf) (0.094g, 0.100 mmol) and approximately 10 mL of tetrahydrofuran. With vigorous stirring, [^{n}Bu$_4$N][N$_3$] (0.029 g, 0.102 mmol) was weighed by difference and added as a white solid. The mixture was stirred for one hour, after which time solvents were removed under reduced pressure. The resulting white powder was washed three times with a 1:1 diethylether and THF mixture to remove the byproduct, tetrabutylammonium triflate. The remaining powder was dried under reduced pressure to yield the product. Analysis for $ZnC_{36}H_{51}N_{10}·SO_3CF_3$: Calcd. C, 53.01; H, 6.13; N, 16.71. Found C, 52.89; H, 6.22; N, 16.49. IR: 1651 cm^{-1} (C=N), 2067 cm^{-1} (N_3), 3226 and 3294 cm^{-1} (NH).

3.5 References

(1) Umena, Y.; Kawakami, K.; Shen, J.-R.; Kamiya, N. Crystal Structure of Oxygen-Evolving Photosystem II at a Resolution of 1.9 Å. *Nature* **2011**, *473*, 55–60.

(2) McEvoy, J. P.; Brudvig, G. W. Water-Splitting Chemistry of Photosystem II. *Chem. Rev.* **2006**, *106*, 4455–4483.

(3) Denisov, I. G.; Makris, T. M.; Sligar, S. G.; Schlichting, I. Structure and Chemistry of Cytochrome P450. *Chem. Rev.* **2005**, *105*, 2253–2278.

(4) Meunier, B.; de Visser, S. P.; Shaik, S. Mechanism of Oxidation Reactions Catalyzed by Cytochrome P450 Enzymes. *Chem. Rev.* **2004**, *104*, 3947–3980.

(5) Tsukihara, T.; Aoyama, H.; Yamashita, E.; Tomizaki, T.; Yamaguchi, H.; Shinzawa-Itoh, K.; Nakashima, R.; Yaono, R.; Yoshikawa, S. Structures of Metal Sites of Oxidized Bovine Heart Cytochrome c Oxidase at 2.8 A. *Science* **1995**, *269*, 1069–1074.

(6) Michel, H.; Behr, J.; Harrenga, A.; Kannt, A. CYTOCHROME *C* OXIDASE: Structure and Spectroscopy. *Annu. Rev. Biophys. Biomol. Struct.* **1998**, *27*, 329–356.

(7) Perutz, M. F.; Mathews, F. S. An X-Ray Study of Azide Methaemoglobin. *J. Mol. Biol.* **1966**, *21*, 199–202.

(8) Maurus, R.; Bogumil, R.; Nguyen, N. T.; Mauk, A. G.; Brayer, G. Structural and Spectroscopic Studies of Azide Complexes of Horse Heart Myoglobin and the His-64-->Thr Variant. *Biochem. J.* **1998**, *332 (Pt 1)*, 67–74.

(9) Lim, M.; Hamm, P.; Hochstrasser, R. M. Protein Fluctuations Are Sensed by Stimulated Infrared Echoes of the Vibrations of Carbon Monoxide and Azide Probes. *Proc. Natl. Acad. Sci.* **1998**, *95*, 15315–15320.

(10) Yoshikawa, S.; Caughey, W. S. Infrared Evidence of Azide Binding to Iron, Copper, and Non-Metal Sites in Heart Cytochrome c Oxidase. *J. Biol. Chem.* **1992**, *267*, 9757–9766.

(11) Jeffrey, G. A. *An Introduction to Hydrogen Bonding*; Topics in physical chemistry; Oxford University Press: New York, 1997.

(12) Messerschmidt, A.; Luecke, H.; Huber, R. X-Ray Structures and Mechanistic Implications of Three Functional Derivatives of Ascorbate Oxidase from Zucchini. *J. Mol. Biol.* **1993**, *230*, 997–1014.

(13) Caignan, G. A.; Deshmukh, R.; Zeng, Y.; Wilks, A.; Bunce, R. A.; Rivera, M. The Hydroxide Complex of *Pseudomonas a Eruginosa* Heme Oxygenase as a Model of the Low-Spin Iron(III) Hydroperoxide Intermediate in Heme Catabolism: ^{13}C NMR Spectroscopic Studies Suggest the Active Participation of the Heme in Macrocycle Hydroxylation. *J. Am. Chem. Soc.* **2003**, *125*, 11842–11852.

(14) Rivera, M.; Caignan, G. A.; Astashkin, A. V.; Raitsimring, A. M.; Shokhireva, T. K.; Walker, F. A. Models of the Low-Spin Iron(III) Hydroperoxide Intermediate of Heme Oxygenase: Magnetic Resonance Evidence for Thermodynamic Stabilization of the D_{xy} Electronic State at Ambient Temperatures. *J. Am. Chem. Soc.* **2002**, *124*, 6077–6089.

(15) Scepaniak, J. J.; Young, J. A.; Bontchev, R. P.; Smith, J. M. Formation of Ammonia from an Iron Nitrido Complex. *Angew. Chem. Int. Ed.* **2009**, *48*, 3158–3160.

(16) Scepaniak, J. J.; Vogel, C. S.; Khusniyarov, M. M.; Heinemann, F. W.; Meyer, K.; Smith, J. M. Synthesis, Structure, and Reactivity of an Iron(V) Nitride. *Science* **2011**, *331*, 1049–1052.

(17) Zolnhofer, E. M.; Käß, M.; Khusniyarov, M. M.; Heinemann, F. W.; Maron, L.; van Gastel, M.; Bill, E.; Meyer, K. An Intermediate Cobalt(IV) Nitrido Complex and Its N-Migratory Insertion Product. *J. Am. Chem. Soc.* **2014**, *136*, 15072–15078.

(18) Matson, E. M.; Park, Y. J.; Bertke, J. A.; Fout, A. R. Synthesis and Characterization of M(II) (M = Mn, Fe and Co) Azafulvene Complexes and Their X_3^- Derivatives. *Dalton Trans* **2015**, *44*, 10377–10384.

(19) Matson, E. M.; Bertke, J. A.; Fout, A. R. Isolation of Iron(II) Aqua and Hydroxyl Complexes Featuring a Tripodal H-Bond Donor and Acceptor Ligand. *Inorg. Chem.* **2014**, *53*, 4450–4458.

(20) Park, Y. J.; Matson, E. M.; Nilges, M. J.; Fout, A. R. Exploring Mn–O Bonding in the Context of an Electronically Flexible Secondary Coordination Sphere: Synthesis of a Mn(III)–oxo. *Chem Commun* **2015**, *51*, 5310–5313.

(21) Matson, E. M.; Park, Y. J.; Fout, A. R. Facile Nitrite Reduction in a Non-Heme Iron System: Formation of an Iron(III)-Oxo. *J. Am. Chem. Soc.* **2014**, *136*, 17398–17401.

Chapter 4
Catalytic nitrite reduction: understanding the role of the secondary coordination sphere

4.1 Introduction

Inorganic nitrite has gained attention as its concentration in drinking water has been increased from industrial and agricultural sources, which can cause severe health and environmental problems.[1,2] For example, high level of nitrite can generate methemoglobin, a form of oxygen-carrying hemoglobin, eventually leading to blue baby syndrome.[3,4] Moreover, nitrite can be converted into carcinogenic nitrosamine compounds, resulting in cancer or lung disease.[5–7]

In biological systems, enzymatic nitrite reduction is effectively achieved by a wide range of metalloenzymes including heme-associated globins, molybdo-flavoproteins, mitochondrial proteins, and cytochrome p450 enzymes.[8–10] In order to understand how these metalloenzymes accomplish catalytic nitrite reduction, as well as to obtain insights into modelling synthetic inorganic complexes capable of nitrite reduction, structural and computational studies of those metalloenzymes have been performed.[10–16] In particular, hydrogen bonding networks in the secondary coordination sphere of the protein scaffold have been proposed to play important roles in several steps, such as stabilizing intermediates or mediating proton/electron transfers to the substrate.[10–16] In cytochrome *cd1* nitrite reductase, for example, a histidine residue proximally positioned to the active site can facilitate nitrite binding to the metal center via hydrogen bonding interactions to the Fe-NO_2 intermediate. Moreover, this pendant histidine is proposed to transfer protons to the oxygen, thereby generating water.[12,13]

Informed by these insights, we expected that our metal complexes bearing the tautomerizable ligand platform, tris(5-cyclohexyliminopyrrol-2-ylmethyl)amine ($H_3[N(pi^{Cy})_3]$), would be a good model for reducing nitrite. Utilizing a Zn(II) complex, we previously demonstrated that the secondary coordination sphere can affect nitrite binding to the metal center by stabilizing the M-nitrito (N-bound nitrite) complex. Moreover, our Fe(II) complex can readily reduce nitrite, resulting in an Fe(III)-oxo which is stabilized by the three amine moieties of the

secondary coordination sphere.[17] This result gave insights into the mechanistic understanding of nitrite reduction and the role of the secondary coordination sphere (Scheme 4.1).

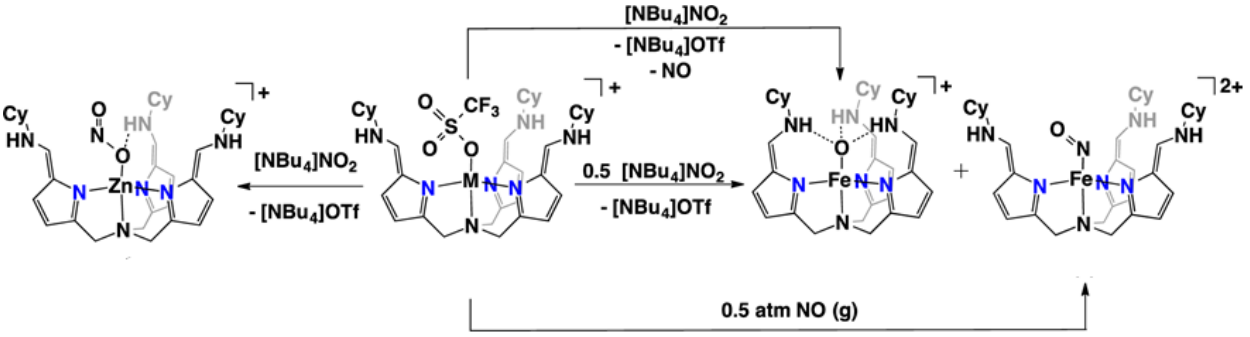

Scheme 4.1 Nitrite reactivity with Fe(II) and Zn(II) complexes.[17]

Thus far, only a few other synthetic inorganic systems capable of nitrite reduction have been reported: Suslick's Mn-porphyrin complex is able to perform nitrite reduction by photolysis,[18] Harrop's nonheme $Fe(NO_2)_2$ complex can undergo nitrite conversion to nitric oxide,[19] and Szymczak's Cu complex featuring a proton-responsive tripodal ligand enables nitrite reduction in homogeneous systems.[20] In the case of catalytic nitrite reduction, examples are only limited to heterogeneous systems such as bimetallic metal catalysts containing noble metals.[21–23]

In this chapter, utilizing a modified ligand, we expand our previous research of stoichiometric nitrite reduction to catalytic nitrite reduction, generating nitric oxide and water. The secondary coordination sphere is able to transfer protons and electrons to an axial ligand, enabling the generation of water over the course of catalytic nitrite reduction, which is rare in synthetic inorganic systems. Catalytic nitrite reduction and its mechanistic study are discussed herein, providing important insights into the nitrite reduction mechanism found in metalloenzymes, such as cytochrome *cd1* nitrite reductase, as well as modelling synthetic inorganic complexes capable of catalytic nitrite reduction.

4.2 Results and discussion

4.2.1 Synthesis of mesityl substituted ligand ($H_3[N(pi^{Mes})_3]$)

Previous studies of hydrogen bonding interactions between substrates and the secondary coordination spheres of a series of iron and manganese complexes with $H_3[N(pi^{Cy})_3]$ have been reported by our research group (described in Chapter 2 and 3).[24,25] The proton movements in the

secondary coordination sphere, as well as the tautomerization of each ligand arm differ depending upon the substrate and the oxidation state of the metal center. Interested in probing the effect of ligand electronics on the reactivity of iron complexes, a ligand variant bearing the more electronic withdrawing, 2,4,6,-trimethylphenyl group in place of the cyclohexyl group was synthesized. Since the pk_a of cyclohexylamine (10.64)[26] and that of 2,4,6-trimethylaniline (4.38)[27] are quite different, we hypothesized that the reactivity and basicity/acidity of the metal complexes with the mesityl substituted ligand ($H_3[N(pi^{Mes})_3]$) would be changed.

To synthesize $H_3[N(pi^{Mes})_3]$, the previously reported formyl derivative of tris-(pyrryl)amine, H_3tap^{CO},[24] and 2,4,6-trimethylaniline were stirred with a catalytic amount of formic acid in anhydrous ethanol at 50 ˚C overnight. Upon workup, we obtained $H_3[N(pi^{Mes})_3]\cdot H_2O$ in 73% yield. Given the highly hygroscopic nature of the ligand, we employed a previously reported drying method using 4Å sieves.[28] The isolated ligand ($H_3[N(pi^{Mes})_3]$) was subsequently characterized by ^1H and ^{13}C NMR spectroscopy and elemental analysis.

4.2.2 Synthesis and characterization of Fe(II) complexes

With ligand in hand, we set out to metallate $H_3[N(pi^{Mes})_3]$ with Fe(II) salts. Synthesis of the desired Fe(II) complexes, $[N(afa^{Mes})_3Fe(OTf)]OTf$ (**$^{Mes}Fe^{II}$-OTf**) and $N(afa^{Mes})(pi^{Mes})_2Fe(OH_2)$ (**$^{Mes}Fe^{II}$-OH_2**) was accomplished using the protocol previously established for the series of Fe(II) and Mn(II) complexes of $H_3[N(pi^{Cy})_3]$ (Scheme 4.2). Characterization of **$^{Mes}Fe^{II}$-OTf** by ^1H NMR spectroscopy revealed broad paramagnetic resonances from -2.9 ppm to 160.6 ppm. The resonances at 39.1 and 21.5 ppm in the ^1H NMR spectrum appear in a similar range to those of the previously reported cyclohexyl derivative, $[N(afa^{Cy})_3Fe(OTf)](OTf)$, and are characteristic of the azafulvene-amine tautomer of the ligand bound to an Fe(II) center. However, the presence of additional paramagnetic resonances for **$^{Mes}Fe^{II}$-OTf** compared to $[N(afa^{Cy})_3Fe(OTf)](OTf)$ is consistent with greater dissymmetry, suggesting the three arms of the ligand in **$^{Mes}Fe^{II}$-OTf** are inequivalent and adopt an asymmetric conformation in solution. Solid state IR spectroscopy further supports an asymmetric ligand coordination, with two different C=N stretches observed at 1621 cm^{-1} and 1636 cm^{-1}. The solution magnetic moment for **$^{Mes}Fe^{II}$-OTf**, obtained via Evans' method was 5.52(6) μ_B which is consistent with a high spin, S=2, Fe(II) metal center.

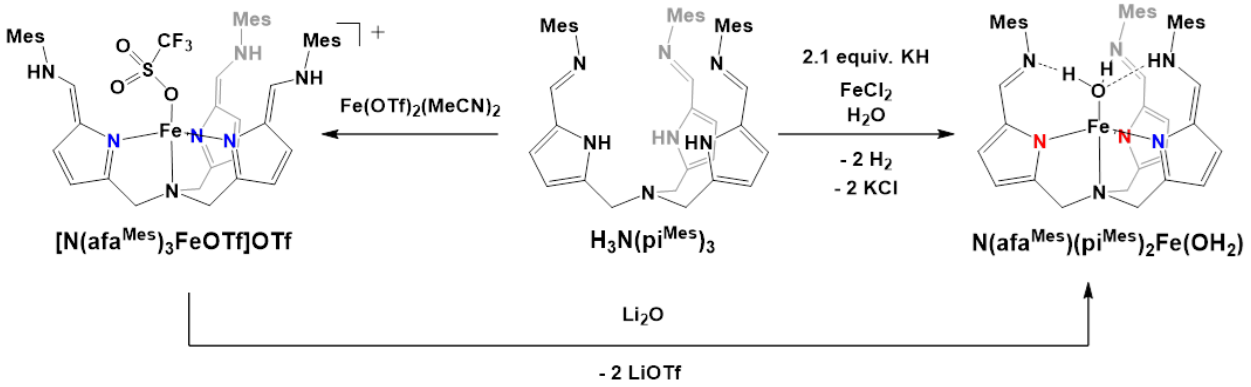

Scheme 4.2 Synthesis of complexes $[N(afa^{Mes})_3Fe(OTf)]OTf$ and $N(afa^{Mes})(pi^{Mes})_2Fe(OH_2)$.

To further establish the structure of **$^{Mes}Fe^{II}$-OTf**, yellow crystals suitable for X-ray diffraction were grown from a concentrated THF solution layered with diethyl ether. Data refinement revealed a five-coordinate Fe(II) center in a pseudo-trigonal bipyramidal geometry with a triflate anion bound *trans* to the apical nitrogen of the tripodal ligand (Figure 4.1). The Fe—N_{pyr} bond distances in the equatorial plane ranging from 2.074(4) – 2.110(4) Å and the Fe-N1 distance of 2.247(4) Å is similar to the previously reported $[N(afa^{Cy})_3Fe(OTf)](OTf)$ complex.[24] A comparison of intraligand bond distances revealed that all three arms were tautomerized to the azafulvene-amine forms coordinating datively to the iron center as previously observed in the structures of $[N(afa^{Cy})_3Fe(OTf)](OTf)$ and $[N(afa^{Cy})_3Mn(OTf)](OTf)$.[24,25] The protons found in the difference map moved from the pyrrole ring to the amines in the secondary coordination sphere, which further supported the tautomerization of the ligand platform. Interestingly, we observed that one of the ligand arms was rotated with the N-H pointing away from the metal center while the other two arms point towards the metal center, resulting in an asymmetric metal complex. This observation is consistent with the data obtained from ^{1}H NMR and IR spectroscopies. Since the bond lengths of each ligand arm are similar, it is assumed that the bulkiness of the mesityl groups and the bound triflate anion causes one of the arms to rotate, thereby relieving the steric strain.

Another Fe(II) complex, $N(afa^{Mes})(pi^{Mes})_2Fe(OH_2)$ (**$^{Mes}Fe^{II}$-OH_2**) which is comparable to the previously reported $N(pi^{Cy})(afa^{Cy})_2FeOH$ compound was also synthesized based on a previously established synthetic protocol. $H_3[N(pi^{Mes})_3]$ was deprotonated by the addition of 2.2 eq. of KH in THF and stirred for three hours at room temperature. Subsequent addition of the

deprotonated ligand to an $FeCl_2$ slurry in THF resulted in a color change from pale yellow to orange (Scheme 4.2). Recrystallization of the solution resulted in an orange crystalline solid in 45% yields. Independent synthesis of ^{Mes}**Fe^{II}-OH$_2$** was successful via the addition of Li_2O to ^{Mes}**Fe^{II}-OTf** (94%) (Scheme 4.2). ^{1}H NMR spectroscopy of complex ^{Mes}**Fe^{II}-OH$_2$** revealed paramagnetic resonances ranging from -4.0 ppm to 29.8 ppm. The number of observed resonances is consistent with C_3-symmetry in solution. The low solubility of the complex precluded a determination of the magnetic moment by Evans' method.

To unambiguously establish the identity of ^{Mes}**Fe^{II}-OH$_2$**, crystals suitable for X-ray diffraction were grown from the slow diffusion of hexanes into a concentrated THF solution of ^{Mes}**Fe^{II}-OH$_2$**. Refinement revealed a pseudo-trigonal bipyramidal Fe(II) center situated on a C_3 axis that included the apical nitrogen of the ligand platform, the iron center, and an oxygen atom. Positioning hydrogens in the electron density map gave a good solution, confirming the presence of a hydrogen atom next to the axially bound oxygen (Figure 4.1), displaying hydrogen bonding to the imine of the secondary coordination sphere with O—H distance of 0.871(14) Å and N—H distance of 2.10(5) Å.[29]

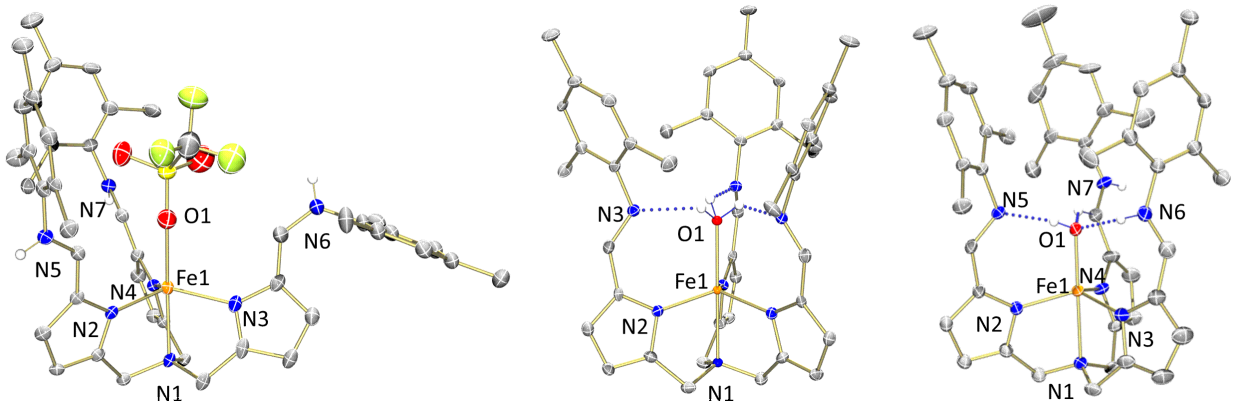

Figure 4.1 X-ray crystal structures of complex ^{Mes}**Fe^{II}-OTf**, ^{Mes}**Fe^{II}-OH$_2$**, and ^{Mes}**Fe^{III}-O(H)**.

Despite the C_3 symmetry observed in the crystal structure of ^{Mes}**Fe^{II}-OH$_2$**, two different C=N stretches at 1616 and 1643 cm^{-1} were observed in the IR spectrum, suggesting both tautomers (afa^{Mes} and pi^{Mes}) of the ligand are present, similar to [N(pi^{Cy})(afa^{Cy})$_2$]FeOH (C=N stretches at 1624 and 1655 cm^{-1}). However, the Fe—O1 bond length of 2.112(7) Å in the structure of ^{Mes}**Fe^{II}-OH$_2$** was longer than the Fe—O1 distance of 2.0339(12) Å in

[N(pi^{Cy})(afa^{Cy})$_2$]FeOH,[24] excluding the possibility of an Fe—OH complex, but similar to K[(N(pi^{Cy})$_3$Fe(H$_2$O)] (2.080(2)Å)[24] and other Fe(II)-aqua complexes reported in literature.[30] Accordingly, we propose that this complex is best described as N(afa^{Mes})(pi^{Mes})$_2$Fe(OH$_2$) (**^{Mes}Fe^{II}-OH$_2$**), which consists of two pyrrol-imine arms and one azafulvene-amine ligand arm, consistent with a water bound to the iron center. Furthermore, this result corroborated the hypothesis that by installing electron withdrawing groups in the secondary coordination sphere results in more acidic protons than those of the cyclohexyl system, thus giving rise to the formation of an Fe-OH$_2$, rather than Fe-OH complex as observed in the cyclohexyl derivative of the ligand.

Table 4.1 Selected structural parameter of complex **^{Mes}Fe^{II}-OTf**, **^{Mes}Fe^{II}-OH$_2$**, and **^{Mes}Fe^{III}-O(H)**.

Bond	**^{Mes}Fe^{II}-OTf (Å)**	**^{Mes}Fe^{II}-OH$_2$ (Å)**	**^{Mes}Fe^{III}-O(H) (Å)**
Fe1—N1	2.247(4)	2.253(8)	2.2499(15)
Fe1—N(pyr)	2.074(4) – 2.110(4)	2.294(5)	2.0089(16) – 2.0404(17)
Fe1—O1	2.141(7)	2.112(7)	1.8539(13)
O1—H1	—	0.871(14)	0.80(4)
NX···H1		X=3, 2.10(5)	X=5, 1.85(4)
O1···H6	—	—	1.72(3)
C=N stretch	1621, 1636 cm^{-1}	1616, 1643 cm^{-1}	1634, 1651 cm^{-1}
Magnetic moment	5.52(6) μ_B	— [a]	5.94(9) μ_B

a. A reliable magnetic moment could not be obtained for complex **^{Mes}Fe^{II}-OH$_2$** due to its insolubility.

4.2.3 Nitrite reduction with [N(afa^{Mes})$_3$Fe(OTf)]OTf

Recently, our research group reported the facile nitrite reduction to nitric oxide utilizing [N(afa^{Cy})$_3$Fe(OTf)](OTf). The crystal structure of a Zn(II)-NO$_2$ analog bearing our tripodal ligand framework revealed that the nitrite is bound through oxygen to the metal center and stabilized by a hydrogen bonding interaction from the secondary coordination sphere (Scheme 4.1). Thus, we proposed that nitrite reduction would proceed via an Fe-nitrito intermediate with subsequent cleavage of the N—O bond to yield NO (g) and the Fe(III)-oxo.[17] This observation is consistent with one of the proposed mechanisms of biological nitrite reduction in hemoglobin, where upon formation of the Fe(III)-oxo, a proximal histidine residue protonates the oxygen, forming an Fe(III)-OH. This proton movement to generate water has been proposed as one of the

important roles of secondary coordination sphere in metalloenzymes.[12] We reasoned that by installing a more electron withdrawing group, 2,4,6-trimethylphenyl, on our ligand, we would enhance the acidity of the protons in the secondary coordination sphere, thereby favoring formation of Fe(III)—OH instead of Fe(III)—O.

Upon addition of $[NBu_4][NO_2]$ to **^{Mes}Fe^{II}-OTf**, an instantaneous color change from yellow to brown was observed, which was consistent with the oxidation of the high spin Fe(II) starting material (**^{Mes}Fe^{II}-OTf**). Following workup, the product, $[N(afa^{Mes})_2(Pi^{Mes})FeOH](OTf)$ (**^{Mes}Fe^{III}-O(H)**) was isolated as a brown crystalline solid. Analysis of the resulting product by ^{1}H NMR spectroscopy revealed two broad characteristic resonances at 77.16 and 60.64 ppm, similar to resonances observed in the ^{1}H NMR spectrum of the C_3 symmetric $[N(afa^{Cy})_3FeO](OTf)$. Characterization by IR spectroscopy, however, revealed two C=N stretches at 1634 and 1651 cm^{-1}, suggesting that the three arms of the ligand are inequivalent, presumably due to different tautomers in the solid state. Finally, the solution magnetic moment, as determined by Evans' method, revealed an average μ_{eff} of 5.94(9) μ_B, consistent with a high-spin, S=5/2, Fe(III) metal center.

To provide a more definitive understanding of the structure of **^{Mes}Fe^{III}-O(H)**, X-ray diffraction analysis was performed. Data refinement revealed a pseudo-trigonal bipyramidal geometry about an Fe(III) center with a bound hydroxo ligand (Figure 4.1). Analysis of intraligand bond distances as well as the location of hydrogens in the electron density map, was consistent with two arms of the ligand in the azafulvene-amine form and the third arm is in the hydrogen bond accepting pyrrole-imine form which is hydrogen bonding to the hydroxo ligand. Hydrogen bonding between one of the amines in the secondary coordination sphere and the oxygen of hydroxo ligand was observed while the remaining amine was partially disordered, oriented both inward toward the substrate and outward.

The azafulvene Fe—N bond distances of 2.0337(17) and 2.0404(17) Å in **^{Mes}Fe^{III}-O(H)**, are consistent with the observed Fe—N distances of the previously reported $[N(afa^{Cy})_3FeO](OTf)$, while the pyrrolyl Fe—N bond distance of 2.0089(16) Å is shorter than azafulvene Fe—N bond distances, consistent with previously observed Fe—pyrrolyl bond distances. The Fe1—O1 distance of 1.8539(13) Å is longer than the Fe—O distance of $[N(afa^{Cy})_3FeO](OTf)$ and similar to other Fe(III)—OH distances (1.869 – 1.9315 Å) found in the literature.[31–33] The O1—H1 distance of 0.80(4) and H1···N7 distance of 1.85(4) Å are well within the range of bond distances

expected for donor-acceptor atoms participating in hydrogen bonding interactions. The X-ray crystal structure demonstrated that the presence of the more electron-withdrawing trimethylphenyl group in **^{Mes}Fe^{III}-O(H)** does, in fact, enhance the acidity of protons in the secondary coordination sphere, as evidenced by the generation of an Fe(III)—OH rather than an Fe-oxo as in the case of the cyclohexyl analogue of the ligand.

4.2.4 Mechanistic studies of cyclic nitrite reduction

In Nature, the conversion of nitrite to nitric oxide proceeds via a metalloenzyme-mediated one electron reduction. In order to perform this catalytically, the Fe(II) metal center at the active site must be regenerated from an Fe(III)—OH intermediate by the addition of 2 eq. of H^+ and 1 eq. of e^-, concomitant with the release of water. In order to provide the requisite $2H^+$ and $1e^-$ in our system, 1.5 eq. of triflic acid (HOTf) and 0.6 eq. of 1,2-diphenylhydrazine (DPH, a source of 2 H^+/2 e^-) were added to reduce **^{Mes}Fe^{III}-O(H)** to **^{Mes}Fe^{II}-OTf** (in order to ensure the complete reduction, a slight excess of both acid and reductant were added). Upon stirring the reaction, the color of the reaction mixture changed from brown to orange. A ^{1}H NMR spectrum of the crude reaction revealed the formation of **^{Mes}Fe^{II}-OTf**, azobenzene, and a small amount of **^{Mes}Fe^{II}-OH$_2$**. The formation of about 1 eq. of water was confirmed by ^{1}H NMR spectroscopy and by Karl-Fisher titration (0.95 eq. by Karl-Fisher, Table 4.2).

Informed by these results, two possible pathways for the reduction of **^{Mes}Fe^{III}-O(H)** are shown in scheme 4.3 and independent synthesis of proposed intermediates was attempted. The addition of acid to **^{Mes}Fe^{III}-O(H)** resulted in the formation of an Fe(III)-aqua intermediate, [N(afa^{Mes})$_2$(pi^{Mes})Fe(OH$_2$)]OTf$_2$, as assayed by IR spectroscopy and mass spectrometry (Scheme 4.3, A-1). However, crystallographic characterization of this intermediate was unsuccessful due to its instability in solution after a few days. Subsequent addition of 0.6 eq. of DPH to the *in situ* generated aqua complex, resulting in the formation of **^{Mes}Fe^{II}-OTf** and 0.8 eq. of water (Scheme 4.3, A-2). Addition of KC_8 to **^{Mes}Fe^{III}-O(H)** generated **^{Mes}Fe^{II}-OH$_2$**, as determined by ^{1}H NMR spectroscopy (Scheme 4.3, B-1). Upon reduction of **^{Mes}Fe^{III}-O(H)**, another proton in the secondary coordination sphere moved to the axially bound oxygen, generating **^{Mes}Fe^{II}-OH$_2$**. This was then treated with 2.1 eq. of HOTf to generate the starting Fe(II) complex (**^{Mes}Fe^{II}-OTf**) and water (1.03 eq.), as confirmed by ^{1}H NMR spectroscopy and a Karl-Fisher titration (Scheme 4.3, B-2).

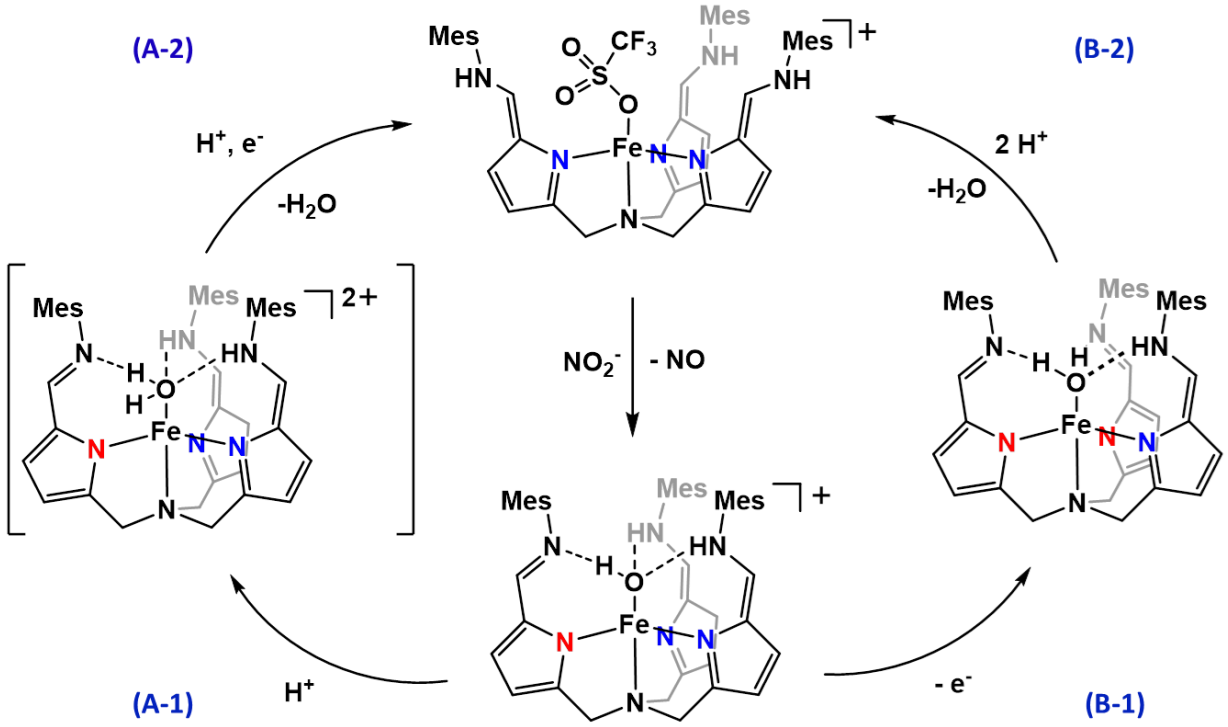

Scheme 4.3 Proposed mechanisms of reduction of $^{Mes}Fe^{III}$-O(H) to $^{Mes}Fe^{II}$-OTf.

Table 4.2 Quantification of water by Karl-Fisher titration.

	Acetonitrile (2 mL)	Reduction of $^{Mes}Fe^{III}$-O(H) to $^{Mes}Fe^{II}$-OTf. (0.5 mL)	Reduction of $[N(afa^{Mes})_3FeOH](OTf)_2$ to $^{Mes}Fe^{II}$-OTf. (0.5 mL)	Conversion of $^{Mes}Fe^{II}$-OH_2 to $^{Mes}Fe^{II}$-OTf. (0.5 mL)
Amount of water (μg)	9.2	61.1	49.8	69.2
	12.0	60.6	52.5	66.6
	14.8	56.6	50.4	63.8
Average	12±2.8	59.4±2.5	50.9±1.4	66.5±2.7
Less Background	-	56.4±2.7	47.9±1.6	63.5±2.9
Equivalent of H_2O detected.	-	0.94	0.80	1.05

4.2.5 Deuterium experiments

Interested in exploring the movements of the hydrogen atoms within the secondary coordination sphere, deuterium experiments were carried out for the conversion of ^{Mes}**Fe^{II}-OH$_2$** to ^{Mes}**Fe^{II}-OTf** (Scheme 4.3, B-2). Reaction between 2.1 eq. of DOTf (deuterated triflic acid) and ^{Mes}**Fe^{II}-OTf** was monitored by ^{1}H, ^{2}H NMR and IR spectroscopies. In the ^{2}H NMR spectrum, two resonances at 13.84 and 7.52 ppm were noted; these resonances match two found in the ^{1}H NMR spectrum of complex ^{Mes}**Fe^{II}-OTf** (Figure 4.2C). We tentatively assigned these resonances as amines in the secondary coordination sphere. Further investigation of the same reaction by IR spectroscopy revealed a broad -ND stretch at 2374 cm^{-1} vs. -NH stretch in ^{Mes}**Fe^{II}-OTf** at 3193 cm^{-1}, with a value of ν_{NH}/ν_{ND} = 1.35 (expected ν_{NH}/ν_{ND} = 1.37) (Figure 4.5).[34,35]

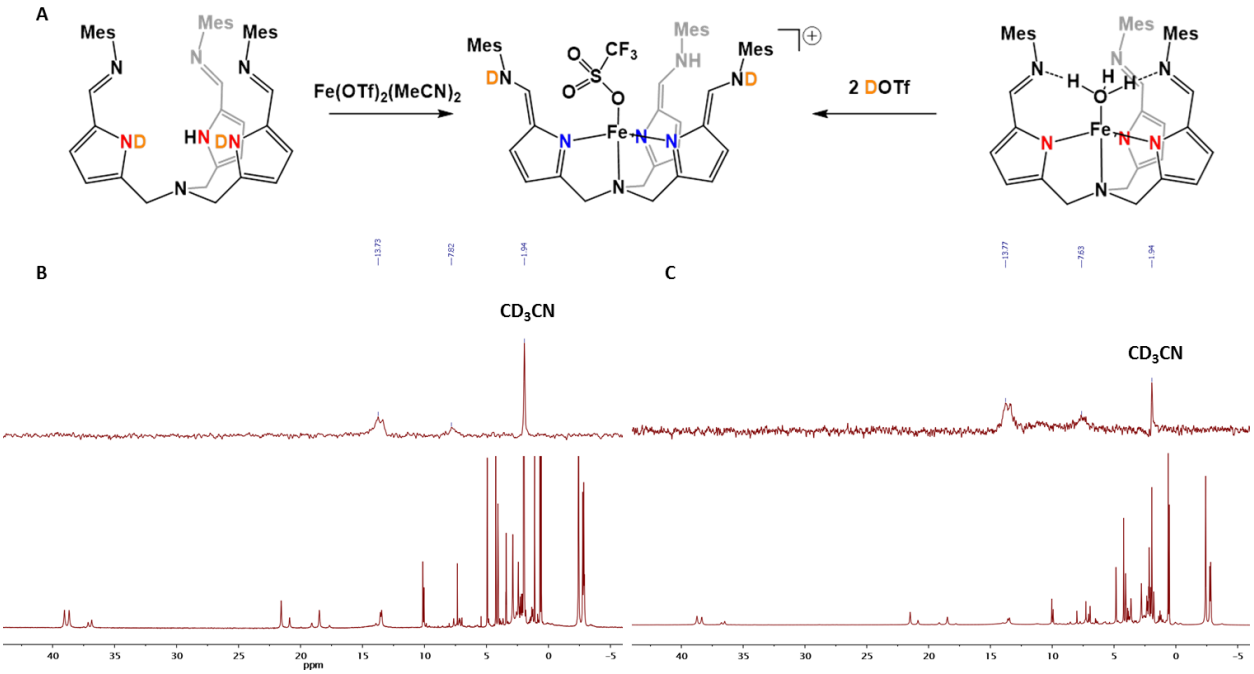

Figure 4.2 (A) Scheme of deuterium labeling experiments. (B) ^{2}H NMR spectrum (CH_3CN, 21°C, upper) and ^{1}H NMR spectrum (CD_3CN,21°C, lower) of ^{Mes}**Fe^{II}-OTf** -d_2. (C) ^{2}H NMR spectrum (CH_3CN,21°C, upper) and ^{1}H NMR spectrum (CD_3CN,21°C, lower) of reaction of ^{Mes}**Fe^{II}-OH$_2$** with 2.2 eq. of DOTf.

In order to confirm the deuterium labelling of ^{Mes}**Fe^{II}-OTf**, independent synthesis with the deuterium labeled ligand was achieved. 2.5 eq. of KH was added to $H_3[N(pi^{Mes})_3]$, followed by addition of 2 eq. of DOTf, resulting in formation of $HD_2[N(pi^{Mes})_3]$, confirmed by ^{1}H and ^{2}H NMR spectroscopy (Figure 4.4B). $Fe(OTf)_2(MeCN)_2$ was then added to a solution of

$HD_2[N(pi^{Mes})_3]$ and the resulting compound, ^{Mes}**Fe^{II}-OTf**-d_2 was characterized by NMR (^{1}H, and ^{2}H) and IR spectroscopies, matched the product of the reaction of ^{Mes}**Fe^{II}-OH$_2$** with DOTf. Lastly, deuterium exchange between D_2O and ^{Mes}**Fe^{II}-OTf** was probed by the addition of D_2O to ^{Mes}**Fe^{II}-OTf**. ^{2}H NMR and IR spectra confirmed the formation of ^{Mes}**Fe^{II}-OTf**-d_2, suggesting that protons can exchange between water and the secondary coordination sphere (Figure 4.7). From these experiments, we proposed that amine protons are capable of transferring among the secondary coordination sphere, the bound substrate, and water; however, the detailed mechanism of proton movements remains unclear.

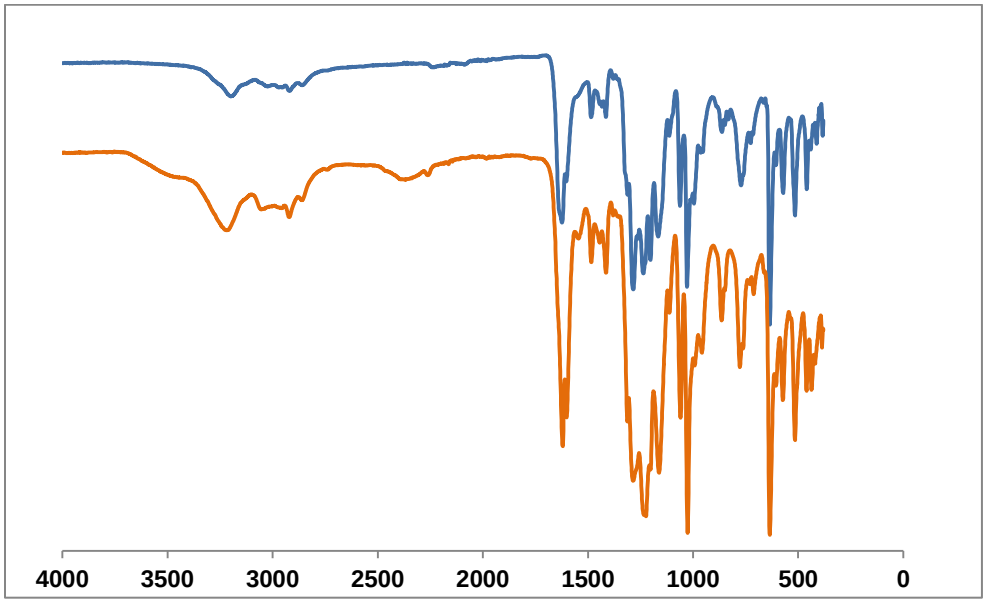

Figure 4.3 IR spectroscopy of ^{Mes}**Fe^{II}-OTf** (blue) and the reaction of ^{Mes}**Fe^{II}-OH$_2$** with 2.2 eq. of DOTf (orange).

4.2.6 Catalytic nitrite reduction

With a stoichiometric nitrite reduction cycle established, we next explored the possibility of rendering the nitrite reduction catalytic. Given the reactivity of triflic acid towards $[^nBu_4][NO_2]$ to generate nitric oxide, we employed sodium nitrite ($NaNO_2$) as the source of nitrite and lutidinium triflate (LuHOTf) as our proton source. Initial attempts used 25 mol % of ^{Mes}**Fe^{II}-OTf**, 1.25 eq. $NaNO_2$, 1.8 eq. of LuHOTf and 1eq. of DPH, with a CoTPP (TPP = 5,10,15,20-tetraphenylporphyrin) solution in a separate vessel for capture and quantification of the NO(g)

generated over the course of the reaction. CoTPP is known to bind NO (g) tightly and generate CoTPP-NO, providing a reliable method for quantification of the amount of NO(g) formed from the catalytic reaction. After 8 hours of stirring, almost 1 eq. of CoTPP was converted to CoTPP-NO, corresponding to a TON of 4 (Table 4.3, entry 1). Decreasing the catalytic loading to 17 % resulted in significant decomposition of the iron complex by the acid, leading to a lower TON. Switching to a more gradual, portion-wise addition of LuHOTf mitigated decomposition, improving catalytic activity (TON = 5.2) (Table 4.3, entry 2).

Seeking to compare the catalytic activity of ^{Mes}**Fe^{II}-OTf** to the previously reported cyclohexyl ligand derivative, the catalytic activity of [N(afa^{Cy})$_3$Fe(OTf)](OTf) was investigated. With 25 mol % of [N(afa^{Cy})$_3$Fe(OTf)](OTf), we observed only 47 % conversion to CoTPP-NO after 8 hours of stirring (Table 4.3, entry 3). Interested in determining the cause of the reduced catalytic activity, fewer equivalents of acid (1.5 eq of LuHOTf) were added, resulting in an increased yield of 67 % within 8 hours (Table 4.3, entry 4), suggesting the acid induces significant decomposition of catalyst.

Table 4.3 Catalytic Nitrite Reduction.

Entry	X (eq.)	Catalyst	CoTPP-NO(%)	Time (hrs)	TON
1	0.25	^{Mes}**Fe^{II}-OTf**	> 99	8	4
2	0.17[a]	^{Mes}**Fe^{II}-OTf**	85	10	5.1
3	0.25	N(afa^{Cy})$_3$Fe(OTf)$_2$	48	8	1.9
4	0.25[b]	N(afa^{Cy})$_3$Fe(OTf)$_2$	61	8	2.5
5		Control	13	8	-
6			17	10	-

a. LuHOTf was added in portions. b. 1.5 equiv of LuHOTf was added.

To test this hypothesis, 7 eq. of LuHOTf, the same amount of acid employed in the catalytic reaction, was added to a solution containing [N(afa^{Cy})$_3$Fe(OTf)](OTf). A ^{1}H NMR spectrum of the reaction revealed significant presence of demetallated, acidified ligand. Integration of the corresponding resonances revealed that greater amounts of demetallated, acidified ligand were present compared to the analogous reaction with ^{Mes}**Fe^{II}-OTf**. Thus, the improved catalytic activity of ^{Mes}**Fe^{II}-OTf** may be due to the increased robustness of the complex towards acid, perhaps a consequence of the lower pKa of the mestiyl derivative

compared to the more basic cyclohexyl variant. Although the turnover number of nitrite reduction is much lower than that observed in the biological system, our complex is the first synthetic inorganic molecule capable of homogeneous catalytic nitrite reduction.

4.3 Conclusions

By modifying the previously reported cyclohexyl variant of the ligand, $[H_3N(pi^{Cy})_3]$, with more acidic protons in the secondary coordination sphere, N-H protons in 2,4,6-trimethylanilin were transferred to the axially bound oxygen to form water throughout the course of catalytic nitrite reduction. The proton transfer from the secondary coordination sphere to the substrate is one of the key steps to complete the cycle of the nitrite reduction and was supported by evidence from deuterium labeling studies. This proton movement is suggested in the study of cytochrome *c* nitrite reductase. To date, the examples of electronically flexible secondary coordination sphere to shuttle protons or electrons are rare. Even though the TON is modest, this result is expected to provide insights into the mechanistic understanding of nitrite reduction by metalloenzymes as well as inorganic model systems for nitrite remediation.

4.4 Experimental section

General Considerations. All manipulations were carried out in the absence of water and dioxygen using standard Schlenk techniques or in an MBraun inert atmosphere drybox under a dinitrogen atmosphere. All glassware was oven dried for a minimum of 8 h and cooled in an evacuated antechamber prior to use in the drybox. Solvents were dried and deoxygenated on a Glass Contour System (SG Water USA, Nashua, NH) and stored over 4 Å molecular sieves purchased from Strem prior to use. Celite 545 (J. T. Baker) was heated to 100°C under dynamic vacuum for 24h prior to use in the drybox. $H_3(tpa^{CO})$,[24] $Fe(OTf)_2(MeCN)_2$,[36] KC_8,[37] and lutidinium triflate (LuHOTf)[38] were prepared according to literature procedures. Chloroform-d and acetonitrile-d_3 were purchased from Cambridge Isotope Laboratories and were degassed and stored over 4 Å molecular sieves prior to use. Potassium hydride was purchased from Sigma-Aldrich washed with hexanes to remove mineral oil, and dried under vacuum prior to use. Ferrous chloride was purchased from Strem and used as received. 2,4,6,-Trimethylaniline, formic acid, lithium oxide, triflic acid, and sodium nitrite were purchased from Sigma-Aldrich and used as received. Tetrabutylammonium nitrite was purchased from Sigama-Aldrich and recrystallized

from a concentrated THF solution layered with hexanes at -35°C. 1,2-Diphenylhydrazine was purchased from Oakwood Chemical and recrystallized from a concentrated diethyl ether solution layered with hexanes at -35°C. Cobalt(II) 5,10,15,20-tetraphenylporphyrin was purchased from Frontier Scientific and used as received.

NMR Spectra were recorded at room temperature on a Varian spectrometer operating at 500 MHz (^{1}H NMR), 126 MHz (^{13}C NMR), 76.7 MHz (^{2}H NMR) and 470 MHz (^{19}F NMR) and referenced to the residual solvent resonance (δ in parts per million, and *J* in Hz). Solid-state infrared spectra were measured using a PerkinElmer Frontier FT-IR spectrophotometer equipped with a KRS5 thallium bromide/iodide universal attenuated total reflectance accessory. Elemental analysis was performed by the University of Illinois at Urbana-Champaign School of Chemical Sciences Microanalysis Laboratory in Urbana, IL. Analysis with mass spectrometry was performed by University of Illinois at Urbana-Champaign School of Chemical Sciences Mass Spectrometry Laboratory. Data of crystal structures were collected on a Bruker D8 Venture Duo or Bruker X8ApexII diffractometer at the George L. Clark X-Ray Facility and 3M Material Laboratory at the University of Illinois at Urbana-Champaign. The quantification of water was performed by an Aquatest CMA Karl Fischer Coulometric Titrator from Photovolt Instruments with HYDRANAL from Fluka Analytical.

Preparation of $H_3[N(pi^{Mes})_3]$. The previously synthesized $H_3(tpa^{CO})$[24] (1.0 g, 2.88 mmol) was dispersed in ethanol (100 % 12 mL). 2,4,6,-Trimethylaniline (1.2 g, 8.93 mmol) was added to the reaction mixture, followed by 6 drops of formic acid added. The reaction was stirred at 50°C for 24 hours, after which time the product $H_3[N(pi^{Mes})_3]\cdot H_2O$ was precipitated as a tan powder. $H_3[N(pi^{Mes})_3]\cdot H_2O$ was collected by filtration and washed with ethanol and acetonitrile several times in a frit (1.45 g, 2.1 mmol, 75%). To dry the $H_3[N(pi^{Mes})_3]\cdot H_2O$, mole sieves(4 Å) was added to diethyl ether solution of $H_3[N(pi^{Mes})_3]\cdot H_2O$ overnight.[28] After evaporating solvents to dryness, the $H_3[N(pi^{Mes})_3]\cdot H_2O$ was recrystallized from diethyl ether/MeCN (2:1) at -35˚C. Analysis for C45H51N7·CH3CN: Calcd. C, 77.23; H, 7.45; N, 15.33. Found C, 76.84; H, 7.33; N, 15.38. ^{1}H NMR (C_6D_6, 21˚C): δ = 2.17 (s, 18H, CH_3-Mes), 2.20 (s, 9H CH_3-Mes), 3.18 (s, 6H, -CH_2), 6.12 (d, 3H, pyr-CH), 6.40 (d, 3H, pyr-CH), 6.82 (s, 6H, Mes-CH), 7.65 (s, 3H, imine-CH), 9.52 (s, 3H, -NH). ^{13}C NMR ($CDCl_3$, 21˚C): δ = 18.50, 20.87, 50.26, 110.29, 115.97, 127.83, 128.81, 130.69, 132.80, 133.38, 148.56, 152.21. (Figure 4.4) IR = 1621 cm^{-1} (C=N).

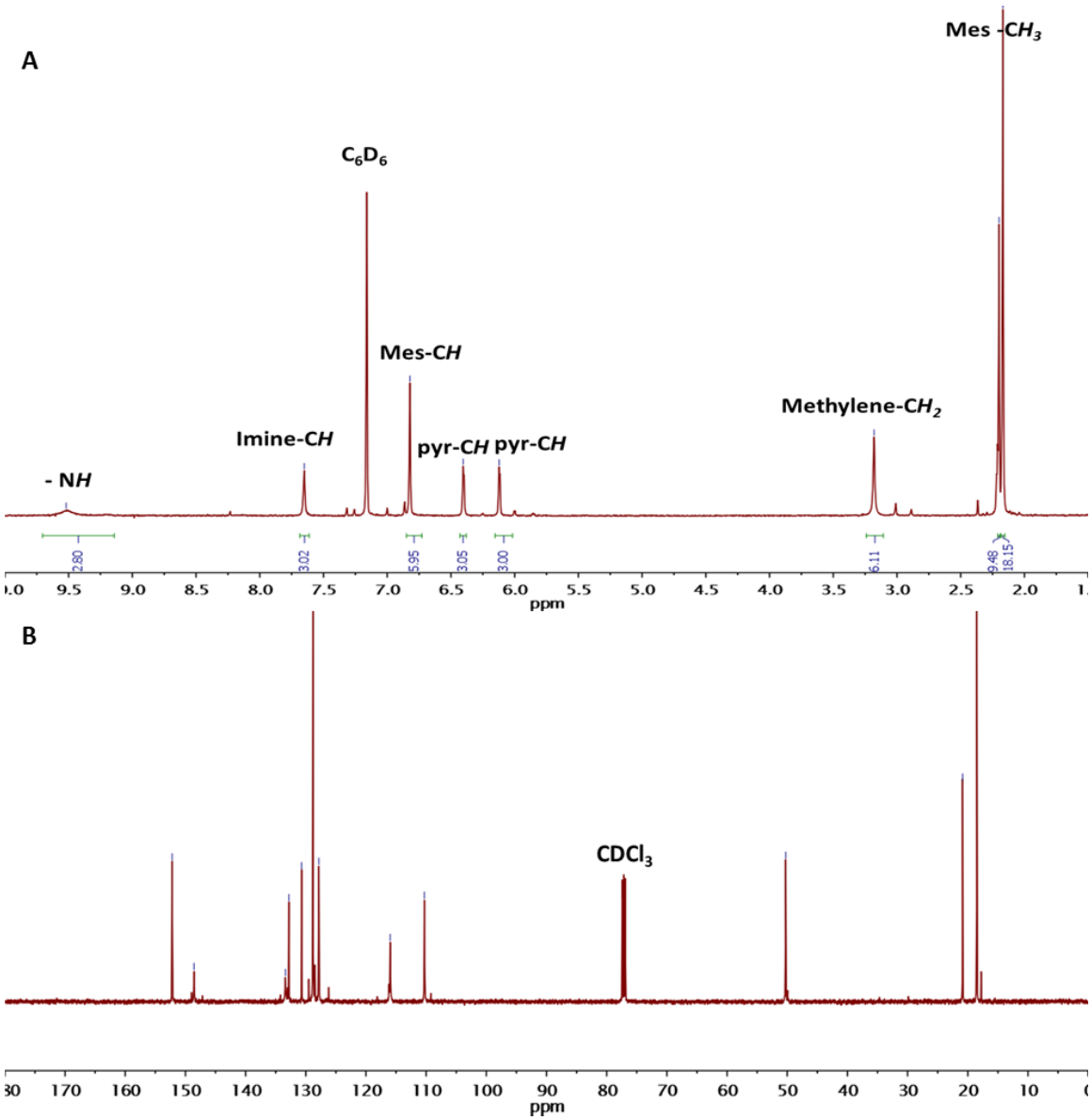

Figure 4.4 (A) ^{1}H NMR spectrum and (B) ^{13}C NMR spectrum of $H_3[N(pi^{Mes})_3]$.

Preparation of $[N(afa^{Mes})_3Fe(OTf)]OTf$. A 20 mL scintillation vial was charged with $Fe(OTf)_2(MeCN)_2$ (0.043 g, 0.100 mmol) and approximately 10 mL of tetrahydrofuran. With vigorous stirring, $H_3N(pi^{Mes})_3$ (0.070 g, 0.101 mmol) was added by difference, resulting in an instantaneous color change to orange. The mixture was stirred for one hour, after which time solvents were removed under reduced pressure. Following removal of volatiles, the orange powder was washed with diethyl ether three times (0.101 g, 97 %). Crystals suitable for X-ray

analysis were from a concentrated solution of tetrahydrofuran layered with diethyl ether at room temperature. Analysis for $FeC_{47}H_{51}N_7S_2F_6O_6$: Calcd. C, 54.08; H, 4.92; N, 9.39. Found C, 54.43; H, 5.01; N, 9.39. ^{19}F NMR (CD_3CN, 21 °C): $\delta = -77.96$ (SO_3CF_3). IR: 1621, 1636 cm^{-1}(C=N), 3193 cm^{-1}(NH) $\mu_{eff} = 5.52(6)\ \mu_B$.

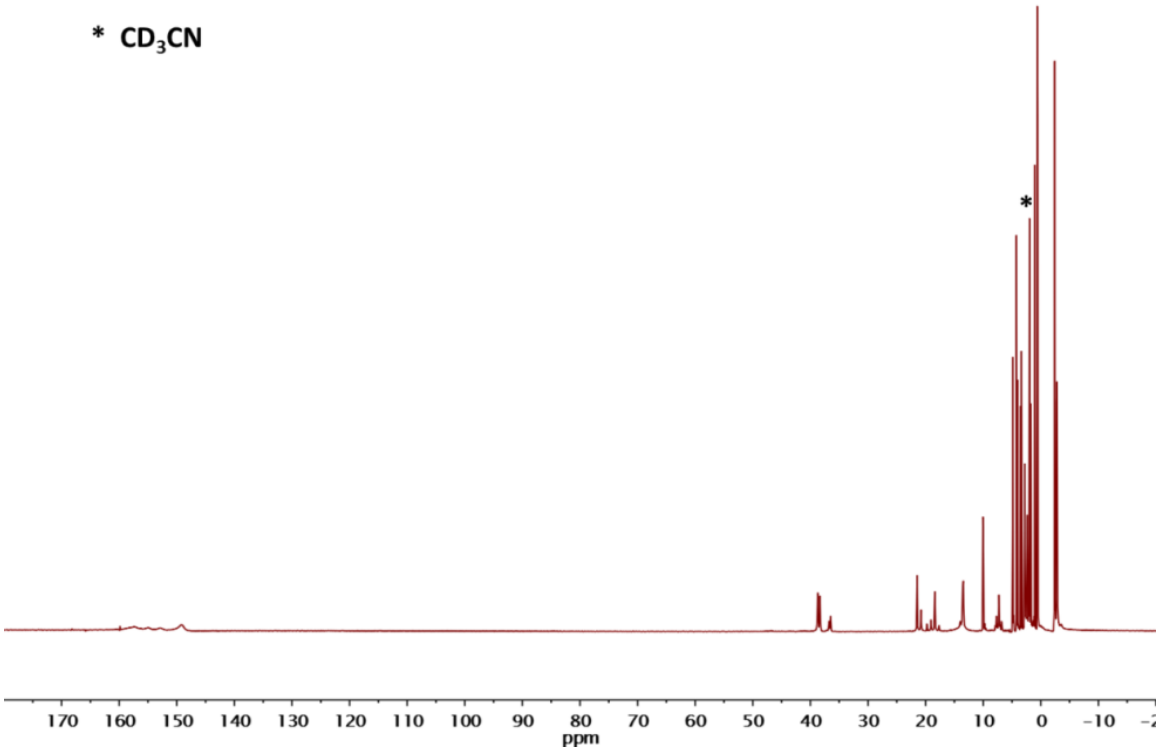

Figure 4.5 ^1H NMR spectrum of $[N(afa^{Mes})_3Fe(OTf)](OTf)$ (CD_3CN, 21°C).

Preparation of $N(afa^{Mes})(pi^{Mes})_2Fe(OH_2)$. $H_3[N(pi^{Mes})_3]$ (0.070 g, 0.101 mmol) was deprotonated by addition of 2.2 eq. KH (0.009 g, 0.22 mmol) to an approximately 10 mL of THF solution. After it was stirred for three hours at room temperature, the mixture was filtered through Celite to remove excess KH. Addition of deprotonated ligand to the $FeCl_2$ (0.013 g, 0.0103 mmol) slurry in THF resulted in a color change from colorless to yellow. After stirring for overnight until all $FeCl_2$ was consumed, the reaction mixture was filtered through Celite to remove KCl and the solvents were removed under reduced pressure. Crystals suitable for X-ray analysis were grown at room temperature from a concentrated solution of THF layered with pentane (0.034g, 45%). Analysis for C45H51FeN7O: Calcd. C, 70.95; H, 6.75; N, 12.87. Found C, 70.59; H, 6.81; N, 12.69, IR: 1643, 1616 cm^{-1} (C=N)

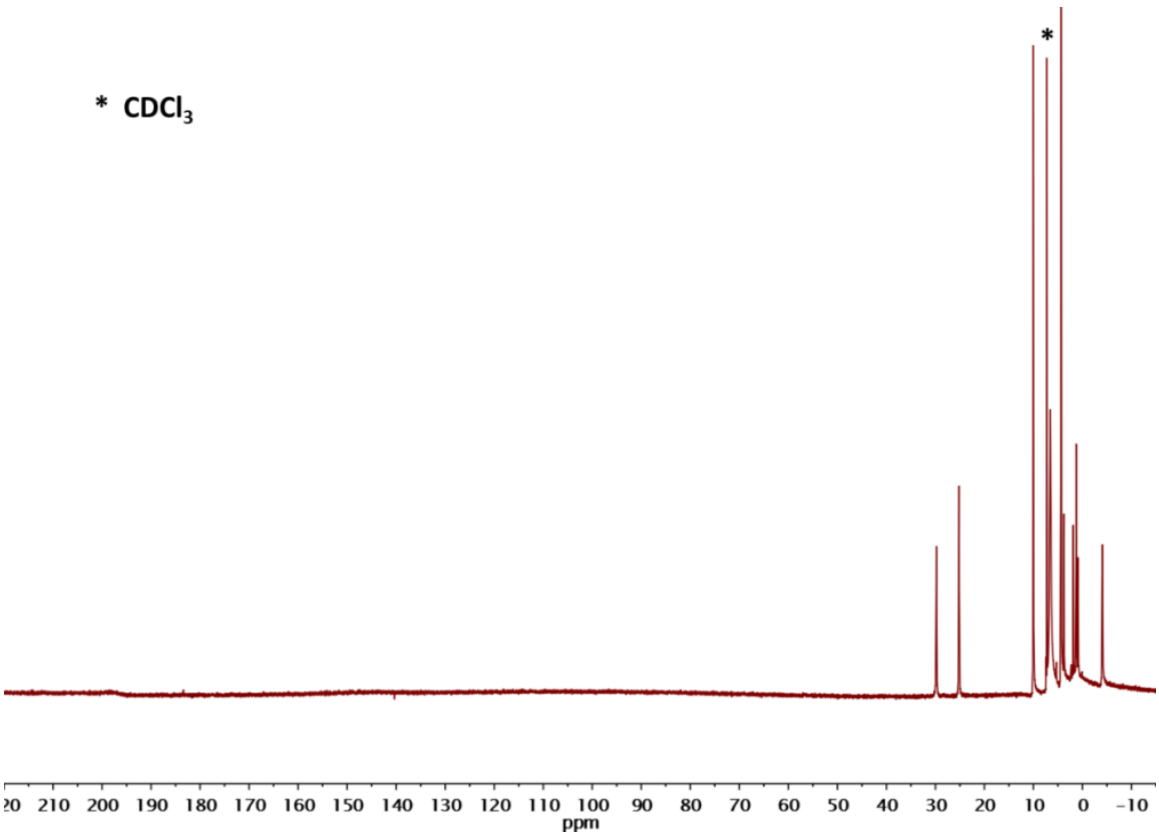

Figure 4.6 ^{1}H NMR spectrum of [N(pi^{Mes})$_3$Fe](OH$_3$) ($CDCl_3$, 21°C).

Alternative Synthesis of [N(afa^{Mes})(pi^{Mes})$_2$Fe(OH$_2$)]. A 20 mL scintillation vial was charged with complex [N(afa^{Mes})$_3$Fe(OTf)]OTf (0.050 g, 0.048 mmol) in an approximately 5 mL of THF. Li_2O (2.5 equiv, 0.0036 g, 0.12 mmol) was added as solid to the aforementioned solution. The mixture was stirred overnight at room temperature, resulting in orange solution. The solution was filtered over Celite to remove excess Li_2O and the solvent was removed under reduced pressure. The residual yellow powder was washed with acetonitrile and dried under vacuum, resulting in an isolation of **3** as orange powder (0.035 g, 0.045 mmol, 94 %), identified via ^{1}H NMR spectroscopy.

Preparation of [N(afa^{Mes})$_2$(Pi^{Mes})FeOH](OTf). A 20 mL scintillation vial was charged with [N(afa^{Mes})$_3$Fe(OTf)]OTf (0.102 g, 0.097 mmol) in an approximately 10 mL of acetonitrile. With vigorous stirring, tetrabutylammonium nitrite ([^{n}Bu$_4$][NO_2]) (0.028 g, 0.100 mmol) was added

as a solid. The mixture was stirred for two hours, after which time solvent was removed under reduced pressure. The product was recrystallized from concentrated THF/benzene solution layered with slow diffusion of diethyl ether (0.068 g, 78 %). Analysis for C46H51O4N7FeS1F3·0.5C5H6: Calcd. C, 61.96; H, 5.73; N, 10.32. Found C, 61.94; H, 5.74; N, 10.14. ^{19}F NMR (CD_3CN, 21 °C): δ = −79.63 (SO_3CF_3). IR: 1634, 1651 cm^{-1} (C=N) μ_{eff} = 5.94(9) μ_B.

One-pot reduction of [N(afa^{Mes})$_2$(Pi^{Mes})FeOH](OTf) to [N(afa^{Mes})$_3$Fe(OTf)]OTf. A 20 mL scintillation vial was charged with [N(afa^{Mes})$_2$(Pi^{Mes})FeOH](OTf) (0.018 g, 0.020 mmol) and DPH (0.022 g, 0.012 mmol) in 3 mL of MeCN. HOTf (0.004 g, 0.032mmol) was added and stirred for 2 hours. In order to quantify the amount of water formed during the reaction, three aliquots of 0.5 mL were removed from the vial using a Hamilton Sample Lock syringe and analyzed by Karl Fischer titration (Table 4.2). The solvent was removed under reduced pressure and the resulting orange oil was washed with diethyl ether and benzene to get rid of azobenzene and unreacted DPH. Characterization by ^{1}H NMR spectroscopy revealed a clean conversion of [N(afa^{Mes})$_2$(Pi^{Mes})FeOH](OTf)to [N(afa^{Mes})$_3$Fe(OTf)]OTf. (0.019 g, 0.0182 mmol, 91 %).

Stepwise Reduction of [N(afa^{Mes})$_2$(Pi^{Mes})FeOH](OTf) to [N(afa^{Mes})$_3$Fe]OTf$_2$.

A-1. Preparation of [N(afa^{Mes})$_3$FeOH](OTf)$_2$ A 20 mL scintillation vial was charged with [N(afa^{Mes})$_2$(Pi^{Mes})FeOH](OTf) (0.018 g, 0.020 mmol) in an approximately 3 mL of MeCN. HOTf (1.5 eq. 0.045 g, 0.03 mmol) was added and stirred for 10 min. The resulting red-brown solution was analyzed by Mass spectrometry using a Hamilton Sample Lock syringe. LRMS (ESI) (m/z): $[M]^{2+}$ calcd. for C45H52FeN7O ([N(afa^{Mes})$_3$FeOH]$^{2+}$) 381.18, found: 381.1. ^{19}F NMR (CD_3CN, 21 °C): δ = −70.70 (SO_3CF_3). IR: 1622, 1649 cm^{-1} (C=N), 3205 cm^{-1} (OH)

A-2. Reduction of [N(afa^{Mes})$_3$FeOH](OTf)$_2$ to [N(afa^{Mes})$_3$Fe(OTf)]OTf. In a solution of [N(afa^{Mes})$_3$FeOH](OTf)$_2$ prepared *in situ*, 0.6 eq. of DPH (0.022 g, 0.012 mmol) was added and stirred for 2 hour. In order to quantify the amount of water formed during the reaction, three aliquots of 0.5 mL were removed from the vial using a Hamilton Sample Lock syringe and analyzed by Karl Fischer titration (Table 4.2). Characterization by ^{1}H NMR spectroscopy confirmed the formation of [N(afa^{Mes})$_3$Fe(OTf)]OTf (0.0155 g, 0.015 mmol,74%).

B-1. Reduction of [N(afa^{Mes})$_3$FeO](OTf) to complex N(afa^{Mes})(pi^{Mes})$_2$Fe(OH$_2$). A 20 mL scintillation vial was charged with [N(afa^{Mes})$_2$(Pi^{Mes})FeOH](OTf) (0.018 g, 0.020 mmol) in an approximately 3 mL of THF. KC_8 (0.0034 g, 26 mmol) was added as a solid and stirred for 10 min. The reaction mixture was filtered over Celite to remove graphite and the solvent was reduced under pressure. The resulting brown solid was dissolved in benzene and filtered over Celite to get rid of KOTf. After the solvent was reduced under pressure, the resulting powder was confirmed the formation of N(afa^{Mes})(pi^{Mes})$_2$Fe(OH$_2$) by ^{1}H NMR spectroscopy (0.0125 g, 0.016 mmol, 82%).

B-2. Reaction of [N(afa^{Mes})(pi^{Mes})$_2$Fe(OH$_2$)] with HOTf to form [N(afa^{Mes})$_3$Fe(OTf)]OTf. A 20 mL scintillation vial was charged with N(afa^{Mes})(pi^{Mes})$_2$Fe(OH$_2$) (0.015 g, 0.020 mmol) in 3 mL of MeCN. HOTf (triflic acid) (2.2 eq. 0.065 g, 0.043 mmol) was added and the reaction was stirred for 30 min. In order to quantify the amount of water formed during the reaction, three aliquots of 0.5 mL were removed from the vial using a Hamilton Sample Lock syringe and analyzed by Karl Fischer titration (Table 4.2). The solution was filtered over Cilite and the solvent was removed under reduced pressure. The yellow oil was washed with benzene to get rid of a small amount of acidified ligand formed during the reaction. Characterization by ^{1}H NMR spectroscopy revealed a conversion of N(afa^{Mes})(pi^{Mes})$_2$Fe(OH$_2$) to [N(afa^{Mes})$_3$Fe(OTf)]OTf (0.019 g, 0.018 mmol, 91%).

Reaction of Complex N(afa^{Mes})(pi^{Mes})$_2$Fe(OH$_2$) with DOTf. A 20 mL scintillation vial was charged with N(afa^{Mes})(pi^{Mes})$_2$Fe(OH$_2$) (0.020 g, 0.026 mmol) in an approximately 0.7 mL of MeCN-d_3. DOTf (deuterium labeled triflic acid) (2.1 eq. 0.008 g, 0.055 mmol) was added and the mixture was stirred for 30 min. The resulting product was confirmed as [N(afa^{Mes})$_3$Fe(OTf)]OTf by ^{1}H NMR spectroscopy. The same reaction was attempted in acetonitrile to take ^{2}H NMR spectroscopy. The reaction mixture was dried and characterized by IR spectroscopy.

Preparation of N(Pi^{Mes})$_3$-*d*$_2$ A 20 mL scintillation vial was charged with H$_3$[N(pi^{Mes})$_3$] (0.035 g, 0.05 mmol) in approximately 5 mL of THF. 2.2 eq. KH (0.009 g, 0.22 mmol) was added to the solution of H$_3$[N(pi^{Mes})$_3$]. After it was stirred for three hours at room temperature, the mixture was filtered through Celite to remove excess KH. DOTf (2.2 eq. 0.0168 g, 0.11mmol) was added

by difference and stirred for 20 min. The solvents were dried under reduced pressure and the resulting powder was washed with acetonitrile. Characterization with ^{1}H and ^{2}H NMR spectroscopy was performed.

Preparation of $^{Mes}Fe^{II}$-OTf -d_2 with of N(Pi^{Mes})$_3$-d_2 A 20 mL scintillation vial was charged with $Fe(OTf)_2(MeCN)_2$ (0.011 g, 0.025 mmol) and approximately 10 mL of tetrahydrofuran. With stirring, $H_3N(pi^{Mes})_3$-d_2 (0.017 g, 0.025 mmol) was added by difference, resulting in an instantaneous color change to orange. The resulting mixture was characterized by both ^{1}H and ^{2}H NMR spectroscopy.

Reaction of $^{Mes}Fe^{II}$-OTf with D_2O A 20 mL scintillation vial was charged with complex $[N(afa^{Mes})_3Fe(OTf)]OTf$ (0.025 g, 0.024 mmol) in an approximately 0.7 mL of acetonitrile. D_2O (1 µl, 0.001 g, 0.05 mmol) was added. After 20 min of stirring, characterization by ^{2}H NMR spectroscopy was performed (Figure 4.7).

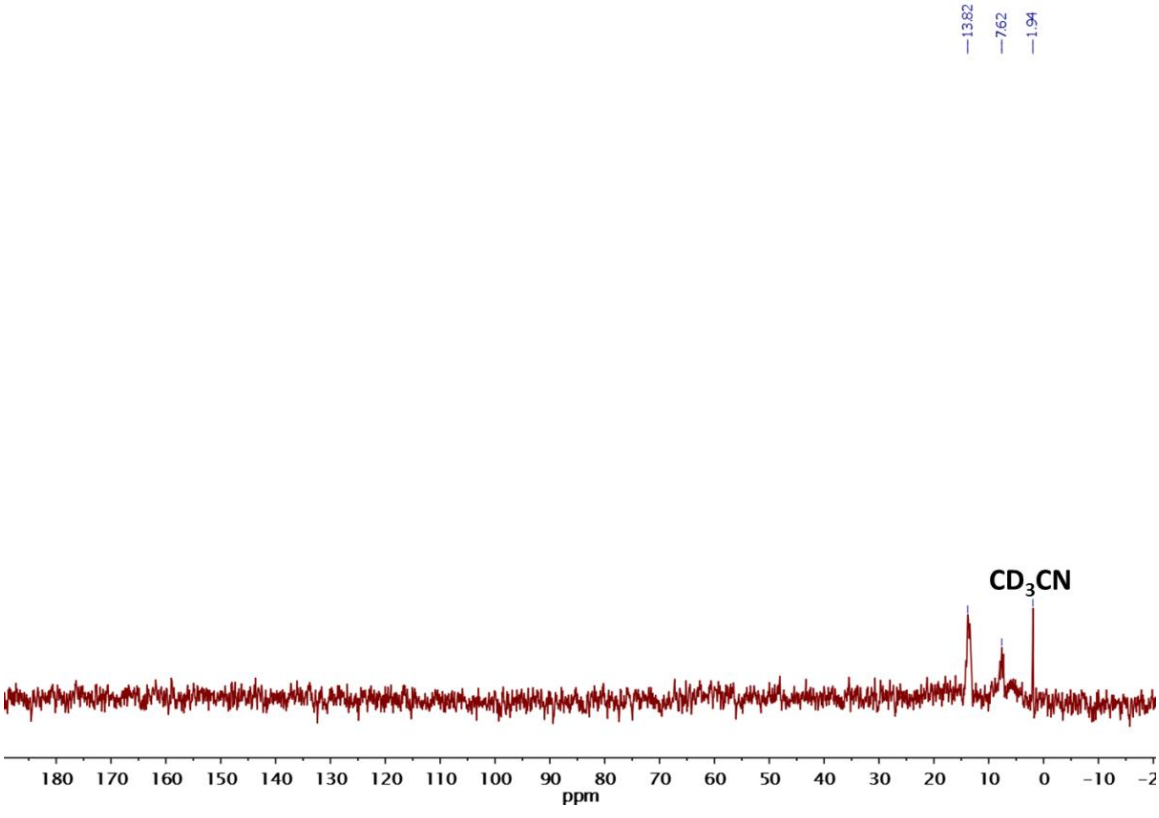

Figure 4.7 ^{2}H NMR spectrum of **$^{Mes}Fe^{II}$-OTf** with D_2O (CH_3CN,21°C).

Procedure for Catalytic Nitrite Reduction with $^{Mes}Fe^{II}$-OTf (Table 4.3, entry 1). A 50 mL three-neck flask was charged with $NaNO_2$ (0.0026 g, 0.038 mmol, 1.25 eq.), 1,2-diphenylhydrazine (0.0056 g, 0.03 mmol, 1 eq.), 15 mg of $MgSO_4$, and 5 mL of acetonitrile. In another 50 mL three-neck flask, cobalt(II) tetraphenylporphyrine (CoTPP) (0.0206 g, 0.03 mmol, 1 eq.) was dissolved in approximately 25 mL of DCM. The 50mL three-neck flasks were connected with tubing and purged with nitrogen for 10 min. $[N(afa^{Mes})_3Fe(OTf)](OTf)$ (0.008 g, 0.0077 mmol, 0.25 eq.) in 1 mL of acetonitrile was added via a Hamilton Sample Lock syringe to the mixture of $NaNO_2$ and 1,2-diphenylhydrazine. After stirring for 10 min, lutidinium triflate (0.0142 g, 0.055 mmol, 1.8 eq.) in 1 mL of acetonitrile was added to the reaction mixture via a Hamilton Sample Lock syringe. 1 mL of aliquot was removed from the solution of CoTPP to analyze the amount of CoTPP-NO after the reaction was stirred for 8 hours. Characterization by ^1H NMR spectroscopy showed that all Co-TPP was converted to CoTPP-NO. Analysis for CoTPP-NO: ^1H NMR ($CDCl_3$, 25°C): δ = 8.91, 8.18, 7.74 ppm. IR = 1693 cm^{-1} (NO).

Procedure for Catalytic Nitrite Reduction with $^{Mes}Fe^{II}$-OTf (0.17 eq.) (Table 4.3, entry 2). A 50 mL three-neck flask was charged with $NaNO_2$ (3.9 g, 0.054 mmol, 1.25 eq.), 1,2-diphenylhydrazine (0.085 g, 0.046 mmol, 1 eq.), 20 mg of $MgSO_4$, and 4.5 mL of acetonitrile. In another 50 mL three-neck flask, cobalt(II) tetraphenylporphyrine (CoTPP) (30.9 g, 0.046 mmol, 1 eq.) was dissolved in approximately 25 mL of DCM. The 50mL three-neck flasks were connected with tubing and purged with nitrogen for 10 min. $[N(afa^{Mes})_3Fe(OTf)](OTf)$ (0.008 g, 0.077 mmol, 0.17 eq.) in 1 mL of acetonitrile was added via a Hamilton Sample Lock syringe to the mixture of $NaNO_2$ and 1,2-diphenylhydrazine. After stirring for 10 min, lutidinium triflate (13.6 g, 0.053 mmol, 1.15 eq.) in 1 mL of acetonitrile was added to the reaction mixture via a Hamilton Sample Lock syringe. After 6.5 hours of stirring, lutidinium triflate (0.008 g, 0.031 mmol, 0.67 eq) in 0.5 mL of acetonitrile was added to the reaction mixture via a Hamilton Sample Lock syringe. 1 mL of aliquot was removed from solution of CoTPP to analyze the amount of CoTPP-NO after the reaction was stirred for 10 hours. Integration by ^1H NMR spectroscopy showed the formation of 85 % of Co-TPP-NO.

Procedure for Catalytic Nitrite Reduction with $[N(afa^{Cy})_3Fe(OTf)]OTf$ (Table 4.3, entry 3). A 50 mL three-neck flask was charged with $NaNO_2$ (0.0026 g, 0.038 mmol, 1.25 eq.), 1,2-

diphenylhydrazine (0.0056 g, 0.03 mmol, 1 eq.), 15 mg of $MgSO_4$, and 5 mL of acetonitrile. In another 50 mL three-neck flask, cobalt(II) tetraphenylporphyrine (CoTPP) (0.0206 g, 0.03 mmol, 1 eq.) was dissolved in approximately 25 mL of DCM. The 50mL three-neck flasks were connected with tubing and purged with nitrogen for 10 min. $[N(afa^{Cy})_3Fe(OTf)](OTf)$ (0.0072 g, 0.0077 mmol, 0.25 eq.) in 1 mL of acetonitrile was added via a Hamilton Sample Lock syringe to the mixture of $NaNO_2$ and 1,2-diphenylhydrazine. After stirring for 10 min, lutidinium triflate (0.0142 g, 0.055 mmol, 1.8 eq.) in 1 mL of acetonitrile was added to the reaction mixture via a Hamilton Sample Lock syringe. 1 mL of aliquot was removed from the solution of CoTPP to analyze the amount of CoTPP-NO after the reaction was stirred for 8 hours. Characterization by ^1H NMR spectroscopy showed that almost 48% of Co-TPP was converted to CoTPP-NO.

Procedure for Control Reaction of Catalytic Nitrite Reduction (8hours, Table 4.3, entry 5). A 50 mL three-neck flask was charged with $NaNO_2$ (0.0026 g, 0.038 mmol, 1.25 eq.), 1,2-diphenylhydrazine (0.0056 g, 0.03 mmol, 1 eq.), 15 mg of $MgSO_4$, and 5 mL of acetonitrile. In another 50 mL three-neck flask, cobalt(II) tetraphenylporphyrine (CoTPP) (0.0206 g, 0.03 mmol, 1 eq.) was dissolved in approximately 25 mL of DCM. The 50mL three-neck flasks were connected with tubing and purged with nitrogen for 10 min. Lutidinium triflate (0.0142 g, 0.055 mmol, 1.8 eq.) in 1 mL of acetonitrile was added to the reaction mixture via a Hamilton Sample Lock syringe. 1 mL of aliquot was removed from the solution of CoTPP to analyze the amount of CoTPP-NO after the reaction was stirred for 8 hours. Characterization by ^1H NMR spectroscopy showed that almost 14% of Co-TPP was converted to CoTPP-NO.

Procedure for Control Reaction of Catalytic Nitrite Reduction (10 hours, Table 4.3, entry 6). A 50 mL three-neck flask was charged with $NaNO_2$ (3.9 g, 0.054 mmol, 1.25 eq.), 1,2-diphenylhydrazine (0.085 g, 0.046 mmol, 1 eq.), 20 mg of $MgSO_4$, and 4.5 mL of acetonitrile. In another 50 mL three-neck flask, cobalt(II) tetraphenylporphyrine (CoTPP) (30.9 g, 0.046 mmol, 1 eq.) was dissolved in approximately 25 mL of DCM. The 50mL three-neck flasks were connected with tubing and purged with nitrogen for 10 min. Lutidinium triflate (13.6 g, 0.053 mmol, 1.15 eq.) in 1 mL of acetonitrile was added to the reaction mixture via a Hamilton Sample Lock syringe. After 6.5 hours of stirring, lutidinium triflate (0.008 g, 0.031 mmol, 0.67 eq) in 0.5 mL of acetonitrile was added to the reaction mixture via a Hamilton Sample Lock syringe. 1 mL

of aliquot was removed from solution of CoTPP to analyze the amount of CoTPP-NO after the reaction was stirred for 10 hours. Integration by ^{1}H NMR spectroscopy showed the formation of 17 % of Co-TPP-NO.

Preparation of $H_3[N(pi^{Mes})_3]$•3HOTf. This preparation was followed the previously reported synthesis of $H_3[N(pi^{Cy})_3]$•3HOTf. A 20 mL scintillation vial was charged with $H_3[N(pi^{Mes})_3]$ (0.011 g, 0.019 mmol) and approximately 0.7 mL of acetonitrile-d_3. Cold HOTf (stored at -35 ºC; 0.009 g, 0.060 mmol) was weighed by difference and added to the suspension. The reaction was stirred at room temperature, resulting in the gradual dissolution of the ligand upon protonation, giving a yellow solution. After stirring for 20 min, solvent was removed *in vacuo* to yield the product, $H_3[N(pi^{Mes})_3]$ • 3HOTf, as a yellow powder, characterized by ^{1}H NMR spectroscopy.

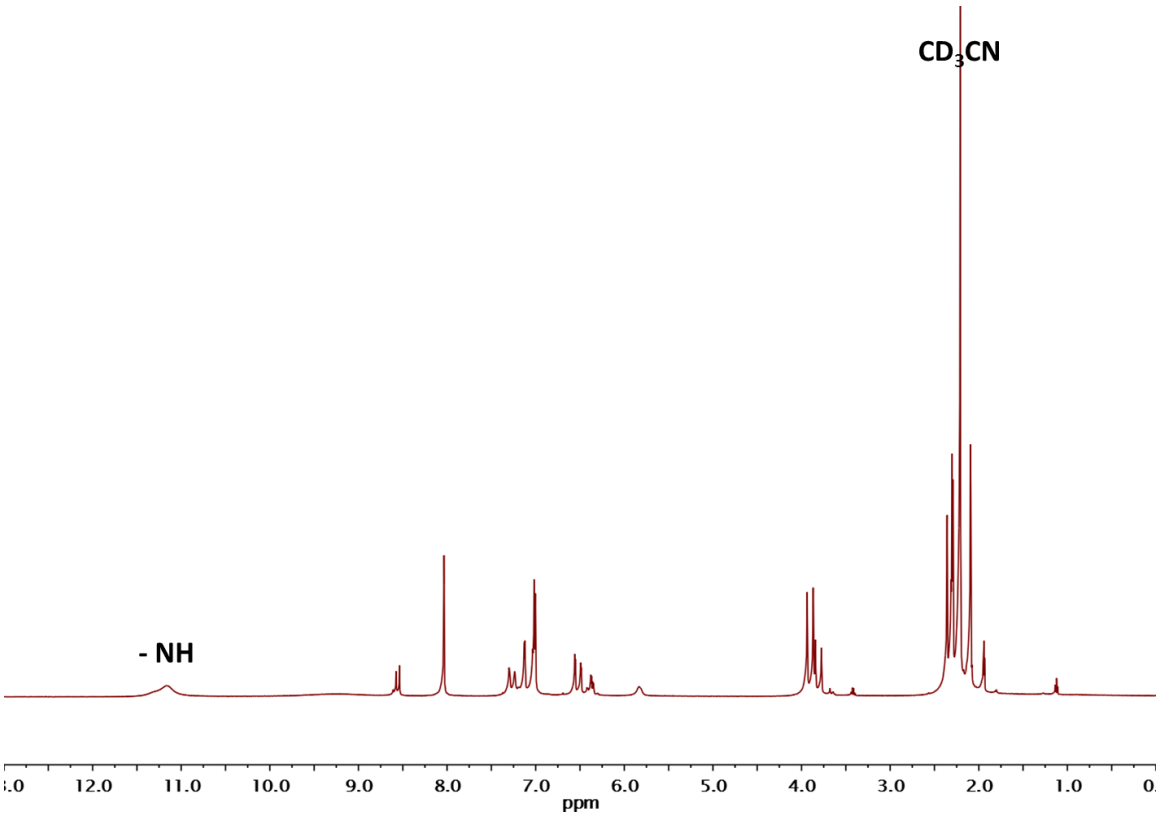

Figure 4.8 ^{1}H NMR spectrum of $H_3[N(pi^{Mes})_3]$•3HOTf (CD_3CN,21°C).

Reaction of $^{Mes}Fe^{II}$-OTf to LuHOTf A 20 mL scintillation vial was charged with complex [N(afa^{Mes})$_3$Fe(OTf)](OTf) (0.006 g, 0.006 mmol) in an approximately 0.7 mL of MeCN-d_3. LuHOTf (7 equiv, 0.0103 g, 0.042 mmol) was added as solid to the aforementioned solution and characterized by ^{1}H NMR spectroscopy (Figure 4.9).

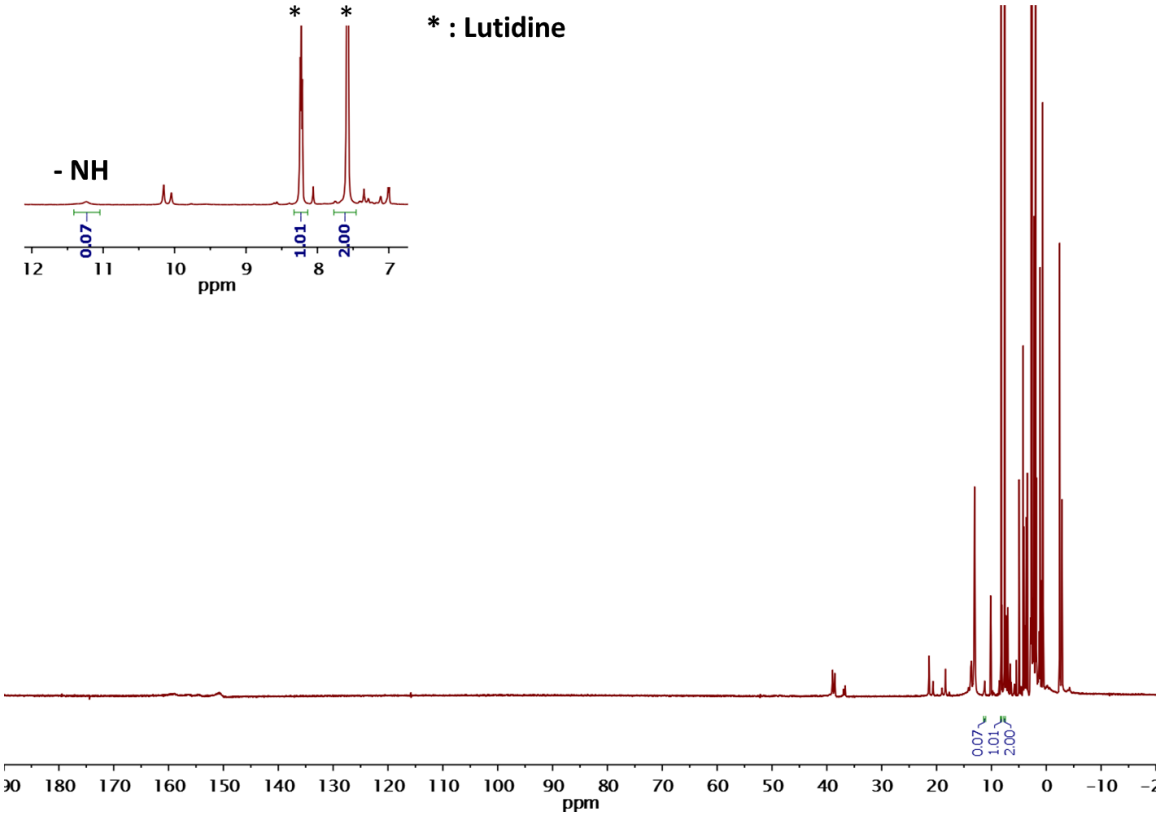

Figure 4.9 ^{1}H NMR spectrum of reaction of $^{Mes}Fe^{II}$-OTf with 7 eq. of LuHOTf (CD_3CN,21°C).

Reaction of [N(afa^{Cy})$_3$Fe(OTf)]OTf with LuHOTf A 20 mL scintillation vial was charged with [N(afa^{Cy})$_3$Fe(OTf)](OTf) (0.054 g, 0.006 mmol) in an approximately 0.7 mL of MeCN-d_3. LuHOTf (7 equiv, 0.0103 g, 0.042 mmol) was added as solid to the aforementioned solution and characterized by ^{1}H NMR spectroscopy (Figure 4.10).

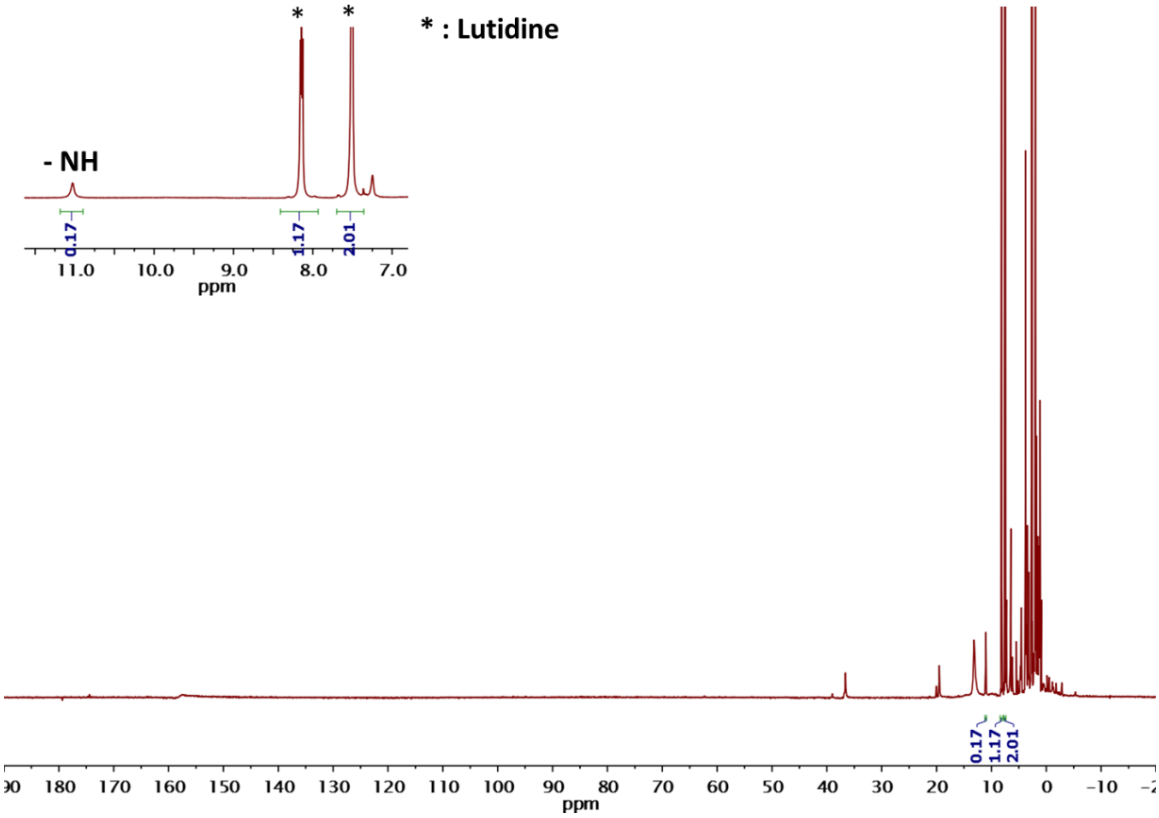

Figure 4.10 ^{1}H NMR spectrum of reaction of [N(afa^{Cy})$_3$Fe(OTf)](OTf) with 7 eq. of LuHOTf (CD_3CN,21°C).

4.5 References

(1) Camargo, J. A.; Alonso, Á. Ecological and Toxicological Effects of Inorganic Nitrogen Pollution in Aquatic Ecosystems: A Global Assessment. *Environ. Int.* **2006**, *32*, 831–849.

(2) Jensen, F. B. Nitrite Disrupts Multiple Physiological Functions in Aquatic Animals. *Comp. Biochem. Physiol. A. Mol. Integr. Physiol.* **2003**, *135*, 9–24.

(3) Buenger, J. W.; Mauro, V. F. Organic Nitrate-Induced Methemoglobinemia. *DICP Ann. Pharmacother.* **1989**, *23*, 283–288.

(4) Fewtrell, L. Drinking-Water Nitrate, Methemoglobinemia, and Global Burden of Disease: A Discussion. *Environ. Health Perspect.* **2004**, *112*, 1371–1374.

(5) Wolff, I. A.; Wasserman, A. E. Nitrates, Nitrites, and Nitrosamines. *Science* **1972**, *177*, 15–19.

(6) Tricker, A. R.; Preussmann, R. Carcinogenic N-Nitrosamines in the Diet: Occurrence, Formation, Mechanisms and Carcinogenic Potential. *Mutat. Res. Toxicol.* **1991**, *259*, 277–289.

(7) Calmels, S.; Ohshima, H.; Bartsch, H. Nitrosamine Formation by Denitrifying and Non-Denitrifying Bacteria: Implication of Nitrite Reductase and Nitrate Reductase in Nitrosation Catalysis. *Microbiology* **1988**, *134*, 221–226.

(8) Gladwin, M. T.; Schechter, A. N.; Kim-Shapiro, D. B.; Patel, R. P.; Hogg, N.; Shiva, S.; Cannon, R. O.; Kelm, M.; Wink, D. A.; Espey, M. G.; *et al.* The Emerging Biology of the Nitrite Anion. *Nat. Chem. Biol.* **2005**, *1*, 308–314.

(9) Omar, S. A.; Webb, A. J. Nitrite Reduction and Cardiovascular Protection. *J. Mol. Cell. Cardiol.* **2014**, *73*, 57–69.

(10) Heinecke, J.; Ford, P. C. Mechanistic Studies of Nitrite Reactions with Metalloproteins and Models Relevant to Mammalian Physiology. *Coord. Chem. Rev.* **2010**, *254*, 235–247.

(11) Zahran, Z. N.; Chooback, L.; Copeland, D. M.; West, A. H.; Richter-Addo, G. B. Crystal Structures of Manganese- and Cobalt-Substituted Myoglobin in Complex with NO and Nitrite Reveal Unusual Ligand Conformations. *J. Inorg. Biochem.* **2008**, *102*, 216–233.

(12) Cutruzzola, F.; Brown, K.; Wilson, E. K.; Bellelli, A.; Arese, M.; Tegoni, M.; Cambillau, C.; Brunori, M. The Nitrite Reductase from Pseudomonas Aeruginosa: Essential Role of Two Active-Site Histidines in the Catalytic and Structural Properties. *Proc. Natl. Acad. Sci.* **2001**, *98*, 2232–2237.

(13) Williams, P. A.; Fülöp, V.; Garman, E. F.; Saunders, N. F.; Ferguson, S. J.; Hajdu, J. Haem-Ligand Switching during Catalysis in Crystals of a Nitrogen-Cycle Enzyme. *Nature* **1997**, *389*, 406–412.

(14) Yi, J.; Orville, A. M.; Skinner, J. M.; Skinner, M. J.; Richter-Addo, G. B. Synchrotron X-Ray-Induced Photoreduction of Ferric Myoglobin Nitrite Crystals Gives the Ferrous Derivative with Retention of the O-Bonded Nitrite Ligand. *Biochemistry (Mosc.)* **2010**, *49*, 5969–5971.

(15) Sundararajan, M.; Neese, F. Distal Histidine Modulates the Unusual O-Binding of Nitrite to Myoglobin: Evidence from the Quantum Chemical Analysis of EPR Parameters. *Inorg. Chem.* **2015**, *54*, 7209–7217.

(16) Ranghino, G.; Scorza, E.; Sjögren, T.; Williams, P. A.; Ricci, M.; Hajdu, J. Quantum Mechanical Interpretation of Nitrite Reduction by Cytochrome *Cd* $_1$ Nitrite Reductase from *Paracoccus Pantotrophus* †. *Biochemistry (Mosc.)* **2000**, *39*, 10958–10966.

(17) Matson, E. M.; Park, Y. J.; Fout, A. R. Facile Nitrite Reduction in a Non-Heme Iron System: Formation of an Iron(III)-Oxo. *J. Am. Chem. Soc.* **2014**, *136*, 17398–17401.

(18) Suslick, K. S.; Watson, R. A. Photochemical Reduction of Nitrate and Nitrite by Manganese and Iron Porphyrins. *Inorg. Chem.* **1991**, *30*, 912–919.

(19) Sanders, B. C.; Hassan, S. M.; Harrop, T. C. NO_2^- Activation and Reduction to NO by a Nonheme $Fe(NO_2)_2$ Complex. *J. Am. Chem. Soc.* **2014**, *136*, 10230–10233.

(20) Moore, C. M.; Szymczak, N. K. Nitrite Reduction by Copper through Ligand-Mediated Proton and Electron Transfer. *Chem Sci* **2015**, *6*, 3373–3377.

(21) Hörold, S.; Vorlop, K.-D.; Tacke, T.; Sell, M. Development of Catalysts for a Selective Nitrate and Nitrite Removal from Drinking Water. *Catal. Today* **1993**, *17*, 21–30.

(22) Gao, W.; Chen, J.; Guan, X.; Jin, R.; Zhang, F.; Guan, N. Catalytic Reduction of Nitrite Ions in Drinking Water over Pd–Cu/TiO2 Bimetallic Catalyst. *Catal. Today* **2004**, *93–95*, 333–339.

(23) Lee, J.; Hur, Y. G.; Kim, M.-S.; Lee, K.-Y. Catalytic Reduction of Nitrite in Water over Ceria- and Ceria–zirconia-Supported Pd Catalysts. *J. Mol. Catal. Chem.* **2015**, *399*, 48–52.

(24) Matson, E. M.; Bertke, J. A.; Fout, A. R. Isolation of Iron(II) Aqua and Hydroxyl Complexes Featuring a Tripodal H-Bond Donor and Acceptor Ligand. *Inorg. Chem.* **2014**, *53*, 4450–4458.

(25) Park, Y. J.; Matson, E. M.; Nilges, M. J.; Fout, A. R. Exploring Mn–O Bonding in the Context of an Electronically Flexible Secondary Coordination Sphere: Synthesis of a Mn(III)–oxo. *Chem Commun* **2015**, *51*, 5310–5313.

(26) Hall, H. K. Correlation of the Base Strengths of Amines [1]. *J. Am. Chem. Soc.* **1957**, *79*, 5441–5444.

(27) Dean, J. A. *Handbook of Organic Chemistry*; McGraw-Hill handbooks; McGraw-Hill Book Co.: New York, 1987.

(28) Matson, E. M.; Gordon, Z.; Lin, B.; Nilges, M. J.; Fout, A. R. Meridional vs. Facial Coordination Geometries of a Dipodal Ligand Framework Featuring a Secondary Coordination Sphere. *Dalton Trans* **2014**, *43*, 16992–16995.

(29) Jeffrey, G. A. *An Introduction to Hydrogen Bonding*; Topics in physical chemistry; Oxford University Press: New York, 1997.

(30) Laine, P.; Gourdon, A.; Launay, J.-P.; Tuchagues, J.-P. Chemistry of Iron with Dipicolinic Acid. 3. Heptacoordinated Iron in [(dipicH)2FeII(OH2)] and [(dipic)2FeII2(OH2)6].cntdot.2dipicH2. *Inorg. Chem.* **1995**, *34*, 5150–5155.

(31) MacBeth, C. E.; Gupta, R.; Mitchell-Koch, K. R.; Young, V. G.; Lushington, G. H.; Thompson, W. H.; Hendrich, M. P.; Borovik, A. S. Utilization of Hydrogen Bonds To Stabilize M−O(H) Units: Synthesis and Properties of Monomeric Iron and Manganese Complexes with Terminal Oxo and Hydroxo Ligands. *J. Am. Chem. Soc.* **2004**, *126*, 2556–2567.

(32) Mukherjee, J.; Lucas, R. L.; Zart, M. K.; Powell, D. R.; Day, V. W.; Borovik, A. S. Synthesis, Structure, and Physical Properties for a Series of Monomeric Iron(III) Hydroxo Complexes with Varying Hydrogen-Bond Networks. *Inorg. Chem.* **2008**, *47*, 5780–5786.

(33) Yeh, C.-Y.; Chang, C. J.; Nocera, D. G. “Hangman” Porphyrins for the Assembly of a Model Heme Water Channel. *J. Am. Chem. Soc.* **2001**, *123*, 1513–1514.

(34) Jonassen, H. B.; Paukert, T.; Henry, R. A. Infrared Spectra of Some 5-Aminotetrazoles and Their Deuterated Derivatives. *Appl. Spectrosc.* **1967**, *21*, 89–91.

(35) Limbach, H.-H. IR-Spectroscopic Study of Isotope Effects on the NH/ND-Stretching Bands of Meso-Tetraphenylporphine and Vibrational Hydrogen Tunneling. *J. Chem. Phys.* **1983**, *78*, 5432.

(36) Hagen, K. S. Iron(II) Triflate Salts as Convenient Substitutes for Perchlorate Salts: Crystal Structures of $[Fe(H_2O)_6](CF_3SO_3)_2$ and $Fe(MeCN)_4(CF_3SO_3)_2$. *Inorg. Chem.* **2000**, *39*, 5867–5869.

(37) Weitz, I. S.; Rabinovitz, M. The Application of C8K for Organic Synthesis: Reduction of Substituted Naphthalenes. *J. Chem. Soc. [Perkin 1]* **1993**, 117.

(38) Curley, J. J.; Bergman, R. G.; Tilley, T. D. Preparation and Physical Properties of Early-Late Heterobimetallic Compounds Featuring Ir–M Bonds (M = Ti, Zr, Hf). *Dalton Trans* **2012**, *41*, 192–200.

Chapter 5

Catalytic nitrate reduction utilizing biomimetic iron complex featuring secondary coordination sphere†

5.1 Introduction

Inorganic nitrate (NO_3^-) is extensively harnessed in many industrial fields including fertilizers, explosives or meat curing processes.[1,2] Because of its high solubility and mobility in water, however, it is considered a major contaminant in drinking water, causing many environmental and health problems.[3–6] Similar to the function of nitrite described in Chapter 4, high concentrations of nitrate in the body can also cause hemoglobin to form oxygen-carrying metalloprotein, methemoglobin, resulting in loss of its ability to carry oxygen.[5] Although its impact on healthy adults is less significant, high levels of nitrate have been related to blue baby syndrome, which can eventually lead to infant death.[5] Moreover, nitrate in groundwater can threaten living organisms in both freshwater and marine systems.[4,7] Thus, remediation of polluted water by reduction of nitrate would have tremendous impact.

The most efficient reduction of nitrate to nitrite is achieved by the microbial metalloenzymes nitrate reductases containing molybdenum center (Figure 5.1), which use this inorganic oxidant as a terminal electron acceptor during anaerobic respiration.[8–11] In the X-ray crystal structure of nitrate reductase, hydrogen bond interactions from alanine and glycine amino acids stabilize the axial oxygen ligand.[9] Moreover, mutation studies revealed that extensive hydrogen bonding networks between two reaction centers are responsible for electron transfers for enzymatic activity.[8] Nitrite is then reduced to nitric oxide by heme containing metalloenzymes including cytochrome *cd1* nitrite reductase, hemoglobin, or myoglobin (Figure 5.1).[12] These enzymes also feature hydrogen bonding networks in the protein scaffold that facilitate the movement of protons and water molecule around the active site and stabilize reactive intermediates (discussed in Chapter 4).

† Portions of this chapter are reproduced from the following publication with permission from the authors. Ford, C. L.*; Park, Y. J.*; Matson, E. M.; Gordon, Z.; Fout, A. R. *Science*, **2016**, *354*, 741-743.

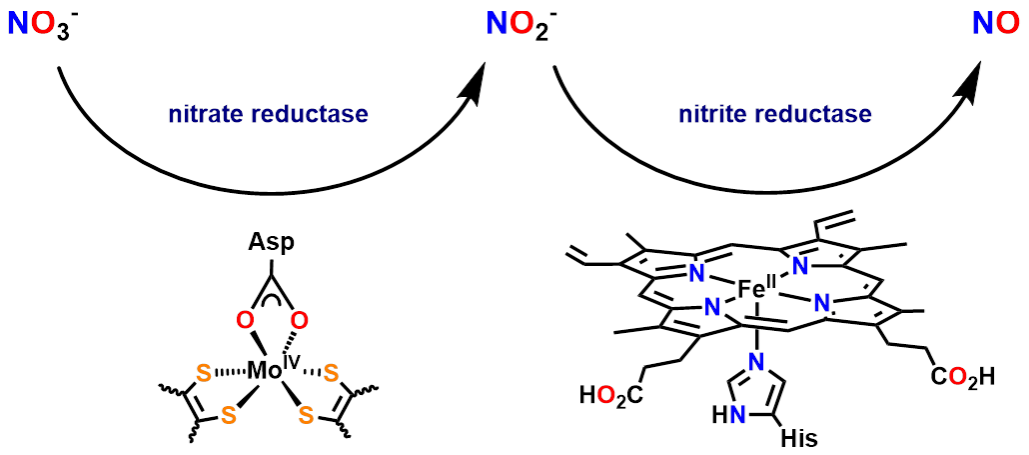

Figure 5.1 Biological processes of nitrate and nitrite reduction.

In synthetic inorganic systems, nitrate reduction has been challenging because of its unfavorable reduction potential as well as its low binding affinity for the transition metal centers. Previous examples of nitrate reduction are limited and typically require to adopt harsh conditions such as low pH, photolysis, or electrocatalysis in both homogeneous and heterogeneous systems.[13–17] Thus, incorporating these secondary sphere interactions into transition metal complexes is expected to aid in nitrate reactivity.

In Chapter 4, a homogeneous inorganic system capable of catalytic nitrite reduction was developed and demonstrated.[18] Given the success of nitrite reduction with our system, we turned our attention to the more difficult three-electrons reduction of nitrate, hypothesizing that the hydrogen bonding interactions in our platform would facilitate the desired reactivity. In this chapter, stoichiometric nitrate reduction with Fe(II) complex, $[N(afa^{Cy})_3FeOTf]OTf$, is described. Using a similar strategy to that in our catalytic nitrite reduction, catalytic nitrate reduction is discussed, which represent the first example of catalytic nitrate reduction to NO and water by a first-row transition metal complex in homogeneous system.

5.2 Results and discussion

5.2.1 Stoichiometric nitrate reduction

As shown previously, the addition of tetrabutylammonium nitrite ($[NBu_4][NO_2]$) to 2 equiv of $[N(afa^{Cy})_3FeOTf]OTf$ (**Fe^{II}-OTf**) afforded the iron(III)-oxo complex, $[N(afa^{Cy})_3FeO]OTf$ (**Fe^{III}-O**) and NO (g), which was trapped by **Fe^{II}-OTf** to furnish the iron(II)-nitrosyl species, $[N(afa^{Cy})_3FeNO]OTf_2$ (**Fe^{II}-NO**).[18] Given the facile one-electron reduction of

nitrite by **Fe^{II}-OTf**, nitrate reduction was then explored. We hypothesized that if the **Fe^{II}-OTf** could perform the two-electron reduction of nitrate to generate nitrite, the reduction of nitrite would then proceed as before to release NO (g).

The addition of 1 equiv of [Bu_4N][NO_3]to **Fe^{II}-OTf** resulted in an immediate reaction, as indicated by a color change from yellow to dark brown. Analysis of the crude reaction mixture by ^{1}H NMR spectroscopy revealed the formation of several products: the previously characterized **Fe^{III}-O** complex, another paramagnetic iron-containing species characterized as **Fe^{III}-OH**, and protodemetallated ligand. The presence of protodemetallated and the loss of a triflate counteranion for the formation of the **Fe^{III}-O** suggested the formation of acid during the nitrate reduction. Accordingly, trimethylamine was added to trap any acid formed during nitrate reduction to generate **Fe^{III}-O** cleanly.

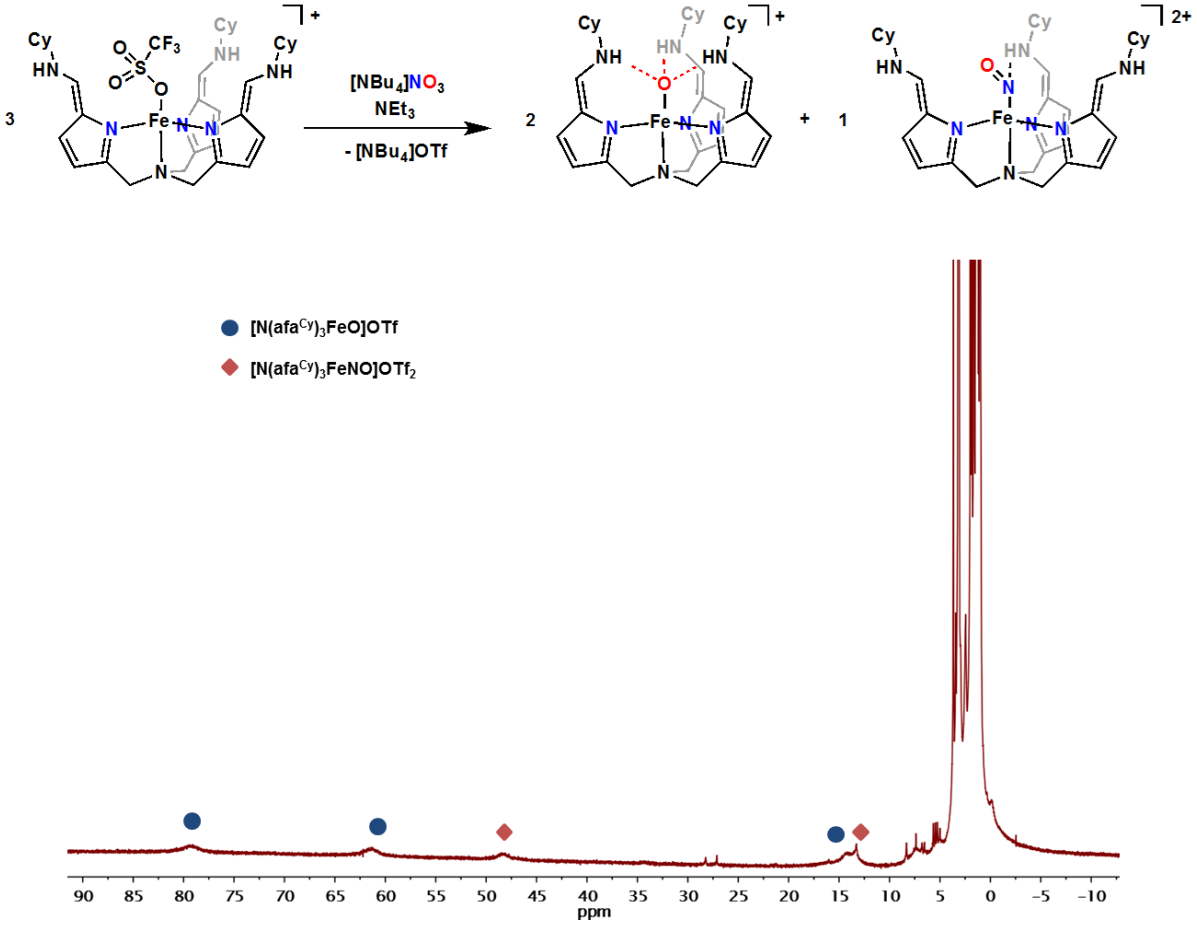

Figure 5.2 Nitrate reduction affords **Fe^{III}-O** and **Fe^{II}-NO**.

When $[NBu_4][NO_3]$ was added to 3 equiv of **Fe^{II}-OTf** in the presence of triethylamine, **Fe^{III}-O** and **Fe^{II}-NO** were formed cleanly, with two-thirds of the isolated product being **Fe^{III}-O** and one-third of **Fe^{II}-NO** (67% and 28% isolated yield, respectively, based on the initial mass of **Fe^{II}-OTf** (Figure 5.2).

5.2.2 Catalytic nitrate reduction

The reduction of **Fe^{III}-O** was investigated to test the possibility that **Fe^{II}-OTf** could be regenerated with concomitant release of water in a similar way of $[N(afa^{Mes})_2(pi^{Mes})Fe(OH)]OTf$ reduction, where two protons and one electron were required. While the method described in the previous chapter utilized LuHOTf and 0.5 eq. of DPH (a $2H^+/2e^-$ source), in this work, DPH and Fc*OTf (as a sacrificial oxidant; Fc*OTf is decamethylferrocenium triflate) were employed due to the instability of **Fe^{II}-OTf** under acidic condition. The reduction of **Fe^{III}-O** resulted in the formation of **Fe^{II}-OTf** in 74% isolated yield, along with the formation of 0.89 equiv of water, as assayed by Karl Fischer titration (Figure 5.3, Table 5.1). Similarly, when **Fe^{III}-O** was generated *in situ* from 0.5 equiv of $NaNO_3$ and reduced under identical conditions, the formation of 0.83 equiv of water was observed by Karl-Fisher titration (Table 5.1).

Having shown that **Fe^{III}-O** is cleanly regenerated with DPH/Fc*OTf, we examined the possibility that the nitrate deoxygenation could be catalytic. A complete reduction of 1 equiv nitrate to nitric oxide and 2 equiv of water requires 3 e^- and $4H^+$, corresponding to 2 equiv of DPH and 1 equiv of Fc*OTf . Using (TPP)Co (TPP, 5,10,15,20-tetraphenylporphyrin) to trap and subsequently quantify the NO(g) produced during the reaction,[19] we tested the reactivity of 3 equiv of $NaNO_3$ (relative to (TPP)Co), 6 equiv of DPH, and 3 equiv of Fc*OTf as a control reaction for nitrate reduction. The amount of (TPP)CoNO formed was quantified by ^1H NMR spectroscopy revealed that NO(g) is produced under these conditions; 0.18 equiv of (TPP)CoNO were detected after 27 hours and 0.24 equiv of (TPP)CoNO after 42 hours (2 equiv of (TPP)CoNO represents a quantitative reaction). When **Fe^{II}-OTf** was added to the reaction mixture over seven times the amount of NO(g) was trapped by (TPP)Co as compared to the control reaction; 1.46 equiv of (TPP)CoNO was detected after 27 hours and 1.74 equiv of (TPP)CoNO after 42 hours resulting in a turnover number (TON, TON is calculated as the number of times the iron catalyst cycles from **Fe^{II}-OTf** to **Fe^{III}-O** and back, based on the NO

formed) of 3.5 (Figure 5.3). Although the TON is modest, this catalytic reaction sequence is the first example of catalytic nitrate reduction by a homogenous system.

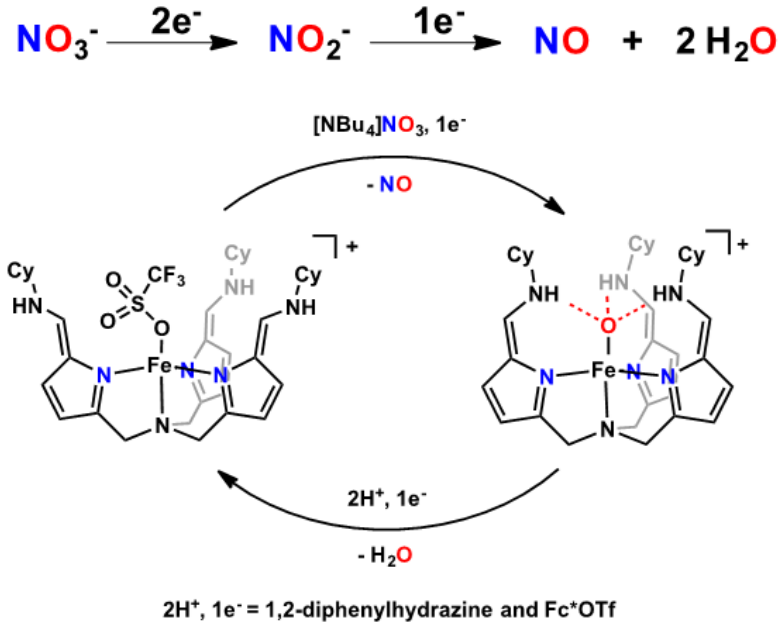

Figure 5.3 Scheme of catalytic nitrate reduction.

5.3. Conclusion

Homogenous first-row transition metal systems that catalytically reduce nitrate are very rare. As demonstrated in the Chapter 4 and this chapter, having the flexible secondary coordination sphere capable of shuttling protons in the metal complex enabled us to perform catalytic reduction of nitrogen-containing oxyanions such as nitrite and nitrate, suggesting that the role of intramolecular interactions in our complexes resembles that of metalloenzymes. Given the concerns caused by nitrogen-containing anions in environmental systems, we expect that this study will provide promising concepts for the design of catalyst for the remediation of nitrite and nitrate.

5.4 Experimental section

General Considerations. To avoid contact with oxygen and water, all manipulations were carried out under an atmosphere of nitrogen in an MBraun inert atmosphere drybox or using

standard Schlenk techniques. Solvents for air- and moisture-sensitive manipulations were dried and deoxygenated using a Glass Contour System (SG Water USA, Nashua, NH) and stored over 4Å molecular sieves purchased from Strem prior to use. Celite 545 (J. T. Baker) was heated to 150°C under dynamic vacuum for 24 h prior to use in the drybox. Sodium nitrate, trifluoromethanesulfonic acid, and ferrocene were purchased from Sigma Aldrich and used as received. Tetrabutylammonium nitrate was purchased from Sigma Aldrich and recrystallized from tetrahydrofuran and hexane under an inert atmosphere prior to use. 1,2-Diphenylhydrazine was purchased from Oakwood Chemical and recrystallized from diethyl ether and hexane under an inert atmosphere prior to use. Triethylamine was purchased from Sigma Aldrich, distilled, and stored over 4Å molecular sieves prior to use. Cobalt(II) tetraphenylporphyrin was purchased from Frontier Scientific and used as received. 1,2,3,4,5-Pentamethylcyclopentadiene was purchased from TCI Chemicals and used as received. Ferrous trifluoromethanesulfonate and decamethylferrocene were prepared according to literature procedure. $H_3[N(pi^{Cy})_3]$ and $[N(afa^{Cy})_3Fe(OTf)](OTf)$ were synthesized according to literature procedure. NMR solvents (acetonitrile-d_3 and chloroform-d_1) were purchased from Cambridge Isotope Laboratories, degassed, and stored over 4Å molecular sieves prior to use. NMR spectra were recorded at ambient temperature on a Varian spectrometer operating at 400 or 500 MHz (^{1}H NMR) and referenced to the peak of the residual solvent (δ parts per million and J in Hz). Solid-state infrared spectra were measured using a PerkinElmer Frontier FT-IR spectrophotometer equipped with a KRS5 thallium bromide/iodide universal attenuated total reflectance accessory. The quantification of water was performed by an Aquatest CMA Karl Fischer Coulometric Titrator from Photovolt Instruments with HYDRANAL from Fluka Analytical.

Synthesis of Decamethylferrocenium Triflate. Decamethylferrocenium triflate was prepared by modifying the synthetic method reported for ferrocenium triflate.[20] A 20 mL scintillation vial was charged with decamethylferrocene (0.013 g, 0.04 mmol) and approximately 5 mL of tetrahydrofuran. After the reaction was cooled to -35°C, AgOTf (0.011 g, 0.043 mmol) was added as a solid. The reaction was stirred for 1 h and filtered. The resulting green powder was washed with tetrahydrofuran three times, yielding green crystalline power (0.0175 g, 0.0368 mmol, 92%). Analysis for $C_{21}H_{30}FeF_3SO_3$: Calcd. C, 53.06; H, 6.36; N, 0. Found C, 52.91; H,

6.16; N, 0.32%. ^{1}H NMR (CD_3CN, 500 MHz, 21°C): δ = -37.29 ppm. ^{19}F NMR (CD_3CN, 470 MHz, 21°C): δ = -79.82 ppm.

Procedure for Stoichiometric Nitrate Reduction. A 20 mL scintillation vial was charged with [N(afa^{Cy})$_3$Fe(OTf)](OTf) (0.0500 g, 0.0534 mmol) and 5 mL of acetonitrile. Tetrabutylammonium nitrate (0.0055 g, 0.0180 mmol) was added as a solid, followed by triethylamine (0.0054 g, 0.0534 mmol) dissolved in 2 mL acetonitrile. The reaction was stirred overnight. Volatiles were removed under reduced pressure and the resulting brown powder was washed with diethyl ether. The addition of 3 mL of tetrahydrofuran and 1 mL of diethyl ether to the brown powder allowed for the separation of [N(afa^{Cy})$_3$FeO](OTf) and [N(afa^{Cy})$_3$FeNO](OTf)$_2$. [N(afa^{Cy})$_3$FeO](OTf) was isolated as powder by filtration of the mixture (0.0290 g, 0.0361 mmol, 67%) whereas [N(afa^{Cy})$_3$FeNO](OTf)$_2$ was soluble in the tetrahydrofuran/diethyl ether mixture. The filtrate was then concentrated under reduced pressure and yielded [N(afa^{Cy})$_3$FeNO](OTf)$_2$ (0.0125 g, 0.0129 mmol, 28%).

When the reaction was completed without the addition of triethylamine, a mixture of 2 paramagnetic iron-containing species, one of which was identified as [N(afa^{Cy})$_3$FeO]OTf, and protodemetallated ligand (N(pi^{Cy})$_3$ • 3HOTf; see preparation and characterization above) were observed by ^{1}H NMR spectroscopy (see Fig. S2 for the diamagnetic window of the ^{1}H NMR spectrum).

Reduction of [N(afa^{Cy})$_3$FeO]OTf with 1,2-Diphenylhydrazine and Decamethylferrocenium Triflate. A 20 mL scintillation vial was charged with [N(afa^{Cy})$_3$FeO]OTf (0.015 g, 0.019 mmol), 1,2-diphenylhydrazine (0.0040 g, 0.021 mmol), decamethylferrocenium trifalte (0.0102 g, 0.021 mmol), 2 mL of acetonitrile, and 1 mL of benzene. The reaction was stirred overnight and concentrated under reduced pressure. The ^{1}H NMR spectrum of crude reaction mixture showed conversion to N(afa^{Cy})$_3$Fe(OTf)$_2$. The solid was washed with diehthyl ether and a mixture of dichloromethane and diethyl ether (1:2) was added to the vial, which was stored at -35° C. N(afa^{Cy})$_3$Fe(OTf)$_2$ was precipitated from the solution overnight (0.0131 g, 0.0146 mmol, 77%). The reaction was repeated and the amount of water formed was quantified by Karl Fischer titration (89%, Table 5.1).

Control Reaction of $N(afa^{Cy})_3Fe(OTf)_2$ with 1,2-Diphenylhydrazine. A 20 mL scintillation vial was charged with $[N(afa^{Cy})_3Fe(OTf)](OTf)$ (0.0281 g, 0.0300 mmol), 1,2-diphenylhydrazine (0.0221 g, 0.120 mmol), $MgSO_4$ (10 mg), and 5 mL of acetonitrile. The reaction was stirred overnight and filtered over Celite. The resulting orange solution was concentrated under reduced pressure. Analysis by ^1H NMR spectroscopy revealed a mixture of the unreacted starting materials.

Procedure for Karl Fischer Titration of Stoichiometric Nitrate Reduction. A 20 mL scintillation vial was charged with $[N(afa^{Cy})_3Fe(OTf)](OTf)$ (0.0234 g, 0.025 mmol), $NaNO_3$ (0.0011 g, 0.013 mmol), 1,2-diphenylhydrazine (0.0046 g, 0.025 mmol), decamethylferrocenium triflate (0.0118 g, 0.025 mmol), 3 mL of acetonitrile, and 1.5 mL of benzene. The reaction vial was sealed with tape and stirring was continued for 16 h. Three aliquots of 0.3 mL were removed from the vial using a gas-tight syringe and analyzed immediately by Karl Fischer titration. The background water content was analyzed by repeating the reaction without $N(afa^{Cy})_3Fe(OTf)_2$ (Table 5.1).

Table 5.1 Quantification of H_2O by Karl Fischer titration (in µg) for the stoichiometric reduction of $[N(afa^{Cy})_3FeO]OTf$ by 0.5 equiv DPH and the stoichiometric reductions of $NaNO_3$ by $[N(afa^{Cy})_3FeOTf]OTf$.

		Fe^{III}-O	**$NaNO_3$**
Background (1.0 mL)		11.5	10.5
		10.2	9.8
		8.9	14.8
	Average:	10.2±1.3	11.7 ± 2.7
Reaction Mixture (0.5 mL of Fe^{III}-O, 0.3 mL of $NaNO_3$, 0.4 mL of $[NBu_4][ClO_4]$)		55.4	27.8
		58.1	27.7
		53.3	29.6
	Average:	55.6±2.4	28.4 ± 1.1
	Less Background:	50.5±2.7	24.9 ± 2.9
	Equiv H_2O Detected:	0.89	0.83

Procedure for Catalytic Nitrate Reduction. A 50 mL three-neck flask was charged with $NaNO_3$ (0.0043 g, 0.05 mmol, 3.5 eq.), 1,2-diphenylhydrazine (0.015 g, 0.08 mmol, 6 eq.), 15

mg of $MgSO_4$, 6 mL of acetonitrile, and 4 mL of benzene. In another 50 mL three-neck flask, cobalt(II) tetraphenylporphyrin (CoTPP) (0.0142 g, 0.021 mmol, 1.5 eq.) was dissolved in 25 mL of DCM. The 50mL three-neck flasks were connected with tubing and purged with nitrogen for 10 min. $[N(afa^{Cy})_3Fe(OTf)](OTf)$ (0.0135 g, 0.014 mmol, 1eq.) in 1 mL of acetonitrile was added via an air-tight syringe to the mixture of $NaNO_3$ and 1,2-diphenylhydrazine. Decamethylferrocenium triflate (0.0195 g, 0.04 mmol, 3 eq.) in 1 mL of acetonitrile was added to the reaction mixture via an air-tight syringe. Aliquots of the solution of CoTPP (1 mL) were analyzed after 27 h and 42 h to quantify the amount of CoTPP-NO that had formed. Integration of ^1H NMR spectra of the aliquots showed conversion of 73% of the Co-TPP to CoTPP-NO after 27 h and 87% after 42 h (Figure 5.4). Analysis for CoTPP-NO (*26*): ^1H NMR ($CDCl_3$, 25°C): δ = 8.91, 8.18, 7.74 ppm. IR = 1693 cm^{-1} (NO).

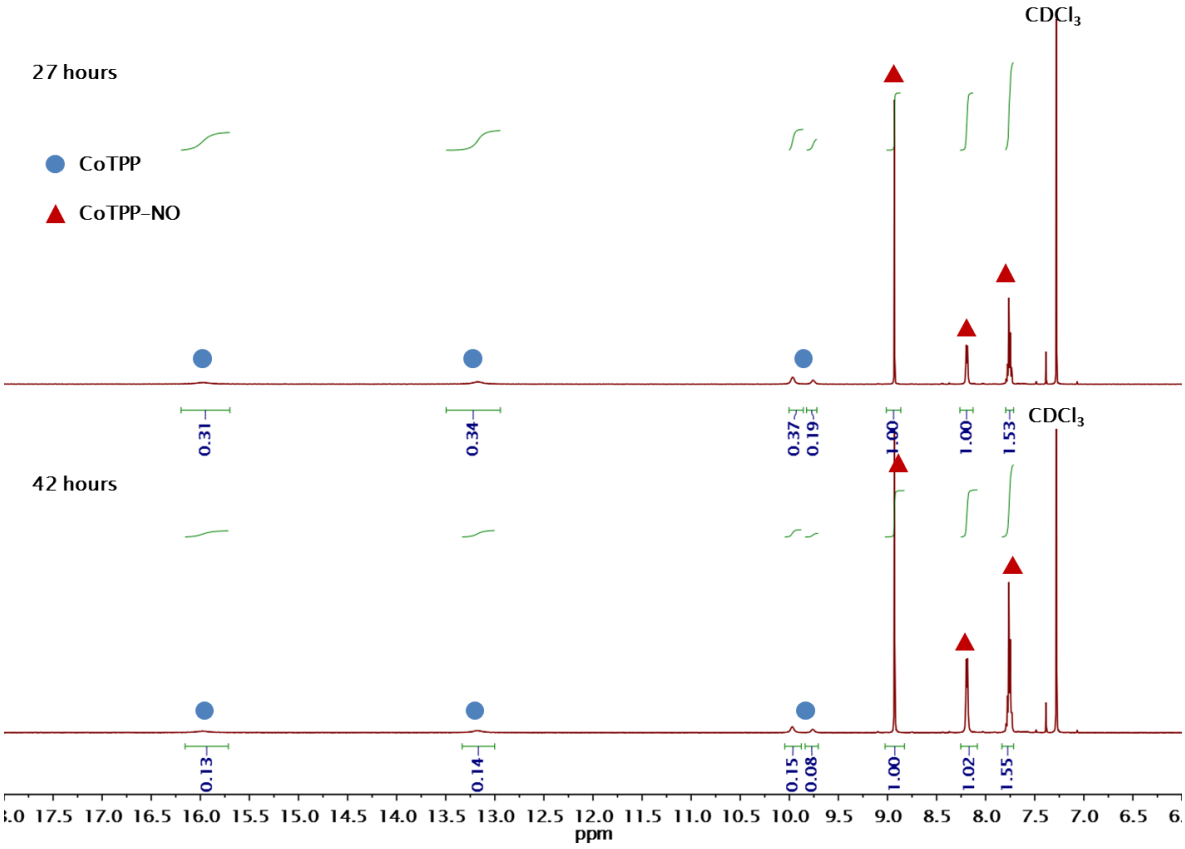

Figure 5.4 ^1H NMR spectrum of CoTPP/CoTPP-NO from catalytic nitrate reduction after 27 hours and 42 hours ($CDCl_3$, 21°C).

Control Reaction of Catalytic Nitrate Reduction. The reaction conditions were identical to those of catalytic nitrate reduction except [N(afa^{Cy})$_3$Fe(OTf)](OTf) was not added to the reaction mixture. CoTPP-NO formation was monitored by ^{1}H NMR spectroscopy. Integration of the ^{1}H NMR spectrum revealed the conversion of 9% of Co-TPP to CoTPP-NO after 27 h and 12% after 42 h (Figure 5.5).

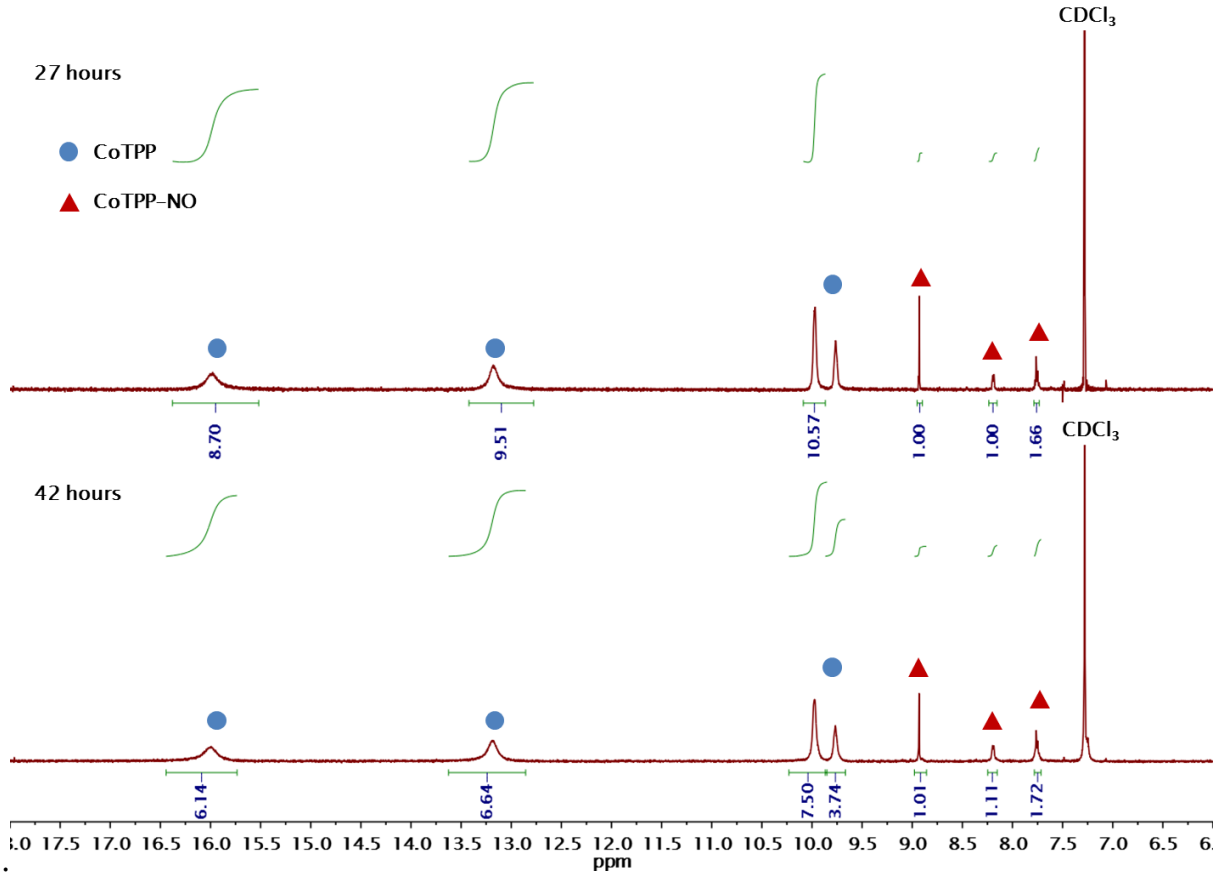

Figure 5.5 ^{1}H NMR spectrum of CoTPP/CoTPP-NO from the control nitrate reduction after 27 hours and 42 hours ($CDCl_3$, 21°C).

5.5 References

(1) Laue, W.; Thiemann, M.; Scheibler, E.; Wiegand, K. W. Nitrates and Nitrites. In *Ullmann's Encyclopedia of Industrial Chemistry*; Wiley-VCH Verlag GmbH & Co. KGaA, Ed.; Wiley-VCH Verlag GmbH & Co. KGaA: Weinheim, Germany, 2000.

(2) Parthasarathy, D. K.; Bryan, N. S. Sodium Nitrite: The "cure" for Nitric Oxide Insufficiency. *Meat Sci.* **2012**, *92*, 274–279.

(3) Addiscott, T. M.; Benjamin, N. Nitrate and Human Health. *Soil Use Manag.* **2006**, *20*, 98–104.

(4) Camargo, J. A.; Alonso, Á. Ecological and Toxicological Effects of Inorganic Nitrogen Pollution in Aquatic Ecosystems: A Global Assessment. *Environ. Int.* **2006**, *32*, 831–849.

(5) Fewtrell, L. Drinking-Water Nitrate, Methemoglobinemia, and Global Burden of Disease: A Discussion. *Environ. Health Perspect.* **2004**, *112*, 1371–1374.

(6) Ward, M. H.; deKok, T. M.; Levallois, P.; Brender, J.; Gulis, G.; Nolan, B. T.; VanDerslice, J. Workgroup Report: Drinking-Water Nitrate and Health—Recent Findings and Research Needs. *Environ. Health Perspect.* **2005**, *113*, 1607–1614.

(7) Camargo, J. A.; Alonso, A.; Salamanca, A. Nitrate Toxicity to Aquatic Animals: A Review with New Data for Freshwater Invertebrates. *Chemosphere* **2005**, *58*, 1255–1267.

(8) Bertero, M. G.; Rothery, R. A.; Palak, M.; Hou, C.; Lim, D.; Blasco, F.; Weiner, J. H.; Strynadka, N. C. J. Insights into the Respiratory Electron Transfer Pathway from the Structure of Nitrate Reductase A. *Nat. Struct. Biol.* **2003**, *10*, 681–687.

(9) Fischer, K. Structural Basis of Eukaryotic Nitrate Reduction: Crystal Structures of the Nitrate Reductase Active Site. *PLANT CELL ONLINE* **2005**, *17*, 1167–1179.

(10) Oosterkamp, M. J.; Mehboob, F.; Schraa, G.; Plugge, C. M.; Stams, A. J. M. Nitrate and (Per)chlorate Reduction Pathways in (Per)chlorate-Reducing Bacteria. *Biochem. Soc. Trans.* **2011**, *39*, 230–235.

(11) Giblin, T.; Frankenberger, W. T. Perchlorate and Nitrate Reductase Activity in the Perchlorate-Respiring Bacterium Perclace. *Microbiol. Res.* **2001**, *156*, 311–315.

(12) Heinecke, J.; Ford, P. C. Mechanistic Studies of Nitrite Reactions with Metalloproteins and Models Relevant to Mammalian Physiology. *Coord. Chem. Rev.* **2010**, *254*, 235–247.

(13) Suslick, K. S.; Watson, R. A. Photochemical Reduction of Nitrate and Nitrite by Manganese and Iron Porphyrins. *Inorg. Chem.* **1991**, *30*, 912–919.

(14) Ghafari, S.; Hasan, M.; Aroua, M. K. Bio-Electrochemical Removal of Nitrate from Water and wastewater—A Review. *Bioresour. Technol.* **2008**, *99*, 3965–3974.

(15) Guy, K. A.; Xu, H.; Yang, J. C.; Werth, C. J.; Shapley, J. R. Catalytic Nitrate and Nitrite Reduction with Pd−Cu/PVP Colloids in Water: Composition, Structure, and Reactivity Correlations. *J. Phys. Chem. C* **2009**, *113*, 8177–8185.

(16) Hamid, S.; Bae, S.; Lee, W.; Amin, M. T.; Alazba, A. A. Catalytic Nitrate Removal in Continuous Bimetallic Cu–Pd/Nanoscale Zerovalent Iron System. *Ind. Eng. Chem. Res.* **2015**, *54*, 6247–6257.

(17) Shen, J.; Birdja, Y. Y.; Koper, M. T. M. Electrocatalytic Nitrate Reduction by a Cobalt Protoporphyrin Immobilized on a Pyrolytic Graphite Electrode. *Langmuir* **2015**, *31*, 8495–8501.

(18) Matson, E. M.; Park, Y. J.; Fout, A. R. Facile Nitrite Reduction in a Non-Heme Iron System: Formation of an Iron(III)-Oxo. *J. Am. Chem. Soc.* **2014**, *136*, 17398–17401.

(19) Richter-Addo, G. B.; Hodge, S. J.; Yi, G.-B.; Khan, M. A.; Ma, T.; Van Caemelbecke, E.; Guo, N.; Kadish, K. M. Synthesis, Characterization, and Spectroelectrochemistry of Cobalt Porphyrins Containing Axially Bound Nitric Oxide. *Inorg. Chem.* **1996**, *35*, 6530–6538.

(20) Curley, J. J.; Bergman, R. G.; Tilley, T. D. Preparation and Physical Properties of Early-Late Heterobimetallic Compounds Featuring Ir–M Bonds (M = Ti, Zr, Hf). *Dalton Trans* **2012**, *41*, 192–200.

Chapter 6

High-valent iron complex capable of C–H bond activation

6.1 Introduction

High-valent iron complexes supported by heme and non-heme ligands are able to oxidize organic substrates in synthetic and biological systems. In particular, a high-spin Fe(IV)-oxo species is proposed to be a reactive intermediate in cytochrome p450 over the course of catalytic C–H bond functionalization reactions such as the hydroxylation of saturated C–H bonds and the oxidation of aromatic substrates, as well as other reactions like epoxidation of alkenes and dealkylation reactions.[1–3] In the proposed mechanism, the reactive Fe(IV)-oxo species is generated from dioxygen, which subsequently reacts with the target hydrocarbon to insert oxygen into the aliphatic position of organic substrate while the other oxygen is reduced to water (Figure 6.1). This finding has inspired both inorganic and organometallic chemists to utilize reactive high-valent metal-oxo complexes to activate such strong bonds.[4–6]

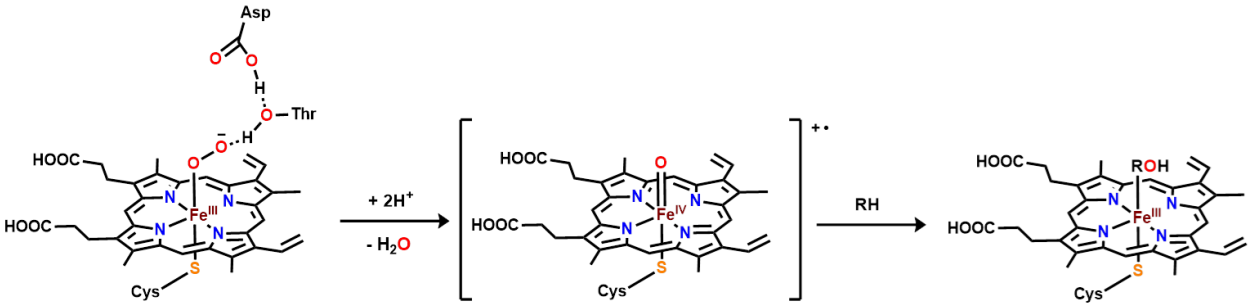

Figure 6.1 Proposed mechanism of hydroxylation of cytochrome P450.

There have been a number of high-valent Fe-oxo complexes capable of C–H bond activation reported in the literature.[7–10] Early examples include olefin epoxidation and alkane hydroxylation by iron porphyrins.[7,8] Mechanistic studies of these reactions demonstrated that the Fe(IV)-oxo porphyrin cation radical was responsible for substrate activations, as suggested for cytochrome p450 (Figure 6.2).[9,10]

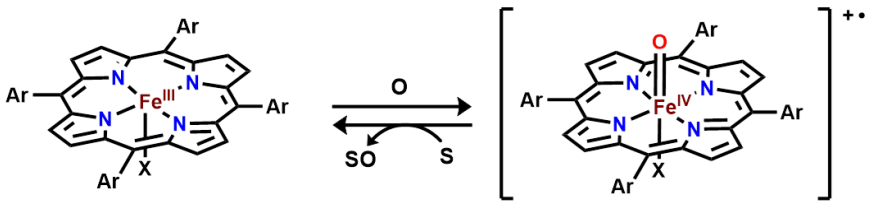

Figure 6.2 Formation of Fe(IV)-oxo porphyrin cation radical from oxygen transfer reagent (O) and oxygenation of substrate (S) with iron-oxo.

Non-heme high-valent iron complexes have also received much attention. For example, Chang and coworkers reported a high-spin Fe(IV)-oxo supported by a trigonal nonheme pyrrolide ligand platform capable of C─H bond activation.[11,12] In these studies they reported isolation of a high-spin Fe(IV)-oxo complex at -40°C and observed C─H bond activation of the ligand platform at room temperature, resulting in Fe^{III}-alkoxide complexes. In an effort to stabilize high-valent Fe-oxos, Borovik and coworkers installed a secondary coordination sphere onto the ligand which allowed for the isolation and crystallographic characterization of an Fe(III)-oxo and an Fe(IV)-oxo at room temperature.[6,13,14] In particular, this system demonstrated the importance of intramolecular interactions within the ligand to stabilize this reactive high-valent iron-oxo bond.

The formation of M(III)-oxo (M = Mn and Fe) or Fe(III)-OH complexes by small molecule activations with M(II) complexes bearing azafulvene-amine moieties (both afa^{Cy} and afa^{Mes}) has been described in previous chapters. The reactivity towards small molecules such as oxygen, nitrite, and oxygen transfer reagents revealed that the M(III)-oxo was easily accessible and such species were stabilized by amine moieties in the secondary coordination sphere. However, the synthesis of M(IV)-oxo was not successful presumably because the neutrally coordinated ligand platform is not sufficiently electron rich to stabilize a M(IV) center. Interested in accessing high-valent iron(IV) complexes with our ligand platforms ($H_3[N(pi^R)_3]$, R = Cy, Mes), iron(II) complexes bearing anionic ligands were synthesized and reacted with oxygen transfer reagents. We expecedt that the anionically bound ligands may provide a better electronic environment to access high-valent iron complexes compared to the neutral bound ligand platform. The resulting Fe(III)-alkoxide complex shows C─H bond activation on one of the arms of the ligand platform, suggesting that the reaction intermediate would proceed via a reactive high-valent iron-oxo complex.

6.2 Results and discussion

In order to generate an Fe(II) complex where $H_3[N(pi^{Mes})]$ is anionically bound to the metal center, 2.1 eq. of KH was added to $H_3[N(pi^{Mes})_3]$, resulting in deprotonation of the ligand. To the solution of the deprotonated ligand, $FeCl_2$ was added to generate $[N(pi^{Mes})_2Fe(afa^{Mes})]$. This complex was characterized by ^1H NMR spectroscopy (Figure 6.3), revealing that a paramagnetic species was formed; however analysis of the structural data was unsuccessful since upon crystallization, the target complex crystallized with water, resulting in formation of $[N(pi^{Mes})_3Fe(OH_3)]$ (described in Chapter4).

Oxidation of $[N(pi^{Mes})_2Fe(afa^{Mes})]$ was attempted by adding either pyridine-N-oxide (PyNO) or iodosylbenzene (PhIO). Since one of the arms was not deprotonated, we expected that it would be a hydrogen bond donor to the substrate and therefore generate a stable reaction intermediate. After adding PyNO to $[N(pi^{Mes})_2Fe(afa^{Mes})]$, the color of the reaction mixture was changed from orange to brown, followed by a change to green over the course of 24 hours. Two color changes are indicative of multiple events, therefore the reaction was monitored over time by ^1H NMR spectroscopy in a C_6D_6 solution to elucidate the progress of the reaction (Figure 6.3).

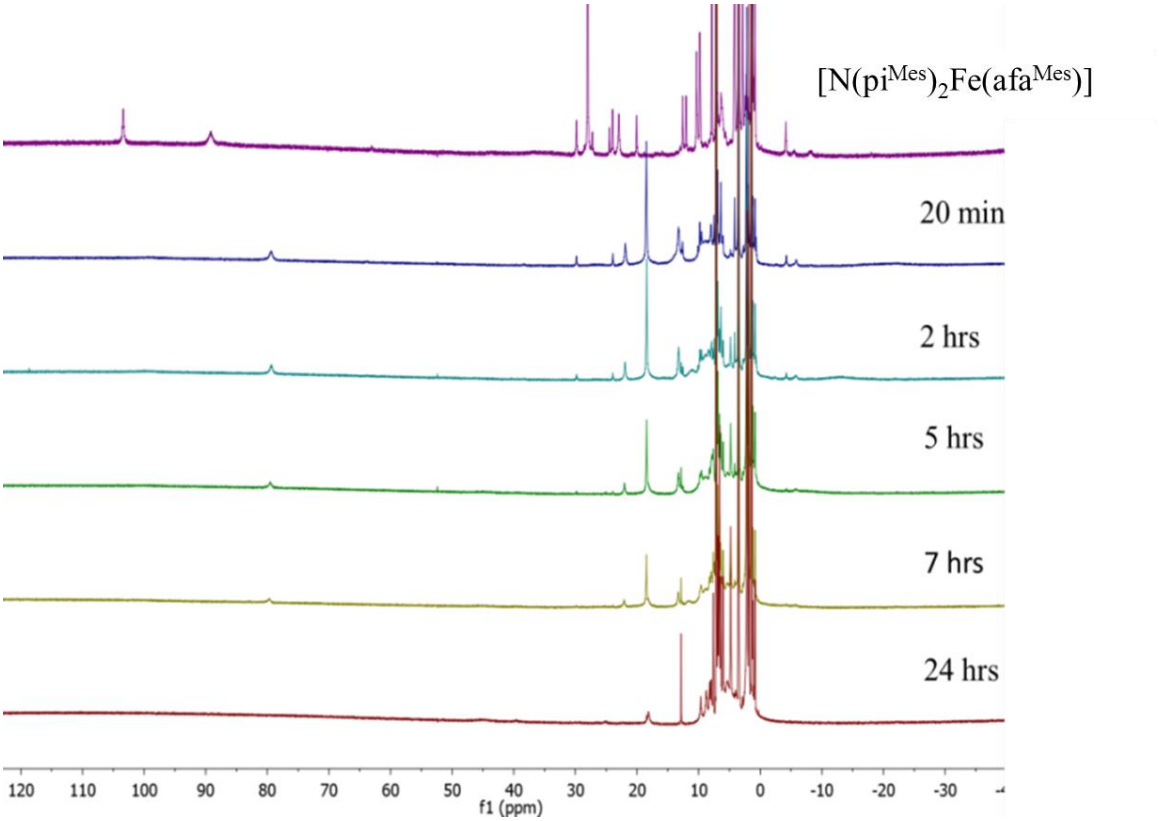

Figure 6.3 ^1H NMR spectroscopy of oxidation of $[N(pi^{Mes})_2Fe(afa^{Mes})]$.

After 20 min, new paramagnetic resonances appeared accompanied by a decrease in the resonances corresponding to the starting compound. After 7 hours, the transient paramagnetic resonances started to disappear, and after 24 hours new broad paramagnetic resonances were observed (45.7 ppm and 18.2 ppm). New diamagnetic resonances similar to those of free ligand were also evident after 24 hours.

To further understand these results, structural characterization was accomplished by X-ray diffraction of crystals grown from a concentrated hexane solution at -35ºC (Figure 6.4C). X-ray analysis revealed that the iron center was in a distorted square pyramidal geometry, bound to four nitrogen atoms, occupying the middle of two arms of the ligand. The axially bound oxygen was appended to one of the mesityl methyl groups, resulting from an intramolecular benzylic C-H bond oxidation of one of the pendant mesityl groups. Analogous C─H bond activation was observed by Chang when $[tpa^{Ph}Fe^{II}]^{+}$ was reacted with trimethylamine N-oxide in acetonitrile.[11,12] The bond length of the reported Fe─O bond was 1.903(5) Å comparable with the distance of the Fe─O bond (1.843(2) Å) of complex $[(afa^{Mes})(pi^{Mes})Fe\text{-}Opi^{Mes}]$. Based on the solid state structure of the C─H bond activated product, we suggest that the diamagnetic resonances similar to the free ligand correspond to the intact arm of the ligand platform, while the paramagnetic resonances correspond to the rest of the ligand including the C-H bond activated methyl group. The IR spectrum was consistent with the X-ray crystal structure, as it contains three different C=N stretches (1584 cm^{-1}, 1608 cm^{-1}, 1622 cm^{-1}) and a broad N─H stretch at 3452 cm^{-1}. We propose that PyNO first forms an adduct with the metal complex (Figure 6.4A), followed by C-H bond cleavage of the ortho-methyl of the mesityl group to form the resulting Fe^{III}-alkoxide compound.[15]

Further characterization by UV-vis spectroscopy confirmed the formation of the high-spin Fe(III) complex. In the UV-vis spectrum of $[(afa^{Mes})(pi^{Mes})Fe\text{-}Opi^{Mes}]$, an absorption band at 629 nm (ε =570 $M^{-1}cm^{-1}$) was detected which did not appear in the spectrum of the starting compound, $[N(pi^{Mes})_2Fe(afa^{Mes})]$. This feature resembles previously reported high-spin Fe(III) complexes,[15,16] suggesting $[(afa^{Mes})(pi^{Mes})Fe\text{-}Opi^{Mes}]$ is a high-spin Fe(III) complex.

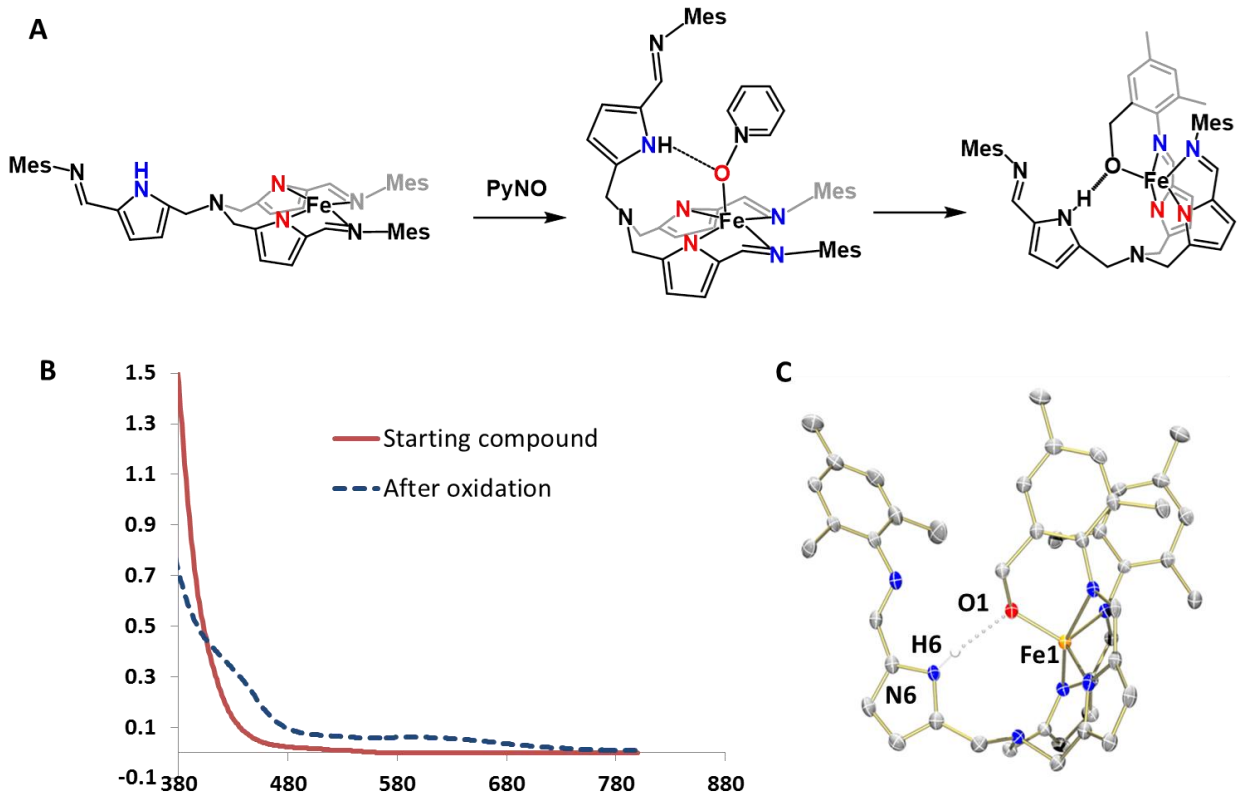

Figure 6.4 (A) Proposed mechanism of [N(pi^{Mes})$_2$Fe(afa^{Mes})] reaction with PhIO. (B) UV-vis spectrum of [(afa^{Mes})(pi^{Mes})Fe-Opi^{Mes}]. (C) Solid structure of [(afa^{Mes})(pi^{Mes})Fe-Opi^{Mes}].

A similar reaction using the [H$_3$N(pi^{Cy})$_3$] ligand was also attempted with PyNO, however, the resulting complex in this reaction was an octahedral Fe(III) complex, [N(pi^{Cy})$_3$Fe^{III}],[17] confirmed by ^{1}H NMR spectroscopy. Since the bond dissociation energy of cyclohexyl group (100 kcal/mol)[18] is higher than that of mesityl group (76 kcal/mol),[19] the C-H bond on the cyclohexyl group is much more difficult to cleave, thus the Fe-ONPy species is unable to activate these C-H bonds.

Attempts to isolate and characterize the reaction intermediate proved unsuccessful. However, the facile generation of the oxygenated product, Fe(III)-alkoxide, from oxygen transfer reagents may imply the formation of a potent iron-centered oxidant such as Fe(IV)-oxo. Moreover, addition of DPH to the mixture of [N(pi^{Mes})$_2$Fe(afa^{Mes})] and PyNO solution resulted in the clean formation of [N(afa^{Mes})(pi^{Mes})$_2$Fe(OH$_2$)] (**^{Mes}Fe^{II}-OH$_2$**). This result also suggests that

generation of the Fe(IV)-oxo complex would subsequently react twice with N–H bonds of DPH to generate $^{Mes}Fe^{II}$-OH_2 complex (Figure 6.5).

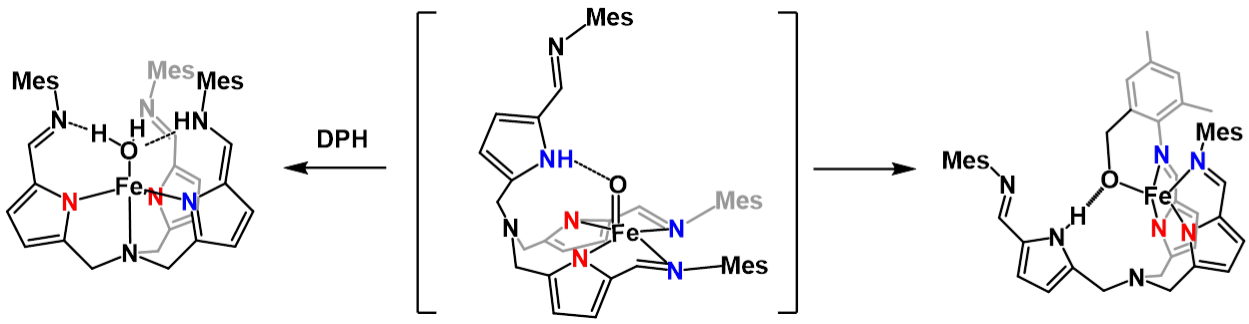

Figure 6.5 Proposed reactivity of Fe(IV)-oxo with either DPH (left) or benzylic methyl group (right).

6.3 Conclusions

Although the isolation of a high-valent Fe(IV) complex was not successful, the formation of th Fe(III)-alkoxide complex as well as $^{Mes}Fe^{II}$-OH_2 by DPH activation featuring an anionically bound ligand implies that a reactive intermediate such as Fe(IV)-oxo would be formed during the oxidation reaction. This study suggested that in order to access a high-valent iron complex, we may need to influence the electronic environment of the ligand platform.

6.4 Experimental section

Preparation of [N(pi^{Mes})$_2$Fe(afa^{Mes})] $H_3[N(pi^{Mes})_3]$ (0.070 g, 0.101 mmol) was deprotonated by addition of 2.2 equivalent KH (0.009 g, 0.22 mmol) to an approximately 10 mL of benezene solution. After it was stirred for three hours at room temperature, the mixture was filtered through Celite to remove excess KH. Addition of deprotonated ligand to the $FeCl_2$ (0.013 g, 0.0103 mmol) slurry in benzene resulted in a color change from colorless to yellow. After stirring overnight until all $FeCl_2$ was consumed, the reaction mixture was filtered through Celite to remove KCl and the solvents were removed under reduced pressure. The resulting orange compound was assayed by ^{1}H NMR spectroscopy (Figure 6.3).

Oxidation of [N(pi^{Mes})$_2$Fe(afa^{Mes})] To the benzene solution of $[N(pi^{Mes})_2Fe(afa^{Mes})]$ prepared *in situ* (described above), pyridine N-oxide (0010 g, 0.105 mmol) was added as a white solid. The

mixture was stirred overnight resulting in green-brown solution, after which time solvent was removed under reduced pressure. The resulting powder was dissolved in hexanes (10mL) and filtered through Celite to remove brown byproduct. The solvent was evaporated again, the green powder was isolated. Green crystals suitable for X-ray analysis were grown from a concentrated hexanes solution at -35°C.

Oxidation of [N(pi^{Mes})$_2$Fe(afa^{Mes})] with DPH present To the benzene solution of [N(pi^{Mes})$_2$Fe(afa^{Mes})] prepared *in situ* (described above), pyridine N-oxide (0.010 g, 0.105 mmol) and diphenylhydrazine(0.018, 0.1 mmol) were added as white solids. The mixture was stirred overnight resulting in an orange solution, after which time solvent was removed under reduced pressure. The resulting compound was assayed by ^{1}H NMR spectroscopy, revealing the formation of [N(afa^{Mes})(pi^{Mes})$_2$Fe(OH$_2$)].

6.5 References

(1) Heinecke, J.; Ford, P. C. Mechanistic Studies of Nitrite Reactions with Metalloproteins and Models Relevant to Mammalian Physiology. *Coord. Chem. Rev.* **2010**, *254*, 235–247.

(2) Denisov, I. G.; Makris, T. M.; Sligar, S. G.; Schlichting, I. Structure and Chemistry of Cytochrome P450. *Chem. Rev.* **2005**, *105*, 2253–2278.

(3) Groves, J. T. High-Valent Iron in Chemical and Biological Oxidations. *J. Inorg. Biochem.* **2006**, *100*, 434–447.

(4) Nam, W. High-Valent Iron(IV)–Oxo Complexes of Heme and Non-Heme Ligands in Oxygenation Reactions. *Acc. Chem. Res.* **2007**, *40*, 522–531.

(5) Bergman, R. G. Organometallic Chemistry: C–H Activation. *Nature* **2007**, *446*, 391–393.

(6) Borovik, A. S. Role of Metal–oxo Complexes in the Cleavage of C–H Bonds. *Chem. Soc. Rev.* **2011**, *40*, 1870.

(7) Groves, J. T.; Nemo, T. E.; Myers, R. S. Hydroxylation and Epoxidation Catalyzed by Iron-Porphine Complexes. Oxygen Transfer from Iodosylbenzene. *J. Am. Chem. Soc.* **1979**, *101*, 1032–1033.

(8) Nam, W.; Goh, Y. M.; Lee, Y. J.; Lim, M. H.; Kim, C. Biomimetic Alkane Hydroxylations by an Iron(III) Porphyrin Complex with H_2O_2 and by a High-Valent Iron(IV) Oxo Porphyrin Cation Radical Complex. *Inorg. Chem.* **1999**, *38*, 3238–3240.

(9) Groves, J. T.; Haushalter, R. C.; Nakamura, M.; Nemo, T. E.; Evans, B. J. High-Valent Iron-Porphyrin Complexes Related to Peroxidase and Cytochrome P-450. *J. Am. Chem. Soc.* **1981**, *103*, 2884–2886.

(10) Groves, J. T.; Watanabe, Y. Reactive Iron Porphyrin Derivatives Related to the Catalytic Cycles of Cytochrome P-450 and Peroxidase. Studies of the Mechanism of Oxygen Activation. *J. Am. Chem. Soc.* **1988**, *110*, 8443–8452.

(11) Harman, W. H.; Chang, C. J. N_2O Activation and Oxidation Reactivity from a Non-Heme Iron Pyrrole Platform. *J. Am. Chem. Soc.* **2007**, *129*, 15128–15129.

(12) Bigi, J. P.; Harman, W. H.; Lassalle-Kaiser, B.; Robles, D. M.; Stich, T. A.; Yano, J.; Britt, R. D.; Chang, C. J. A High-Spin Iron(IV)–Oxo Complex Supported by a Trigonal Nonheme Pyrrolide Platform. *J. Am. Chem. Soc.* **2012**, *134*, 1536–1542.

(13) MacBeth, C. E. O2 Activation by Nonheme Iron Complexes: A Monomeric Fe(III)-Oxo Complex Derived From O2. *Science* **2000**, *289*, 938–941.

(14) Lacy, D. C.; Gupta, R.; Stone, K. L.; Greaves, J.; Ziller, J. W.; Hendrich, M. P.; Borovik, A. S. Formation, Structure, and EPR Detection of a High Spin Fe^{IV} —Oxo Species Derived from Either an Fe^{III} —Oxo or Fe^{III} —OH Complex. *J. Am. Chem. Soc.* **2010**, *132*, 12188–12190.

(15) Wang, B.; Lee, Y.-M.; Seo, M. S.; Nam, W. Mononuclear Nonheme Iron(III)-Iodosylarene and High-Valent Iron-Oxo Complexes in Olefin Epoxidation Reactions. *Angew. Chem. Int. Ed.* **2015**, *54*, 11740–11744.

(16) Soo, H. S.; Komor, A. C.; Iavarone, A. T.; Chang, C. J. A Hydrogen-Bond Facilitated Cycle for Oxygen Reduction by an Acid- and Base-Compatible Iron Platform. *Inorg. Chem.* **2009**, *48*, 10024–10035.

(17) Matson, E. M.; Bertke, J. A.; Fout, A. R. Isolation of Iron(II) Aqua and Hydroxyl Complexes Featuring a Tripodal H-Bond Donor and Acceptor Ligand. *Inorg. Chem.* **2014**, *53*, 4450–4458.

(18) Tian, Z.; Fattahi, A.; Lis, L.; Kass, S. R. Cycloalkane and Cycloalkene C−H Bond Dissociation Energies. *J. Am. Chem. Soc.* **2006**, *128*, 17087–17092.

(19) Zhang, X.-M.; Bordwell, F. G. Homolytic Bond Dissociation Energies of the Benzylic Carbon-Hydrogen Bonds in Radical Anions and Radical Cations Derived from Fluorenes, Triphenylmethanes, and Related Compounds. *J. Am. Chem. Soc.* **1992**, *114*, 9787–9792.